Generation of Bipartite Quantum Features and Transfer of Quantum States in Hybrid Optomechanical System with an Optical Parametric Amplifier

Abraham Abebe Kibret

A PhD Dissertation Submitted to the Department of Applied Physics,
School of Applied Natural Science

Presented in the Partial Fulfillment of the Requirements for the Degree of Doctor of Philosophy in Applied Physics (Quantum Optics and Information)

Office of Graduate Studies
Adama Science and Technology University

June 2024
Adama, Ethiopia

Generation of Bipartite Quantum Features and Transfer of Quantum States in Hybrid Optomechanical System with an Optical Parametric Amplifier

PhD Candidate:
Abraham Abebe Kibret

Major-supervisor:
Dr. Tesfay Gebremariam[1] (Associate Professor)

Co-supervisor:
Dr. Tewodros Yirgashewa [2] (PhD)

[1]Arba Minch University, Department of Physics, Faculty of Natural Science, P. O. Box 21, Arba Minch, Ethiopia

[2]Adama Science and Technology University, Department of Applied Physics, P.O.Box 1888, Adama, Ethiopia

A Dissertation Submitted to the Department of Applied Physics, School of Applied Natural Science

Presented in a Partial Fulfillment of the Requirement for the Degree of Doctor of Philosophy in Applied Physics (Quantum Optics and Information)

Office of Graduate Studies
Adama Science and Technology University

June 2024
Adama, Ethiopia

DECLARATION

I hereby declare that this PhD Dissertation entitled "**Generation of Bipartite Quantum Features and Transfer of Quantum States in Hybrid Optomechanical System with an Optical Parametric Amplifier**" is my original work and has not been submitted the award of any academic degree, diploma or certificate in any other university. All sources of material used for this dissertation have been duly acknowledged through appropriate citations.

(Name of Candidate)	Signature	Date

RECOMMENDATION

I/we, the supervisor(s) of this dissertation, hereby certify that I/we have read and revise the dissertation entitled "Generation of Bipartite Quantum Features and Transfer of Quantum States in Hybrid Optomechanical System with an Optical Parametric Amplifier" prepared under my/our guidance by **Abraham Abebe Kibret** submitted in the partial fulfillment of the requirements for the degree of Doctor of Philosophy in **Applied Physics (quantum optics and information)**. Therefore, I/we recommend the submission of the dissertation to the department for further review and defense.

(Supervisor)	Signature	Date
(Co-supervisor)	Signature	Date

APPROVAL SHEET

I/We, certify that the recommendations and suggestions made by the board of examiners are appropriately incorporated into the final version of the dissertation entitled "Generation of Bipartite Quantum Features and Transfer of Quantum States in Hybrid Optomechanical System with an Optical Parametric Amplifier" by **Abraham Abebe Kibret**.

(Supervisor)	Signature	Date
(Co-supervisor)	Signature	Date

We, the undersigned, members of the Board of Examiners of the dissertation open defense by **Abraham Abebe Kibret** have read and evaluated the dissertation entitled "Generation of Bipartite Quantum Features and Transfer of Quantum States in Hybrid Optomechanical System with an Optical Parametric Amplifier" and examined the candidate during open defense. This is therefore to certify that the dissertation is accepted for partial fulfillment of the requirement of the degree of Doctor of Philosophy in **Applied Physics (quantum optics and information)**

(Chairperson)	Signature	Date
(Internal Examiner 1)	Signature	Date
(Internal Examiner 2)	Signature	Date
(External Examiner 1)	Signature	Date
(External Examiner 2)	Signature	Date

Final approval and acceptance of the dissertation proposal is contingent upon submission of its final copy to the Office of Postgraduate Studies (OPGS) through the Department Graduate Council (DGC) and School Graduate Committee (SGC).

(Department Head)	Signature	Date
(School Dean)	Signature	Date
(Office of Postgraduate Studies, Dean)	Signature	Date

ABBREVIATIONS AND SYMBOLS

OPA	Optical Parametric Amplifier
EPR	Einstein-Podolsky-Rosen
CV	Continuous Variable
GQD	Gaussian Quantum Discord
EN	Logarithmic Negativity
EN^1	Entanglement in the absence of atoms
EN^2	Entanglement in the presence of two-level atoms
EN^3	Entanglement in the presence of three-level atoms
D_1	Gaussian quantum discord without atoms
D_2	Gaussian quantum discord in the presence of two-level atoms
D_3	Gaussian quantum discord in the presence of three-level atoms
$C1-M1$	The first cavity -mechanical oscillator modes
$C2-M2$	The second cavity-mechanical oscillator modes
$M1-M2$	The two mechanical oscillator modes
$C1-C2$	The two cavity modes

ACKNOWLEDGMENT

First and foremost, I would like to express my gratitude to the Almighty God for giving me good health, wisdom, and endurance during my research endeavors. I also appreciate his tolerance for all of life's challenges, complexities, ups and downs, and, in the end, for enabling me to overcome them with tremendous battle. Next, I would like to express my heartfelt gratitude to **Dr. Tesfay Gebremariam**, who is my **instructor** and **supervisor** for this research and for showing me all the ways during my research work. His broad knowledge and research interests have always been an inspiration to me, motivating and encouraging me when I felt discouraged and providing constructive suggestions and scientific criticism on my trials, which opens my mind and drives me to explore various optomechanical systems in quantum optics and information. His scientifically integral view of research, his overly enthusiasm, and his original work on quantum optics and quantum information have made a deep impression on me. I am very grateful to have had his guidance, trust, and encouragement over the past few years. The philosophy and attitude that I learned from **Dr. Tesfay** have deeply influenced me, not only giving me confidence to face all the challenges in research but also benefiting my future career and life. Furthermore, I appreciate his brotherly and fatherly approach during this research. I would also like to express my strong gratitude and respect to my **instructor** and **Co-Advisor Dr. Tewodros Yirgashew**, who offered me the opportunity to study and work in such a wonderful field of study and for his valuable guidance, continuous support, helpful suggestions, and encouragement. I also appreciate him for his kind, thoughtful, and helpful remarks, opinions, and recommendations throughout the dissertation work. He was not only my **instructor** and **co-advisor** but also a true brother or father. They kindly read different papers and offered invaluable, detailed advice on organization and the theme of this dissertation. This dissertation is made possible with their help and support.

I would like to express my heartfelt gratitude to **Dr. Sintayehu Tesfa** for his unwavering support and for his invaluable comments and suggestions, which have been indispensable throughout my journey. I extend my sincere thanks to **Dr. Fekadu Tolesa**, the head of the Applied Physics department, **Dr. Minisha Alemu**, **Dr. Megersa Wedajo**, as well as to all the staff members in the Applied Physics department at Adama Science and Technology University and Wollega University. Their guidance and encouragement, especially during challenging times when my dissertation were not progressing well, have been immensely supportive. I am also deeply thankful to Wollega University for their generous sponsorship and support over these years. Again, I'd like to thank my parents for their morale, encouragement, and financial support. I also have to express my strong feelings of appreciation, love, and respect for my wife, **Tizita Ferede**, for her commitment, praying, and patience in embracing all the responsibilities of our family during all these years.

TABLE OF CONTENTS

LIST OF FIGURES

LIST OF TABLES

ABSTRACT

In this dissertation, the generation of bipartite quantum features and entanglement transfer between distance parties have been investigated using hybrid optomechanical system with an optical parametric amplifier and three-level atoms. In the first part of our work, we examined the degree of steady-state entanglement in a hybrid optomechanical system incorporating a parametric amplifier. We used logarithmic negativity to quantify the steady-state entanglement under the linearization approximation. The entanglement between the cavity-mechanical oscillator and two cavity modes was analyzed by varying the nonlinear gain of the OPA, optical cavity detuning, and cavity-cavity coupling strength. We found that the steady-state entanglement increases with the nonlinear gain of the OPA medium and normalized detuning. Additionally, we demonstrated that the generation of entanglement can be significantly influenced by the coupling strengths. In the second part of our work, we investigated the stationary entanglement and quantum discord between the cavity and mechanical oscillator mode in an optomechanical system containing three-level atoms. We explored how the shared entanglement and correlations are affected by the number of atoms injected into the cavity. By optimizing the injection of atoms and tuning the optical cavity detuning, we analyzed the impact of these parameters on the degree of steady-state entanglement and quantum discord. We confirmed that both entanglement and Gaussian quantum discord are enhanced in the presence of three-level atoms, with maximum entanglement occurring near the resonance condition. Lastly, we studied the generation of quantum correlations using an OPA in a single cavity of two distant Fabry-Perot cavities connected by cavity-cavity coupling. We analyzed steady state entanglement, quantum discord, and steering. Our findings demonstrate that under OPA, higher nonlinear gain enhances quantum correlations, resulting in stronger entanglement. However, the decay rates significantly impact the sustainability of these correlations. Additionally, we shown that Gaussian quantum discord contributes to broader quantum correlations beyond entanglement. We also characterize quantum steering by examining the steerability between subsystems, revealing that strong coupling under OPA boosts quantum steering between cavity modes. Our results may have potential applications in constructing long-distance quantum communication networks and facilitating the manipulation of quantum state transfer.

***Key Words**: Optomechanical Systems, Optical Parametric Amplifer, Three-Level Atoms, Entanglement, Quantum Correlations, and Quantum Information Process.*

1. INTRODUCTION

1.1. Background

Quantum entanglement is an important resource in the fields of quantum information to realize quantum communication, quantum computation, quantum cryptography, and quantum teleportation (Nielsen and Chuang, 2010; Gebremariam et al., 2017; Horodecki et al., 2009; Zubair et al., 2017). Recently, entanglement has attracted great attention and experimental realization using different physical quantum systems and information carriers (Liu et al., 2021; Lin et al., 2020; Riedinger et al., 2018). Specifically, mechanical resonators at mesoscopic scales are beginning to be available as candidate systems to study various macroscopic quantum features, whereas optomechanical systems have emerged as particularly promising platforms due to their versatility in design, fabrication, and control (Aspelmeyer et al., 2014; Gebremariam et al., 2017).

In recent years, there has been a surge of interest in investigating entanglement phenomena, specifically within mesoscopic systems and two-qubit states (Berrada et al., 2010; Tesfahannes and Getahune, 2020). This heightened attention underscores the significance of unraveling the intricacies of entanglement at intermediate scales, driving forward our understanding of quantum phenomena in complex systems (Bai et al., 2016; Mancini et al., 2002). On the other hand, optomechanics is one of the emerging research areas that focuses on the interaction of light with mechanical motion due to radiation pressure forces associated with momentum (Meystre, 2013; Nichols and Hull, 1901). Cavity optomechanical systems have recently garnered significant attention due to their experimental realization, making them crucial components of quantum technology. For the existing coherent phonon-photon interaction, the pertinent entanglement has been studied in various optomechanical systems by transferring the quantum behavior of photons to movable mirrors of coupled optical cavities. In this respect, different authors have studied the entanglement of two dielectric membranes suspended inside a cavity (Hartmann and Plenio, 2008), macroscopic quantum states in two superconducting qubits (Berkley et al., 2003), dynamical quantum steering (Gebremariam et al., 2019), nano-mechanical oscillators in a ring cavity by feeding squeezed light (Huang and Agarwal, 2009b), optomechanically induced transparency (Tesfahannes, 2021), processing quantum information (Zhang et al., 2015; Li et al., 2015b), and enhancing optomechanical force sensing (Gebremariam et al., 2020; Liu et al., 2012).

Furthermore, the bipartite entanglement between the cavity mode and the mode of oscillating mirrors has also been demonstrated with the help of an optomechanical array in which the optical cavities are connected to one oscillating end mirror via a photon hopping mechanism (Tesfahannes, 2020). In addition, authors have studied observation and measures of robust correlations for continuous variable systems (Gebremariam et al., 2017), steady-state entanglement in a hybrid optomechanical system (Kibret et al., 2023), cooling a mechanical oscillator to its quantum ground state (Marquardt et al., 2008; Zhang et al., 2016b), dynamical quantum steering (Gebremariam et al., 2019), generating side band comb (Xiong et al., 2014), and optomechanically induced transparency (Tesfahannes, 2021). Exploring quantum features in macroscopic systems has also made nanomechanical oscillators attractive candidates (Huang and Agarwal, 2011; Miao et al., 2009). Entwining two mirrors in a cavity is a proposal put forth by some researchers (Zhang et al., 2003; Huang and Agarwal, 2009b). Research has been done on the entanglement that occurs between a vibrating end mirror and a cavity field (Genes et al., 2008; Mi et al., 2013). Furthermore, generation of the bipartite entanglement and correlations in an optomechanical array (Gebremariam et al., 2017).

Moreover, many authors have devoted their effort to studying the effect of the parametric amplification process on entanglement in a cavity where both ends of the mirrors are fixed (Alebachew, 2007; Adamyan and Kryuchkyan, 2004). In particular, there are also indications that placing an optical parametric amplifier inside the optomechanical cavity leads to cooling of the optomechanical oscillation (Huang and Agarwal, 2009a), strengthening the optomechanical coupling (Lü et al., 2015), and splitting the normal mode (Huang and Agarwal, 2009c). In the same way, the OPAs in a single optomechanical cavity have also been shown to improve entanglement between a cavity mode and a mechanical mode (Mi et al., 2013; Yang et al., 2017).

Recent results suggest that various applications in quantum information theory can be captured by quantum correlations. Several measures of these quantum correlations have been investigated in the literature (Henderson and Vedral, 2001; Modi et al., 2010). Remarkably, one of the quantum correlation measures that Ollivier and Zurek introduced is quantum discord (Ollivier and Zurek, 2001). The quantum discord is the most popular candidate for such general quantum correlations and has recently received a great deal of attention (Datta et al., 2008; Ferraro et al., 2010), and some of these have been verified experimentally (Lanyon et al., 2008; Xu et al., 2010). Furthermore, quantum discord has been proposed as the key resource in certain quantum communication tasks and quantum computational models, despite containing minimal entanglement. Specifically, its asymptotic dynamics in open quantum systems (Berrada et al., 2011), advancements in quantum communication techniques (Bub, 2014; Navascués et al., 2015), and the novel type of quantum computing problems (Zidan et al., 2021) are widely used for the application of quantum information processing.

Furthermore, the interaction between a single two-level atom and an electromagnetic field, which is the Jaynes-Cummings model, has been at the forefront of quantum optics and quantum information. Subsequently, the atomic medium plays an essential role during the interaction with the hybrid quantum system. Specifically, when the atomic medium is trapped in a cavity with a micromechanical oscillator, some interesting phenomena have been revealed. For example, cooling the ground state of a micromechanical system through a two-level atomic system (Genes et al., 2009b) and the two-level atoms effectively enhance the radiation pressure of the optical cavity field (Ian et al., 2008) have been extensively studied based on atom-assisted hybrid optomechanical systems. Particularly, hybrid systems composed of an atomic ensemble can achieve a strong coupling between a mechanical oscillator and a single trapped atom (Hammerer et al., 2009b). Recently, the nondegenerate three-level laser coupled to a two-mode thermal reservoir with atomic coherence has been investigated (Ayehu, 2021).

In contrast to earlier considerations of linear optomechanical coupling schemes in two optomechanical cavities in the absence of degenerate OPAs (Gebremariam et al., 2017), we seek to study the effect of degenerate OPA and the strength of coupling between two separate optomechanical cavities on the degree of entanglement. With this in mind, we strive to study steady-state bipartite entanglement in a hybrid optomechanical system using optical parametric amplifiers. To this end, we obtain the dynamics of the optomechanical system by applying the corresponding Hamiltonian using the quantum Langevin equations, in which the dissipation and fluctuation terms are added to the Heisenberg equations of motion. We then find the steady-state and the linearized quantum fluctuation of the system. Afterward, the steady-state bipartite entanglement is quantified by applying logarithmic negativity. Due to the presence of degenerate OPA inside each cavity, the steady-state entanglement is found to significantly vary with the value of the nonlinear gain of OPA.

Furthermore, we consider steady-state entanglement and correlations in an optomechanical system whose cavity is injected by three-level atoms, in contrast to considerations of entanglement measurement with early works of a Fabry-Pérot cavity without atoms of an oscillating micro-mirror and driven by coherent light (Vitali et al., 2007). In light of this, we employ the quantum Langevin equations, which add the dissipation and fluctuation terms to the Heisenberg equations of motion, to apply the corresponding Hamiltonian and derive the dynamics of the optomechanical system. Next, we determine the system's steady-state and linearized quantum Langevin equations of fluctuation. After that, logarithmic negativity is used to quantify the steady-state entanglement. However, the quantum correlation is investigated by means of Gaussian quantum discord. In this way, we explore the effect of atoms injected into an optomechanical cavity on the degree of steady-state entanglement and quantum discord. This study shows that the cavity field and the oscillating mirror can be entangled. Furthermore, with the assistance of atomic enhancement, the logarithmic negativity and Gaussian quantum discord that separate the entanglement and correlation between the two modes are enhanced.

Moreover in this dissertation, we investigated quantum correlations in a hybrid cavity optomechanical system where one of the optical cavities contains an optical parametric amplifier (OPA), and the two cavity modes are coupled through cavity-cavity coupling strength. We focused on generating quantum correlations in hybrid systems, incorporating optical parametric amplification and photon-hopping processes. Under weak conditions, we examine the system's ability to create quantum correlations through the OPA. Specifically, we characterize the quantum correlations among the subsystems using various quantum correlation measures. We have thoroughly utilized logarithmic negativity to quantify bipartite entanglement and assess state transfer among the subsystems. While the quantum steering is used to measure the steerability of the two entangled bipartite states. Additionally, Gaussian quantum discord is utilized to evaluate the correlation between two Gaussian states, extending our analysis beyond entanglement.

Our findings indicate that introducing an optical parametric amplifier within the cavity system significantly enhances quantum correlations between subsystems. We explore the impact of the nonlinear gain and phase of the OPA, cavity-cavity coupling strength, and environmental temperature on quantum correlations. Specifically, we show that under OPA, higher nonlinear gain enhances quantum correlations, resulting in stronger entanglement. However, the decay rates significantly impact the sustainability of these correlations. Furthermore, our results show that increasing the cavity-cavity coupling strengthens the interactions and correlations between the modes, promoting conditions necessary for higher quantum transfer between subsystems. Our comprehensive approach demonstrates the potential to enhance quantum correlations within the hybrid system. We believe our findings hold significant promise for advancing quantum correlations through nonlinear interactions and facilitating the manipulation of quantum state transfer.

1.2. Statement of the problem

Optomechanics is the latest field of research and has received great attention in a vast variety of systems, ranging from nanomechanical cantilevers, vibrating microtoroids, membranes, and ultra-cold atoms to gravitational wave detectors. In the last decade, much theoretical attention has been given to optomechanical systems. On the other hand, due to research progress and technological developments, these systems are now becoming experimentally accessible. Furthermore, the coupling between the cavity field and the movable mirror in optomechanics has been a great attraction for researchers because it is helpful to create non-classical states of both the cavity field and the mirror. Also, it has been used for quantum noise reduction. The interaction between optical cavity mode and the degree of freedom of a mechanical object, cavity optomechanics, is, at this point, a mature research field in which many different platforms have been demonstrated that couple energy in a mechanical resonator to the energy stored in an optical cavity (Metcalfe, 2014; Li et al., 2021; Liu et al., 2018; Amazioug et al., 2018; Anetsberger et al., 2009; Fogliano et al., 2021).

Currently, the study of mesoscopic quantum states and their correlation properties is a captivating area of research as it gives

- improved compatibility between small quantum states like photons and atoms in a cavity and existing quantum technologies in terms of information storage, transport, and computation,
- a means to examine various nonclassical behaviors on a scale that falls between the microscopic and macroscopic levels,

On the other hand, squeezing of the cavity field is generated by the OPA, which can be used to improve the sensitivity of mechanical quadrature measurements. An OPA inside the cavity can enhance optomechanical cooling, optomechanical coupling strength, and normal mode splitting. The enhanced coupling strength makes it even possible to implement cavity optomechanics in the single-photon strong coupling regime. Currently, significant progress has been reported on the study of the enhanced entanglement of two optical modes in optomechanical systems. Therefore, the enhancement of entanglement and correlation in two-cavity modes of optomechanical systems via an optical parametric amplifier is the subject of an active research field (Zhang et al., 2016a; Paschotta, 2014; Lakhfif et al., 2022; Pan et al., 2023; Elsaesser et al., 1998; Budriūnas et al., 2021; Artigas et al., 2002). Motivated by these interesting features, we propose the generation of bipartite quantum features and the transfer of quantum states in a hybrid optomechanical system with an optical parametric amplifier and three-level atoms. In this dissertation, different behaviors quantum states and nonclassical states in quantum optomechanical systems, such as entanglement, quantum discord, steering, their interactions with OPA's effects, and atomic cavities, are studied. So, using radiation from the interaction of OPA and atoms with the cavity field, will entanglement and quantum correlations in the modes of the cavity and mechanical oscillators be established in this dissertation? Furthermore, what impact do OPA and atoms injected into an optomechanical cavity have on steady-state entanglement, quantum discord, and steering?

1.3. Objective of the study

1.3.1 General objective

The general objective of this dissertation is to investigate the generation of bipartite quantum features and the transfer of quantum states in a hybrid optomechanical system with an optical parametric amplifier and the three-level atoms.

1.3.2 Specific objectives

The specific objectives of this work are to:

- describes the model, the Hamiltonian of the system, and examine the equation of motion via the quantum Langevin equations,
- generates quantum features such as Gaussian quantum discord, and Gaussian steering between the subsystems under the effect of OPA and three-level atoms.
- describe bipartite entanglement, quantum discord, and steering between subsystems under different parameters.

1.4. Significance of the study

Quantum entanglement and correlation properties are applicable, particularly in the fields of physics, quantum communication, quantum information processing, computer science, engineering, and other sciences. A hybrid optomechanical system is used to achieve quantum control of micromechanical and nanomechanical resonators using the electromagnetic field, which has been very helpful for recent applications in quantum technologies such as quantum metrology, quantum cryptography, quantum teleportation, quantum computation, and others. The development of efficient hybrid optomechanical systems is also important in bridging the gap between theory and implementation of quantum communication, computations, and quantum information processing.

Therefore, the results of this dissertation will contribute to these applications that are used for technological advancements and provide a promising platform for the realization of bipartite CV quantum information processing and a framework for future remote entanglement and correlation preparation. Furthermore, the theoretical physicist may use mathematical procedures to develop further optomechanical models. In addition to that, the results of this research will be used as input for other researchers and postgraduate students to apply to other hybrid optomechanical systems. Moreover, it will serve as a platform for other scientific researchers.

1.5. Scope of the study

Based on the principles of quantum optomechanical systems, this dissertation explores their applications in various fields, such as quantum communications and quantum information science.

This study investigates the advancements in hybrid optomechanical systems, focusing on their entanglement, Gaussian quantum discord, and Gaussian steering. The analysis is carried out using the quantum Langevin equations for various quantum states of the system. The study is limited to linear analysis and a good cavity limit. The interaction between the OPA and the cavity field, as well as the interaction between the atoms and the cavity field, are considered to be significantly stronger than the optomechanical coupling. However, the external environments connected to cavity radiation and quantum harmonically oscillating mirrors are Markovian. The parameters utilized in this study are restricted to a specific range. Particularly, the main focus of these investigations was to ascertain the effects of OPA and atomic injection into the cavity of a hybrid optomechanical system on steady-state bipartite entanglement, Gaussian quantum discord, and Gaussian steering between subsystems. Specifically, by selecting the nonlinear gain of OPA, normalizing detuning function, cavity-cavity coupling strength, the cavity driving laser, coupling rate, decay rate of the cavity, and ambient temperature.

2. LITERATURE REVIEW

2.1. Overview of the study

In this chapter, we present a comprehensive theoretical overview of the principles of optomechanics. A number of significant topics will be covered, such as the development of ptomechanical systems, the importance of optomechanical systems, the basic concepts of optomechanics, radiation pressure force, optomechanical coupling, and correlated emission lasers. This chapter also covers the Hamiltonian formulation, Heisenberg quantum Langevin equations, and linearization approximation approach. After that, we talk about entanglement through logarithmic negativity, Gaussian quantum discord, and Gaussian steering, respectively.

2.2. The development of optomechanical systems

Any system that has a coupling between an optical and a mechanical element is an optomechanical system. One area of current quantum physics that is expanding quickly is optomechanics. An optical cavity connected to a mechanical oscillator makes up a quantum optomechanical system, to put it simply. Nanophysics and quantum optics converge in optomechanics. Optomechanics deals with the interaction of light and a mechanical oscillator, e.g., a mirror attached to a spring or a cantilever. Radiation pressure force is the force that light applies to an oscillating mirror or mechanical oscillator. In optomechanics, radiation force is the fundamental element. The next part will go into depth on radiation pressure force; in the meantime, in an optomechanical system, light can be used to measure and control the mechanical oscillator. A simple example, sometimes referred to as cavity-optomechanics, of a Fabry-P´erot cavity consists of one mirror that is fixed while the other one is free to move in a harmonic potential, as shown in Figure 1 of the cavity modes of frequency. ω_a is driven by a laser, and the light inside the cavity will push the mirror due to radiation pressure. When combined, these two mechanisms can produce a wide range of optomechanical phenomena, including normal mode splitting, optomechanically induced transparency, high-sensitivity quantum ground state cooling of mechanical resonators, and quantum coherent coupling between light and mechanical oscillators (Mari, 2012). The mirror oscillates in a harmonic potential of frequency ω_b, which changes the length of the cavity, modulating the phase of the light.

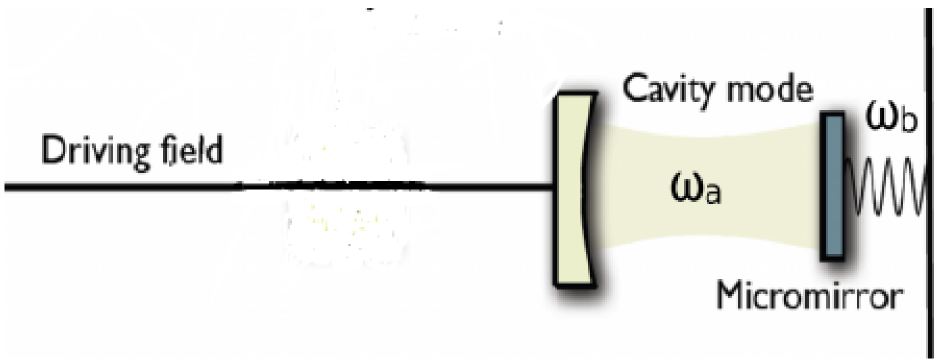

Figure 1: Typical shape of cavity optomechanics (Mari, 2012)

2.3. The importance of optomechanical systems

Furthermore, optomecanics systems, which relate macroscopic mechanical objects to electromagnetic degrees of freedom, offer a way to realize new types of dynamical control in both the quantum and classical domains and to explore quantum effects on macroscopic scales (Chen, 2013). These days, optomechanics is a rapidly developing topic that has drawn significant scientific attention and is now the basis of numerous research initiatives (Gebremariam et al., 2017). In two-mode compressed states, a number of intriguing optomechanical devices can be employed to process quantum information and make high-precision measurements while examining the shifts from micro-to-macro entanglement.

Additionally, optomechanical systems are a fundamental component of many research endeavors, as previously noted (Bariani et al., 2014) and (Barzanjeh et al., 2019). Numerous optomechanical device investigations are applicable in the two-mode squeezed condition (Woolley and Clerk, 2014). In the quantum application of optomechanical systems, a strong coupling rate with low optical and mechanical losses was the main concern (Kippenberg and Vahala, 2007). Devices with well-coupled mechanical and optical modes play an important role in many fields of physics and a wide range of applications, including the study of optomechanically induced transparency, gravitational wave detection, precision measurements of small displacement and force, quantum ground state cooling of mechanical resonators, light readout, and information processing for storage.

Entanglement is now understood to be a resource; it must be generated, manipulated, and stored to process quantum information (Mathieu et al., 2009). A hybrid quantum system is a coupling between two quantum systems of a different physical nature, such as light and mechanical vibration, useful for purposes such as quantum information processing. In order to combine the advantages of different physical systems in one architecture, some systems may be strongly interacting (good for computation), some are very coherent (good for long-term storage), and others are easily transported over long distances (good for communication).

A light beam passing through an optomechanical cavity and then an atom cloud carries information in its quadratures about the sum and difference of position and momentum variables of the mechanics and the spin state that allow to generate CV entanglement between an optical cavity and mechanical mode. It was recently suggested that light might also be used to couple the collective spin of an atom cloud to a nano-mechanical oscillator in such a setup (Hammerer et al., 2009a).

2.4. The basic concepts of optomechanics

It is well known that optomechanical systems can be created when a mechanical resonator is coupled to electromagnetic fields (to say, an optical or microwave cavity) through radiation pressure. It has been shown both theoretically and experimentally that mechanical resonators can be used to convert optical quantum states to microwave ones via optomechanical interactions between a mechanical resonator and a single-mode field of both optical and microwave wavelengths (Wang et al., 2014b). Figure 2 shows that when a weak coherent probe field is applied to the cavity of an optomechanical system, the mechanical resonator can act as a switch to control the probe photon transmission such that photons can pass through the cavity one by one or two by two in the limit of the strong single-photon optomechanical coupling. Moreover, optomechanical systems can also become transparent to a weak-probe field when a strong driving field is applied to the cavity field. This is an optomechanical analogy of electromagnetically induced transparency.

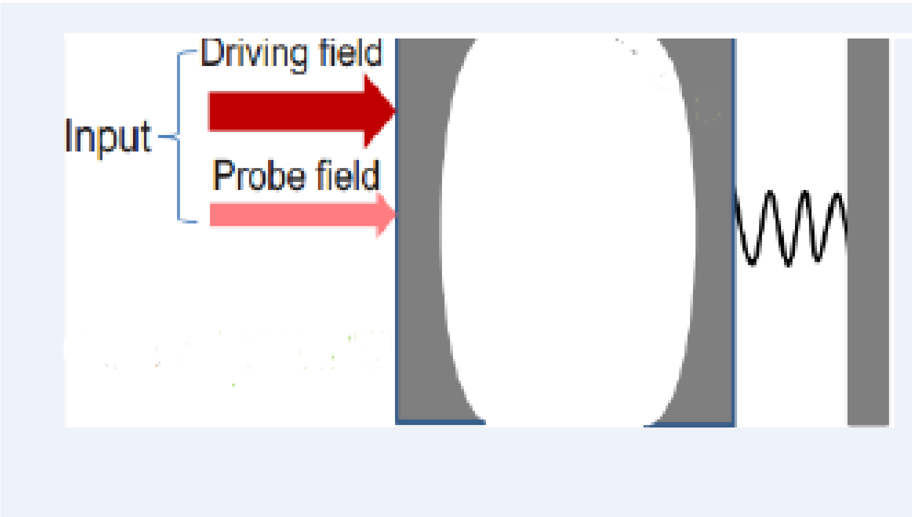

Figure 2: set up of optomechanics (Wang et al., 2014b)

2.5. Radiation pressure force and optomechanical coupling

In optomechanics, radiation pressure force is the fundamental element. The early 17th century saw discussions about radiation pressure, also known as radiation pressure force, acting due to the photon momentum of light. Johannes Kepler first recognized that a mechanical force from the sun might be the cause of comet tail tilts. The comet's tails are actually the result of solar energy vaporizing particles from the comet's surface. Maxwell later postulated that an object can experience force from an electromagnetic field. In the 20th century, the radiation pressure force of photons was experimentally established following these predictions (Nichols and Hull, 1901; Lebedev, 1901). These were the first experimental indications of Maxwell's predicted radiation pressure force. It was necessary to thoroughly examine these trials in order to decipher the phenomenon from the radiative influence that had guided previous studies. The dual nature of the wave particle of black body radiation was revealed by Einstein in 1909 when he developed the statistics of fluctuations theory (Einstein, 1909). This theory included a radiation pressure fluctuation force acting on the movable mirror along with a radiation pressure frictional effect. Beth (Beth, 1936) and Frisch (Frisch, 1933) demonstrated the angular and linear momentum of photon transport to atoms and macroscopical objects in a different experiment.

Therefore, in a quantum context, radiation pressure can be intuitively understood in terms of photons. transferring their momentum to a surface (Gröblacher, 2012). As seen in Figure 3, one of the end-mirrors in a Fabry-Prot cavity is hung and can be thought of as a damped harmonic oscillator with a mass of m and a resonance frequency of ω_m. It is connected to the light inside the cavity by the radiation-pressure force and is susceptible to an external temperature bath. The following qualitative description can be used to characterize the interaction between the mechanical and optical systems: When light with a wave length of λ strikes a moving mirror, each photon imparts momentum of $2\hbar k$ to the mechanism, with the light's wave vector being $k = \frac{2\pi}{\lambda}$. The light force causes a slight displacement of the mirror, which alters the cavity's length and, in turn, the light field's phase.

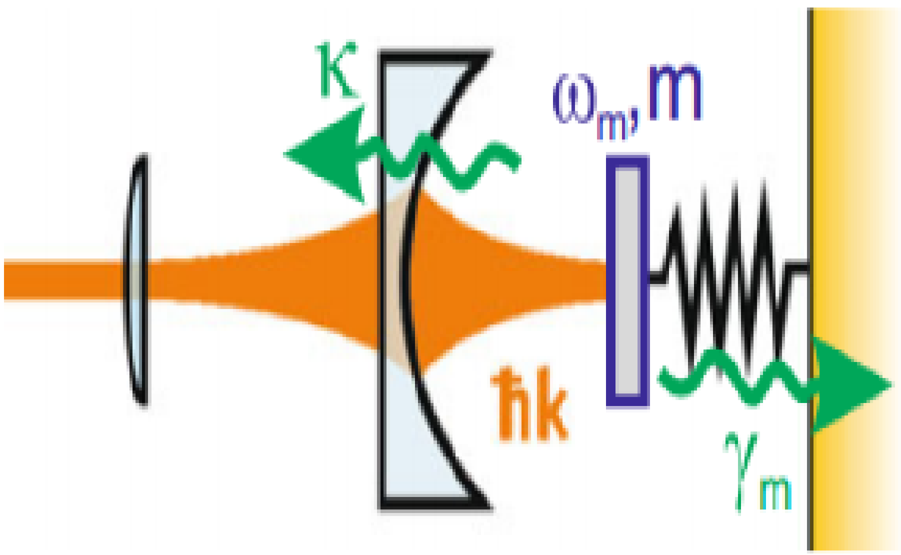

Figure 3: Description of radiation pressure interaction (Gröblacher, 2012)

Two complimentary modes exist in which matter and light interact. In optics, matter is an inert tool or expertise that is used to determine the direction in which photons propagate. When a photon travels through an optical system, it encounters several atoms, none of which significantly affect the photon's speed. However, the total effect can be rather large. In atom optics, light is a tool that can be used to accelerate, decelerate, cool, or deflect material particles. Since a significant number of photons are known to be present in the powerful laser fields, each photon interacts with the atom at least once, providing a tiny momentum boost. What occurs when the two kinematics of the light-matter interaction are considered, especially when light is simultaneously deflected significantly by matter and deflected by it? In this regime, which is also known as optomechanical coupling, light is used to transmit a mechanical connection between the material particles. The optomechanical interaction between the cavity mode and mirror, or the cavity field and atom, plays a crucial role. In addition to the optomechanical spring effect (Meystre et al., 1985; Sheard et al., 2004), optomechanical normal mode splitting (Dobrindt et al., 2008; Marquardt et al., 2007; Teufel et al., 2009; Huang and Agarwal, 2010), self-induced oscillation (Höhberger and Karrai, 2004; Carmon et al., 2005; Metzger et al., 2008),and optomechanically induced transparency (Safavi-Naeini et al., 2011; Agarwal and Huang, 2010; Lin et al., 2010; Schliesser and Kippenberg, 2014), the optomechanical coupling in such a system induces various nonlinear behaviors. Optomechanical connections can be classified into two main groups. These couplings are dispersive and dissipative, with different physical interpretations depending on the parameters. In the strong coupling regime, the mechanical response exhibits two discrete peaks separated by $2g$. This is an example of how a peak feature that split into two oscillator modes hybridized. In the case of a cavity mode driven by a laser, coherent excitation can also be exchanged between the laser-driven mode and the mechanical mode. Optomechanical coupling has also been accomplished using superconducting resonators (Regal et al., 2008) by injecting a nano-mechanical beam into a superconducting microwave cavity or by placing an aluminum membrane into a superconducting resonator. In contrast to the strong coupling regime, the situation is different in the weak coupling regime ($g < \kappa$). However, weak coupling is also a major topic in optomechanics research.

2.6. Correlated emission laser

The emission of light is attributed to multiple significant aspects, including the interaction of radiation with multi-level atoms and atomic coherence. Given this claim and with the intention of examining the non-classical aspects of the radiation arising from this interaction, we choose to focus on the cascade three-level scheme in the hopes that the methodology to be created can be easily transferred to other schemes. The scenario where the intermediate energy level is assumed to have a different parity from the upper and lower energy levels and, therefore, direct transition between the upper and lower energy levels is absolutely forbidden makes sense for understanding the cascading three-level atom. Keep in mind that the configuration that results when two photons of the same frequency are produced is known as degenerate. A three-level laser is a type of quantum optical device in which a single-port mirror connects a cavity containing three-level atoms to a vacuum reservoir to produce light. In one model of a three-level laser, three-level atoms initially prepared in a coherent superposition of the top and bottom levels are injected into a cavity and then removed from the cavity after they have decayed due to spontaneous emission (Scully and Zubairy, 1988). The squeezed-out light is caused by the superposition or connection of the top and bottom levels. The preparation of the atoms in a coherent superposition of the top and bottom levels prior to their injection into the cavity seems to be rather challenging. Furthermore, it ought to be difficult to discover that the atoms spontaneously disintegrated prior to being extracted from the hollow.

From a theoretical standpoint, within the framework of hybrid optomechanical systems aided by three-level atoms, the temperatures of $300K$, $4K$, and $100mK$ represent distinct thermal environment tiers: $300K$ (room temperature): This temperature corresponds to typical room conditions where the system is at thermal equilibrium with its surroundings. At this temperature, thermal effects are relatively strong, and quantum phenomena may be influenced by thermal fluctuations. $4K$ (pulse tube cryostat): This temperature represents a cryogenic environment achieved using a pulse tube cryostat. Cryogenic temperatures like 4K are often used in experiments to reduce thermal noise and enhance the coherence of quantum systems. It allows for better control over quantum effects and reduces the impact of thermal fluctuations on the system. $100mK$ (dilution refrigerator): This temperature indicates an even lower cryogenic level achieved with a dilution refrigerator. Dilution refrigerators can achieve temperatures close to absolute zero $(0K)$, providing an ultra-low temperature environment for studying quantum behavior with minimal thermal disturbances. At $100mK$, quantum effects dominate, and thermal noise is greatly suppressed, allowing for the observation of delicate quantum phenomena.

Our findgs specifically delves into the generation of stationary entanglement and quantum discord facilitated by three-level atoms within optomechanical systems operating under cryogenic conditions. Cryogenic temperatures typically span from millikelvins (mK) to a few kelvins (K) to facilitate and observe quantum phenomena effectively. These low temperatures are essential for inducing quantum behavior, manipulating entanglement, and observing coherent dynamics. This is evidence that cryogenic temperatures are often used in optomechanical systems to reduce thermal noise and achieve quantum effects. Hence, considering a temperature in the cryogenic range is typically required to achieve quantum effects, manipulate entanglement, and observe coherent behavior in such systems. Furthermore, as evidence, optomechanical experiments are conducted at temperatures in the cryogenic range to achieve ground state cooling and observe quantum behavior in the system. Consequently, under a cryogenic temperature range, the stability conditions of our system ensure it operates within a stable regime, effectively controlling quantum effects. Therefore, temperatures in this low range are typically required to observe and study quantum phenomena and correlation effects in cascaded three-level atoms coupled to an optomechanical cavity.

2.7. Hamiltonian formulation

A subharmonic generator has been considered a typical source of squeezed light. It is one of the most interesting and well-characterized optical devices in quantum optics. In quantum optics, subharmonic generation can be employed to create entangled photon pairs or to manipulate quantum states, facilitating experiments in quantum information processing. In this device, a pump photon interacts with a nonlinear crystal inside a cavity and is down-converted into two highly correlated photons. If these photons have the same frequency, the device is called a one-mode subharmonic generator; otherwise, it is called a two-mode subharmonic generator. However, in this dissertation, we consider only a one-mode subharmonic generator (degenerate subharmonic generation). In a degenerate subharmonic generating system, a pump photon of frequency 2ω is down converted into a pair of signal photons, each of frequency ω. With the pump mode treated classically, the process of degenerate subharmonic generation is described by the Hamiltonian (Kassahun, 2014).

$$\hat{H} = \frac{i\varepsilon}{2}(\hat{a}^2 - \hat{a}^{\dagger 2}), \tag{2.1}$$

where ε, considered to be real and constant, is proportional to the amplitude of the pump mode and $\hat{a}$ is the annihilation operator for the signal mode. We can see how to pump the OPA to produce a signal mode that generates squeezed light. This squeezed light is useful to entangle the state of the system. Consider three Hamiltonian of the systems: the free Hamiltonian of the optical and mechanical modes, which are represented by quantum harmonic oscillators ($\hat{H}_{free}$), the optomechanical interaction between the optical mode and the mechanical mode ($\hat{H}_{int.}$), and optical driving of the system, which is power pumped by the degenerate subharmonic generating system ($\hat{H}_{derive}$) illustrated at Eq. 2.1. Then the total Hamiltonian is given by

$$\hat{H} = \hat{H}_{free} + \hat{H}_{int} + \hat{H}_{derive}. \tag{2.2}$$

The first term $\hat{H}_{free}$ is described by

$$\hat{H}_{free} = \omega_c \hat{a}^\dagger \hat{a} + \omega_m \hat{b}^\dagger \hat{b}. \tag{2.3}$$

Here, both of the optical and mechanical modes are represented by quantum harmonic oscillators, where $\hat{a}(\hat{a}^\dagger)$ is the bosonic annihilation (creation) operator of the optical cavity mode, $\hat{b}(\hat{b}^\dagger)$ is the bosonic annihilation (creation) operator of the mechanical mode, and ω_c, ω_m are the corresponding angular resonance frequency. The commutation relations

satisfy $[\hat{a},\hat{a}^\dagger]=1$ and $[\hat{b},\hat{b}^\dagger]=1$.
The displacement operator of the mechanical mode is given by

$$x = x_{zf}(\hat{b}^\dagger + \hat{b}), \tag{2.4}$$

where x_{zf}= $\sqrt{\frac{\hbar}{(2m_{eff}w_m}})$ is the zero-point fluctuation, with m_{eff} being the effective mass of the mechanical mode.

The second term of Eq. 2.2 represents the optomechanical interaction between the optical mode and the mechanical mode, which is written as

$$\hat{H}_{int} = g\hat{a}^\dagger\hat{a}(\hat{b}^\dagger + \hat{b}), \tag{2.5}$$

where g = $[\partial\omega_c(x)/\partial x]x_{zf}$ represents the single-photon optomechanical coupling strength. This Hamiltonian can be obtained by simply considering that the cavity resonance frequency is modulated by the mechanical position and using Taylor expansion. $\omega_c(x) = \omega_c + x\partial\omega_c(x)/\partial x + \vartheta(x) \simeq \omega_c + g(\hat{b}^\dagger + \hat{b})$. Therefor, the total Hamiltonian derived from Eq. 2.1- 2.5 becomes

$$\hat{H} = \omega_c\hat{a}^\dagger\hat{a} + \omega_m\hat{b}^\dagger\hat{b} + g\hat{a}^\dagger\hat{a}(\hat{b}^\dagger + \hat{b}) + \frac{i\varepsilon}{2}(\hat{a}^2 - \hat{a}^{\dagger 2}). \tag{2.6}$$

Furthermore, we consider a generic cavity optomechanical system with a single optical cavity mode coupled to a mechanical mode, which is canonically modeled as a Fabry-P´erot cavity with one fixed mirror and one movable mirror attached on a spring (Liu et al., 2013). In the frame rotating at the input laser frequency ω_{in}, the system Hamiltonian is transformed to

$$\hat{H} = -\Delta\hat{a}^\dagger\hat{a} + \omega_m\hat{b}^\dagger\hat{b} + g\hat{a}^\dagger\hat{a}(\hat{b}^\dagger + \hat{b}) + (\Omega^*\hat{a} + \Omega\hat{a}^\dagger), \tag{2.7}$$

where $\Delta = \omega_{in} - \omega_c$ is the input-cavity detuning. Here, ω_{in} is the input laser frequency, and $\Omega = \sqrt{k_{ex}P/(\hbar\omega_{in})}e^{i\phi}$ denotes the driving strength, where P is the input laser power, ϕ is the initial phase of the input laser, and k_{ex} is the input cavity coupling rate.

Moreover, the effective cavity-atom coupling in a cascade configuration of three-level atoms using the Holstein-Primakoff (HP) approximation and Bra-ket notation (Holstein and Primakoff, 1940), can be obtained as follows: Start with the Hamiltonian that describes the interaction between the atoms and the cavity field. In the HP approximation, the Hamiltonian can be written as:

$$\hat{H} = \hat{H}_0 + \hat{H}_{int}, \tag{2.8}$$

where $\hat{H}_0$ is the free Hamiltonian of the system (without interaction) and $\hat{H}_{int}$ is the interaction Hamiltonian. The free Hamiltonian for a three-level system can be written as:

$$\hat{H}_0 = \hbar\omega_c\hat{a}^\dagger\hat{a} + \hbar\omega_a|a\rangle\langle a| + \hbar\omega_b|b\rangle\langle b| + \hbar\omega_c|c\rangle\langle c|, \tag{2.9}$$

where ω_c is the cavity frequency, ω_a and ω_b are the frequencies of levels $|a\rangle$ and $|b\rangle$, respectively. The interaction Hamiltonian can be written using the HP approximation, which involves expanding the atomic operators in terms of bosonic operators. For a cascade configuration with levels $|a\rangle$, $|b\rangle$, and $|c\rangle$, the interaction Hamiltonian can be written as:

$$\hat{H}_{int} = \hbar g_1(\hat{a}^\dagger \hat{\sigma}_{ab}^- + \hat{a}\hat{\sigma}_{ab}^+) + \hbar g_2(\hat{a}^\dagger \hat{\sigma}_{bc}^- + \hat{a}\hat{\sigma}_{bc}^+), \tag{2.10}$$

where g_1 and g_2 are the coupling constants for transitions $|a\rangle$ to $|b\rangle$ and $|b\rangle$ to $|c\rangle$, respectively. $\hat{\sigma}_{ij}^-$ and $\hat{\sigma}_{ij}^+$ are the lowering and raising operators for transitions between levels $|i\rangle$ and $|j\rangle$. In the HP approximation, we represent the atomic operators using bosonic operators as follows:

$$\hat{\sigma}_{ab}^- = \sqrt{N_a - \hat{a}^\dagger \hat{a}}.\hat{a}, \hat{\sigma}_{ab}^+ = \hat{a}^\dagger.\sqrt{N_a - \hat{a}^\dagger \hat{a}}, \tag{2.11}$$

$$\hat{\sigma}_{bc}^- = \sqrt{N_b - \hat{b}^\dagger \hat{b}}.\hat{b}, \hat{\sigma}_{bc}^+ = \hat{b}^\dagger.\sqrt{N_b - \hat{b}^\dagger \hat{b}}, \tag{2.12}$$

where N_a and N_b are the maximum occupation numbers for $|a\rangle$ and $|b\rangle$, respectively. After applying the HP approximation and simplifying the interaction Hamiltonian, the effective cavity-atom coupling for the cascade configuration can be expressed in terms of the bosonic operators $\hat{a}$ and $\hat{b}$ as:

$$\hat{H}_{eff} = \hbar g_{eff}(\hat{a}^\dagger \hat{b} + \hat{b}^\dagger), \tag{2.13}$$

where g_{eff} is the effective coupling constant given by:

$$g_{eff} = g_1\sqrt{N_a} + g_2\sqrt{N_b}. \tag{2.14}$$

This represents the effective interaction between the cavity field and the atoms in the cascade configuration of three-level atoms.

2.7.1 The Heisenberg equation

The Heisenberg approach is used to characterize the dynamics of system-reservoir interactions through the dynamics of the system operators, and the corresponding equations of motion are obtained by using the quantum mechanical average density matrix. Furthermore, for dissipative systems, the analog of the Heisenberg equations of motion are the quantum Langevin equations. More importantly, the Heisenberg-Langevin approach has attracted many applications and plays a crucial role in certain calculation benefits in the determination of phase diffusion coefficient and to calculate the laser linewidth (Scully and Zubairy, 1997). The quantum Langevin equation in optomechanics (Dodonov and

Dodonov, 2006) for any operator $\hat{z}$ can be written as

$$\frac{d\hat{z}}{dt} = \frac{-i}{\hbar}[\hat{z},\hat{H}] - \beta\hat{z} + \sqrt{2\beta}\hat{z}_{in}, \tag{2.15}$$

where $\hat{H}$ is the total Hamiltonian of the system. We discuss the general formulation of the quantum Langevin equation for a system (S) interacting with the environment (E), which is also called a " heat bath". The total Hamiltonian of the system is given by (Gardiner and Zoller, 2004).

$$\hat{H} = \hat{H}_s(\hat{Z}) + \sum_j \left\{ \frac{\hat{p}_j^2}{2m_j} + \frac{k_j}{2}(\hat{q}_j - \hat{X})^2 \right\}. \tag{2.16}$$

Here $\hat{X}$ and $\hat{p}$ represent the coordinate and momentum operators for the system $\hat{Z}$, and $\{\hat{q},\hat{p}\}$ describe the set of coordinate and momentum operators for the environment (reservoir). While k_j characterizes the coupling coefficients between the system and reservoir, the first term represents the system Hamiltonian; such a system could be a two-level atom or macroscopic LC circuit. The second term $\sum_j \left\{ \frac{\hat{p}_j^2}{2m_j} + \frac{k_j}{2}(\hat{q}_j - \hat{X})^2 \right\} \to \hat{H}_B$ describes the Hamiltonian of the heat bath, and the potential energy depends on the derivation of position $\hat{X}$ from all $\hat{q}_j$. The Hamiltonian of the whole system, which is the coupling between the system and the bath Eq. (2.16), can be simplified by the following transformation:

$$\begin{cases} \hat{q}_j \to \dfrac{\hat{p}_j}{k_j}, \\ \hat{p}_j \to -\hat{q}_j\sqrt{k_j}, \\ \dfrac{k_j}{m_j} \to \omega_j^2, \\ \sqrt{k_j} \to k_j, \end{cases} \tag{2.17}$$

and therefore, based on these transformations, the Hamiltonian Eq. (2.16) becomes

$$\hat{H}_s(Z) + \frac{1}{2}\sum_j \left\{ (\hat{p}_j - \kappa_j\hat{X})^2 + \omega_j^2\hat{q}_j^2 \right\}. \tag{2.18}$$

The above Hamiltonian and its operators satisfy the following commutation relations:

$$[\hat{Z},\hat{p}_j] = [\hat{Z},\hat{q}_j] = 0, \left[\hat{p}_i,\hat{p}_j\right] = \left[\hat{p}_j,\hat{p}_i\right] = 0, \left[\hat{p}_i,\hat{p}_j\right] = i\hbar\delta_{ij}. \tag{2.19}$$

To derive the Heisenberg-Langevin equations of motion, first solve the equation of motion for the harmonic oscillator in terms of variable $\hat{Z}$, and then substitute it into the evolution equation of $\hat{Z}$. Finally, we can determine the exact quantum Langevin equation for the system variable $\hat{Z}$. Therefore, the Heisenberg equation of motion for the harmonic oscillator variable is given by

$$
\begin{aligned}
\dot{\hat{q}}_j &= \frac{i}{\hbar}[\hat{H},\hat{q}_j] = \hat{q}_j - k_j\hat{X}, & (2.20)\\
\dot{\hat{p}}_j &= \frac{i}{\hbar}[\hat{H},p_j] = -\omega_n^2\hat{q}_j. & (2.21)
\end{aligned}
$$

Next, we introduce the creation and annihilation operators in the following forms:

$$
\begin{aligned}
\hat{a}_j &= \frac{\omega_j\hat{q}_j + i\hat{p}_j}{\sqrt{2\hbar\omega_j}},\\
\hat{a}_j^{\dagger} &= \frac{\omega_j\hat{q}_j - i\hat{p}_j}{\sqrt{2\hbar\omega_j}},
\end{aligned}
\tag{2.22}
$$

and using Eq. (2.19), we obtained the corresponding equations of motion.

$$
\hat{a}_j(t) = e^{-\omega_j(t-t_0)}\hat{a}_j(t_0) - \kappa_j\sqrt{\frac{\omega_j}{2\hbar}}\int_{t_0}^{t} e^{-\omega_j(t-t')}\hat{X}(t')dt', \tag{2.23}
$$

and similarly, we can also obtain the corresponding Hermitian conjugate equation for $\hat{a}_j^{\dagger}$. It is straightforward to extend the result of this equation of motion for any arbitrary system operator; $\hat{Y}$ can be simplified as

$$
\begin{aligned}
\dot{\hat{Y}} &= \frac{i}{\hbar}\left[\hat{H},\hat{Y}\right] - \frac{i}{\hbar}\left[\hat{H}_s,\hat{Y}\right] + \frac{i}{2\hbar}\sum_j\left[\left[[\hat{Y},\hat{p}_j - k_i\hat{X}\right]_+, k_j\hat{X}\right]\\
&= \frac{i}{\hbar}\left[\hat{H}_s,\hat{Y}\right] + \frac{i}{2\hbar}\sum_j\left[\left[\hat{Y},k_j\hat{X}\right],\hat{p}_j - k_j\hat{X}\right]. & (2.24)
\end{aligned}
$$

By substituting Eqs. (2.21) and (2.22) and after using the partial integration's, we obtained the simplified form of the quantum Langevin equations of motion.

$$
\begin{aligned}
\dot{\hat{Y}} &= \frac{i}{\hbar}\left[\hat{H}_s,\hat{Y}\right] - \frac{i}{2\hbar}\left[X,\left[\hat{Y},\xi(t) - \int_{t_0}^{t} f(t-\acute{t})\dot{\hat{X}}(\acute{t})\,d\acute{t} - f(t-t_0)\hat{X}(t_0)\right]\right]\\
&= \frac{i}{\hbar}\left[\hat{H}_s,\hat{Y}\right] - \frac{i}{2\hbar}\left[\left[\hat{X},\hat{Y}\right],\xi(t) - \int_{t_0}^{t} f(t-\acute{t})\dot{\hat{X}}(\acute{t})\,d\acute{t} - f(t-t_0)\hat{X}(t_0)\right], & (2.25)
\end{aligned}
$$

where

$$
\begin{aligned}
\xi(t) &= i\sum_j k_j\sqrt{\frac{\hbar\omega_j}{2}}\left[-\hat{a}_j(t_0)e^{-i\omega_j(t-t_0)} + \hat{a}_j^{\dagger}(t_0)e^{i\omega_j(t-t_0)}\right],\\
f(t) &= \sum_j \kappa_j^2\cos\left(\omega_j t\right). & (2.26)
\end{aligned}
$$

The above Eq. (2.25) represents the fully quantum Langevin equation. Moreover, from a fundamental physics perspective, it is a very useful equation in optomechanical point of view and most widely used to characterize the time evolution of the system, damping, and noise terms of the optomechanical system (Aspelmeyer et al., 2014; Gebremariam et al., 2017).

2.7.2 Input-Output formulation

To illustrate the formulation of input-output, we consider a system of single cavity mode interacting with an external field. The total system Hamiltonian is given by (Walls and Milburn, 2008).

$$\hat{H} = \hbar\omega_c \hat{a}^\dagger \hat{a} + \hbar\omega_m \int_0^\infty \hat{b}^\dagger(\omega)\hat{b}(\omega)\,d\omega + i\hbar \int_0^\infty g(\omega)\left(\hat{b}(\omega)\hat{a}^\dagger - \hat{a}\hat{b}^\dagger(\omega)\right)d\omega, \tag{2.27}$$

where the first term represents the single cavity mode with frequency ω_c, the second term characterizes the external (electromagnetic) mode, and the last term is the interaction between a system of the single cavity mode and heat bath, respectively. $g(\omega)$ characterizes the coupling strength between the modes. While $\hat{a}$ is the annihilation operator for the intra-cavity field, with the commutation relations $[\hat{a}, \hat{a}^\dagger] = 1$, and $\hat{b}(\omega)$ are the annihilation operators for the external field, with $[\hat{b}(\omega), \hat{b}^\dagger(\omega')] = \delta(\omega - \omega')$ (Walls and Milburn, 2008). In the Heisenberg equation of motion for cavity and external mode, we have

$$\dot{\hat{a}}(\omega) = -i\omega_c \hat{a} - \int_{-\infty}^{\infty} d\omega g(\omega)\hat{a}(\omega), \tag{2.28a}$$

$$\dot{\hat{b}}(\omega) = -i\omega\hat{b}(\omega) + g(\omega)\hat{a}. \tag{2.28b}$$

By using the initial condition time $t_0 < t$, we obtained

$$\hat{b}(\omega) = e^{-i\omega(t-t_0)}\hat{b}_0(\omega) - g(\omega)\int_t^{t_0} dt' e^{-i\omega(t-t')}\hat{a}(t'), \tag{2.29}$$

and in a similar manner, we can substitute the final condition time $t < t_1$, and we have

$$\hat{b}(\omega) = e^{-i\omega(t-t_1)}\hat{b}_1(\omega) - g(\omega)\int_t^{t_1} dt' e^{-i\omega(t-t')}\hat{a}(t'). \tag{2.30}$$

From the above Eqs. (2.29) and (2.30), $\hat{b}_0(\omega)$ is the value of $\hat{b}(\omega)$ at $t = t_0$, and $\hat{b}_1(\omega)$ is the value of $\hat{b}(\omega)$ at $t = t_1$. Thus, the time evolution of the cavity field in terms of the solution with initial conditions Eq. (2.28a) becomes

$$\dot{\hat{a}} = -i\omega_c\hat{a} - \int_{-\infty}^{\infty} g(\omega)e^{-i\omega(t-t_0)}b_0(\omega)d\omega - \int_{-\infty}^{\infty} d\omega g^2(\omega)\int_{t_0}^{t} e^{-i\omega(t-t')}\hat{a}(t')dt'. \tag{2.31}$$

We now assume that $g(\omega)$ is independent of frequency, then we substitute $g^2(\omega) \Rightarrow \sqrt{\frac{\kappa}{2\pi}}$; this is known as the first Markov approximation process. Accordingly, we introduce the input and output field formulation operators.

$$\hat{a}_{IN}(t) = \frac{1}{2\pi}\int_{-\infty}^{\infty} d\omega e^{-i\omega(t-t_0)}\hat{b}_0(\omega), \tag{2.32}$$

$$\hat{a}_{Out}(t) = \frac{1}{2\pi}\int_{-\infty}^{\infty} d\omega e^{-i\omega(t-t_1)}\hat{b}_1(\omega), \tag{2.33}$$

where these operators satisfy the commutation relations. $[\hat{a}_{IN}(t), \hat{a}_{IN}(t)] = [\hat{a}_{Out}(t), \hat{a}_{Out}(t)] = \delta(t-t')$. Finally, using the above equation (2.33), we can formulate the input and output relations.

$$\hat{a}_{IN}(t) + \hat{a}_{Out}(t) = \sqrt{\kappa}\hat{a}(t). \tag{2.34}$$

The above equation of Eq. (2.34) characterizes the boundary condition relating each of the far field amplitudes outside the cavity to the corresponding internal cavity field, and the interference terms between the input and the cavity field may contribute to the observed moments when measurements are made on $\hat{a}_{Out}$.

Note that the quantum Langevin equations used to describe the full dynamics of the system, including the fluctuation and dissipation terms affecting the optomecanical system, interact with the environment. It interacts in the external environment with corresponding decay or damping rate β and input noise Z_{in}, respectively.

2.7.3 The linearization approximation approach

The quantum dynamics of the full non-linear system are difficult to analyze. So we linearize the dynamics of the quantum fluctuations around the semi-classical fixed points where the cavity is intensely driven under a strong field (Genes et al., 2009a). We expand each Heisenberg operator as a sum of its semi-classical steady-state value plus quantum fluctuation for any relevant operators. The general form of linearization approach for any operator α is given by

$$\alpha = \alpha_s + \delta\alpha, \tag{2.35}$$

where α is an operator and α_s is a real number denoting the optical, microwave, and mechanical amplitudes, and $\delta\alpha$ is the quantum fluctuation operator.

2.7.4 Entanglement via Logarithmic negativity

In quantum information processing schemes that involve two sites, entanglement between more than two quantum states has the potential to be a valuable resource. This can be extended to an arbitrary number of parties sharing a multipartite entanglement. These days, it is also widely acknowledged that the high practical realization efficiency of continuous variable quantum entanglement is one of its most valuable characteristics. For instance, quantum error correction, entanglement swapping, unconditional quantum teleportation, and universal quantum computation have all successfully used continuous variable entangled states.

In quantum information processing and quantum communications, transferring quantum states between two distant parties is a significant and fulfilling task. A number of schemes utilizing cavity quantum electrodynamics have been proposed (Kraus and Cirac, 2004; Li and Paraoanu, 2009). Recently, there has been interest in quantum state transfer in quantum optomechanics, where mechanical modes are connected to the optical modes through radiation pressure (Tian and Wang, 2010; Wang and Clerk, 2012; Tian, 2012; Singh et al., 2012; McGee et al., 2013; Palomaki et al., 2013). In quantum information processing, in particular, entanglement transmission between two spatially separated cavities is attractive. Entangling an optical ring cavity's two movable mirrors (Mancini et al., 2002), entangling two mirrors of two different cavities illuminated by entangled light beams (Zhang et al., 2003), and entangling two mirrors of a double-cavity setup coupled to two independent squeezed vacuums (Pinard et al., 2005) have been considered.

It is also possible to argue that several sufficient inseparability criteria for a composite state can be proposed for a continuous variable system. One such possibility is logarithmic negativity. Logarithmic negativity is the most popular tool to measure the degree of the entanglement between two systems of any size. Researchers use this tool to compute the entanglement of mixed states to investigate their distribution in space, to capture quantum correlation, and to quantify the continuous-variable Gaussian-type bipartite state because it is the only one that can always be explicitly computed, and it is also additive (Lee and Vidal, 2013). Therefore, we use this tool to study the two possible bipartite entanglements generated by the interaction between two optical cavities and the optical cavity, the mechanical resonator of the subsystem. The generated CV bipartite entanglement measure in terms of logarithmic negativity E_N (Vidal and Werner, 2002) defined as E_N

$$E_N = max[0, -\ln 2\bar{\eta}], \tag{2.36}$$

where $\bar{\eta}$ is the symplectic eigenvalue of the bipartite system and it is given by the equation.

$$\bar{\eta} \equiv 2^{\frac{-1}{2}}[\sum(V) - \sqrt{\sum(V)^2 - 4detV}]^{\frac{1}{2}}, \tag{2.37}$$

where

$$\sum(V) = \begin{pmatrix} V_A & V_C \\ V_C^T & V_B \end{pmatrix} \tag{2.38}$$

and $\sum(V) \equiv detV_A + detV_B - 2detV_C$, where V_A, V_B, and V_C are 2 x 2 block matrices.

2.7.5 Gaussian quantum discord

It is thought that a good indicator of the quantum nature of the correlations is quantum discord. Even so, there is no such direct criterion to confirm the existence of discord for a given quantum state because optimization of the conditional entropy is necessary because of the involved local measurement process. This is true even though there is growing evidence for the relevance of quantum discord in characterizing non-classical resources in information processing. Fortunately, a closed analytical relation that can be used to quantify the quantum discord for the two-mode Gaussian states can be outlined under restricted Gaussian measurements.

There is just one approximation to the quantum discord for continuous variable systems, known as Gaussian quantum discord, created by (Adesso and Datta, 2010) and simultaneously by (Giorda and Paris, 2010). The primary limitation of this approximation is that it is limited to the set of Gaussian measurements for the optimization over all measurements over a single mode. Because of this, the unrestricted quantum discord can only be approximated by the Gaussian quantum discord (with the exception of a family of states for which Gaussian measurements are known to be ideal).

Quantum discord has been the subject of numerous recent studies in a variety of optomechanical systems (Chakraborty and Sarma, ; Amazioug et al., 2018). When compared to optomechanical entanglement in the presence of cross-Kerr nonlinearity or in two spatially separated Fabry-Perot cavities, the *GQD* is more resilient and can withstand high thermal bath temperatures.

It has already been observed that the increase of squeeze parameter in an optomechanical system with two spatially separated Fabry-P´erot enhances the *GQD* but it decreases with the increase of thermal effects (Amazioug et al., 2020b), whereas purity and quantum discord remain nonzero when entanglement between the mechanical modes and optical modes vanishes under thermal effect (Amazioug et al., 2020a). It is well known that even some separable states contain nonclassical correlations (Henderson and Vedral, 2001; Ollivier and Zurek, 2001) where the "nonclassicality" of bipartite correlations can be measured via quantum discord, which was first introduced as a measure of all quantum correlations in a bipartite state, including entanglement. The quantum correlation quantifier is a fundamental notion allowing for the description of the quantumness of the correlations present in the state of a quantum system. In our case, the Gaussian quantum discord denotes non-classical correlations if the two distant cavity fields, a mirror and a distant cavity field, and two distant mirrors are separable or not.

To study the quantum correlation properties of the hybrid system, utilize the linearization of quantum fluctuation and rewrite the compact matrix. Specifically, in this section, we will measure the quantum correlation between the subsystems. In this sense, we will quantify the bipartite correlations among the possible subsystems. In this manner, we will measure the correlations between the subsystems through the quantum quantifier of quantum discord. Specifically, Gaussian quantum discord provides a means to identify and quantify whether non-classical correlations between various modes, such as optical-to-mechanical, are separable or not. We can define the two-mode Gaussian state covariance matrix (Giorda and Paris, 2010) as

$$C = \begin{pmatrix} A & D \\ D^T & B \end{pmatrix}, \tag{2.39}$$

where A, B, and D are 2×2 matrices, one can define four local symplectic invariants: $Z_1 = detA, Z_2 = detB, Z_3 = detD, Z_4 = detC$. In the case of continuous variables and Gaussian states, in terms of those sympathetic invariants, specifically, we can define the Gaussian quantum discord for the optical mode as follows:

$$GQD_A = f\left(\sqrt{detB}\right) - f(\sqrt{\Theta_+}) - f(\sqrt{\Theta_-}) + f(\eta), \tag{2.40}$$

the symplectic eigenvalues given by

$$\Theta \pm = \frac{\sqrt{Z_\upsilon \pm \sqrt{Z_\upsilon^2 - 4Z_4}}}{\sqrt{2}}, \tag{2.41}$$

where $Z_\upsilon = Z_1 + Z_2 + 2I_3$ and η is defined by

$$\eta = \frac{\sqrt{\det A + 2\sqrt{\det A \det B} + 2I_3}}{1 + 2\sqrt{\det B}}, \tag{2.42}$$

where I_3 is 2×2 identity matrix, represents the vacuum noise contribution on each mode. Similarly, we can determine the quantum discord for the mechanical mode as follows:

$$GQD_B = f\left(\sqrt{detA}\right) - f(\sqrt{\Theta_+}) - f(\sqrt{\Theta_-}) + f(\eta'), \tag{2.43}$$

where

$$\eta' = \frac{\sqrt{\det B + 2\sqrt{\det A \det B} + 2I_3}}{1 + 2\sqrt{\det A}}, \tag{2.44}$$

where the function f defined by

$$f(x) = \left(x+\frac{1}{2}\right)\ln\left(x+\frac{1}{2}\right) - \left(x-\frac{1}{2}\right)\ln\left(x-\frac{1}{2}\right). \tag{2.45}$$

The quantum states of the mechanical and optical modes are said to be entangled when the Gaussian quantum discord in Eqs. (2.40) and (2.43) satisfies $GQD_A > 1 : GQD_B > 1$. Moreover, if the condition $0 \leq GQD_A \leq 1 : 0 \leq GQD_B \leq 1$ is satisfied, the mechanical mode and optical mode can be in an entangled state or not. Note that; the Gaussian discord can be non-zero even when a state is not entangled. Specifically, for certain mixed states, particularly those that are separable (non-entangled), Gaussian discord can still manifest. For $GQD_A = 0$ the subsystem A has no quantum correlations beyond classical correlations. In practical terms, this means that the state of the system is either completely separable or can be described purely classically. There is no quantum advantage to be gained from measuring or manipulating the subsystem A. On the other hand, $0 < GQD_A < 1$ values in this range signify the presence of quantum correlations in subsystem A. The closer the value is to 1, the stronger the non-classical correlations are. This suggests that subsystem A possesses some degree of entanglement or other quantum effects that can be utilized for tasks like quantum communication or computation. Similarly, $GQD_A = 1$ represents a theoretical upper bound of Gaussian quantum discord. While not all systems can reach this value, achieving $GQD_A = 1$ implies that the quantum correlations in subsystem A are maximal, indicating a fully non-classical state that can harness the full power of quantum phenomena.

2.7.6 Gaussian Steering

Steering is a form of quantum correlation that exhibits a fundamental asymmetry in the properties of quantum systems. Quantum correlation refers to the correlations between subsystems of a composite quantum system, including Bell nonlocality, steerability, quantum entanglement, and quantum discord. Conversely, the (He and Ficek, 2014) proposal about the quantification and measure of the Gaussian steering quantifier for CV systems is relatively new. As noted by (Bennett et al., 2011), a measure of steering quantifies the amount of correlations in a given state. In this case, a measure of the degree of steerability is obtained by evaluating the maximum violation of a selected steering criterion as revealed by optimal measurements. This is a manifestation of these correlations that can be observed by the violation of appropriate EPR-steering criteria. One anticipates that the state will be more helpful in tasks and a focus of focused research using quantum steering as a resource, the higher the violation (i.e., number of correlations) (Reid et al., 2009). By observing these correlations as a breach of suitable EPR-steering criteria, the degree of steerability can be quantitatively estimated. To do this, the maximum violation of a certain steering criterion as revealed by optimal measurements is evaluated. Said another way, let's say Alice tries to persuade Bob, who doesn't trust her, that she is in a tangled relationship with him. Assume Bob asks Alice to remotely prepare a set of states for his subsystems in order for Alice to be persuaded. Imagine that Alice took the required measurements without Bob knowing about them and informed him of the outcome. It is interesting to note that Bob can certify using the idea of quantum steering whether or not the measurements originate from an entangled state, given the nature of quantum measurement and an examination of Alice's prepared conditional states. To achieve steerability, A and B might switch roles. For the time being, it is noteworthy that the quantum steering observed in this form is associated with bipartite entanglement, which is measurable by quantum discord and logarithmic negativity. The ability to change the state of the remote system without necessarily interacting with it is represented by the higher degree of steerability, which could be useful for reliably teleporting quantum information. It is also a measure of the asymmetry between two subsystems' entangled observers. It also offers a means of measuring the degree of steerability that each of the two independent modes possesses. The steerability of $A \to B$ is defined as (Kogias et al., 2015) if we utilize the covariance matrix of mechanical oscillators to examine the information flow between Alice A and Bob B.

$$S^{A\to B} = max\left[0, \frac{1}{2} ln(\frac{\det \mathbf{A}}{4 \det \mathbf{C}})\right]. \tag{2.46}$$

The corresponding measure of the Gaussian steerability $B \to A$ can be found by

$$S^{B\to A} = max\left[0, \frac{1}{2} ln(\frac{\det \mathbf{B}}{4 \det \mathbf{C}})\right]. \tag{2.47}$$

As can be seen from the above, there are two possible scenarios for quantum steering between A and B: two-way steering if $S^{A\to B} = S^{B\to A} > 0$, and no-way steering, in which Alice cannot steer Bob and vice versa even in cases where they are not separable. Actually, a steerable state is always not separable, whereas a non-separable state is not necessarily a steerable state. If the two matrices involved in a steerability analysis are singular, it indicates that the matrices do not have full rank, which can affect the evaluation of quantum steering.

3. MATERIALS AND METHODS

3.1. Materials

The system under discussion consists of OPA inserted into a hybrid optomechanical system's cavities and externally coupled through the cavity-cavity coupling parameter. Additionally, three-level atoms are injected into an optomechanical system's cavity in a cascade configuration by an externally powered laser aimed at the OPA and atoms.

3.2. Methods

In this section, we formulate a model of the system under study, utilizing the system's quantum Hamiltonian, and solving the system's quantum Langevin equations are the techniques to be employed in this investigation. Determine steady-state values and linearized QLE using these findings. A drift matrix was developed following the linearization of the quantum Langevin equations. Then, we obtain logarithmic negativity by utilizing the acquired drift matrix. We discussed the created steady-state bipartite entanglement feature between subsystems in this regard. In particular, we looked at how generated bipartite entanglement in the subsystems was affected by OPA and three-level atoms. Moreover, Gaussian quantum discord and Gaussian steering quantify quantum correlations. Additionally, we discussed the quantum correlation strength among subsystems using the cavity-cavity parameter.

3.3. Steady-state entanglement in a hybrid optomechanical system enhanced by optical parametric amplifiers

3.3.1 Model and Hamiltonian of the system

The optomechanical cavities in the system model depicted in Figure 4 have two fixed cavity mirrors and two moving mirrors. The cavity contents of each optomechanical cavity are OPA, effective mass m, and frequency ω_{mj}. It is believed that every cavity mode is powered by a laser, which communicates with the movable mirror through radiation pressure. The coupling parameter of the physical system connecting the optomechanical oscillators is denoted by J (Kibret et al., 2023).

The total Hamiltonian that characterizes the system reads

$$\hat{H} = \sum_{j=1}^{2}\Big(\hbar\omega_{cj}\hat{a}_j^\dagger\hat{a}_j + \hbar G_{mj}\hat{a}_j^\dagger\hat{a}_j\hat{q}_j + \frac{1}{2}\hbar\omega_{mj}(\hat{q}_j^2+\hat{p}_j^2)$$
$$+ i\hbar E_j(\hat{a}_j^\dagger e^{-i\omega_{0j}t} - \hat{a}_j e^{i\omega_{0j}t}) + i\hbar\Omega(e^{i\theta}\hat{a}_j^{\dagger 2}e^{-i\omega_{0j}t} - e^{-i\theta}\hat{a}_j^2 e^{i\omega_{0j}t})\Big)$$
$$+ \hbar J(\hat{a}_1^\dagger\hat{a}_2 + \hat{a}_2^\dagger\hat{a}_1), \tag{3.1}$$

where the first term describes the sum of the energy corresponding to the optical cavity modes with photon operators $\hat{a}_j$ or $\hat{a}_j^\dagger$ and frequency ω_{cj}, While the second term denotes the radiation pressure with the rate G_{mj}, the third term is the energy of the mechanical oscillator with the position and momentum operators $\hat{q}_j$ and $\hat{p}_j$, the fourth term stands for driving field, the fifth term denotes the coupling between the OPA and the two cavity modes, Ω is the nonlinear gain of the OPA and θ is the phase of the optical field driving the OPA. We have assumed the nonlinear gain Ω and the phase θ to be similar for the two independent nonlinear processes, and the last term to describe the coupling between the two cavity modes $\hat{a}_1$ and $\hat{a}_2$, with a cavity-cavity coupling term of intensity J. The Hamiltonian of the whole

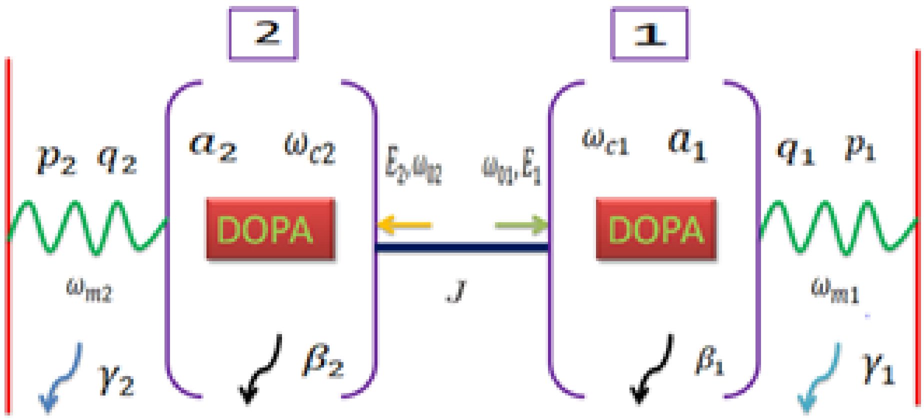

Figure 4: The schematic model of a hybrid optomechanical system is under consideration. Thus, the separate cavities with a degenerate optical parametric amplifier (OPA) are externally coupled, with J being the coupling parameter, β_j being the cavity decay rate, γ_j as the mechanical damping rate, ω_j as the frequency of the mechanical oscillator, and the other symbols defined in the main text.

system is written as follows after a frame rotates:

$$\hat{H} = \sum_{j=1}^{2}\Big(\hbar\triangle_j\hat{a}_j^\dagger\hat{a}_j + \hbar G_{mj}\hat{a}_j^\dagger\hat{a}_j\hat{q}_j + \frac{1}{2}\hbar\omega_{mj}(\hat{q}_j^2+\hat{p}_j^2) + i\hbar E_j(\hat{a}_j^\dagger - \hat{a}_j)$$
$$+ i\hbar\Omega(e^{i\theta}\hat{a}_j^{\dagger 2} - e^{-i\theta}\hat{a}_j^2)\Big) + \hbar J(\hat{a}_1^\dagger\hat{a}_2 + \hat{a}_2^\dagger\hat{a}_1), \tag{3.2}$$

where $\triangle_j = \omega_{cj} - \omega_{0j}$ is the optical detuning, $|E_j|$ is the driving amplitude related to driving power P, and the cavity decay rate β_j by $|E_j| = \sqrt{2P_{j\beta}/\hbar\omega_{0j}}$ in which $\beta_1 = \beta_2 = \beta = \pi c/2FL$ and F is the cavity finesse and c is the speed of light. The driving amplitude can refer to the amplitude of an external force or signal applied to a system, influencing its behavior. In addition, $G_{mj} = (\omega_{cj}/L)\sqrt{\hbar/m\omega_{mj}}$ is the single-photon optomechanical coupling associated with the cavity mode with frequency ω_{cj}, where L is the cavity length and m is the effective mass.

3.3.2 Dynamics of the system

The dynamics of the system are obtained from quantum Langevin equations. Starting from the Hamiltonian Eq. (3.2), we see that

$$\begin{aligned}\hat{H} &= \hbar\triangle_1 \hat{a}_1^\dagger\hat{a}_1 + \hbar\triangle_2 \hat{a}_2^\dagger\hat{a}_2 + \hbar G m_1 \hat{a}_1^\dagger\hat{a}_1\hat{q}_1 + \hbar G m_2 \hat{a}_2^\dagger\hat{a}_2\hat{q}_2 + \frac{1}{2}\hbar\omega_{m1}(\hat{q}_1^2 + \hat{p}_1^2) \\ &+ \frac{1}{2}\hbar\omega_{m2}(\hat{q}_2^2 + \hat{p}_2^2) + i\hbar E_1(\hat{a}_1^\dagger - \hat{a}_1) + i\hbar E_2(\hat{a}_2^\dagger - \hat{a}_2) + \hbar J(\hat{a}_1^\dagger\hat{a}_2 + \hat{a}_2^\dagger\hat{a}_1) \\ &+ i\hbar\Omega(e^{i\theta}\hat{a}^{\dagger 2}_1 - e^{-i\theta}\hat{a}_1^2) + i\hbar\Omega(e^{i\theta}\hat{a}^{\dagger 2}_2 - e^{-i\theta}\hat{a}_2^2).\end{aligned} \tag{3.3}$$

Employing Eqs. (2.15) and (3.3) together, that means

$$\frac{d\hat{q}_1}{dt} = -i/\hbar[\hat{q}_1, \hat{H}], \tag{3.4}$$

$$\begin{aligned}\dot{\hat{q}}_1 = -i\Big(&\triangle_1 [\hat{q}_1, \hat{a}_1^\dagger\hat{a}_1] + \triangle_2[\hat{q}_1, \hat{a}_2^\dagger\hat{a}_2] + G m_1 \hat{a}_1^\dagger\hat{a}_1[\hat{q}_1, \hat{q}_1] + G m_2 \hat{a}_2^\dagger\hat{a}_2[\hat{q}_1, \hat{q}_2] \\ &+ \frac{1}{2}\omega_{m1}[\hat{q}_1, \hat{q}_1^2 + \hat{p}_1^2] + \frac{1}{2}\omega_{m2}[\hat{q}_1, \hat{q}_2^2 + \hat{p}_2^2] + iE_1[\hat{q}_1, \hat{a}_1^\dagger - \hat{a}_1] + iE_2[\hat{q}_1, \hat{a}_2^\dagger - \hat{a}_2] \\ &+ J[\hat{q}_1, \hat{a}_1^\dagger\hat{a}_2] + J[\hat{q}_1, \hat{a}_2^\dagger\hat{a}_1] + i\Omega e^{i\theta}[\hat{q}_1, \hat{a}^{\dagger 2}_1] - i\Omega e^{-i\theta}[\hat{q}_1, \hat{a}_1^2] \\ &+ i\Omega e^{i\theta}[\hat{q}_1, \hat{a}^{\dagger 2}_2] - i\Omega e^{-i\theta}[\hat{q}_1, \hat{a}_2^2]\Big),\end{aligned} \tag{3.5}$$

$$\dot{\hat{q}}_1 = \omega_{m1}\hat{p}_1. \tag{3.6}$$

Similarly,

$$\dot{\hat{q}}_2 = \omega_{m2}\hat{p}_2. \tag{3.7}$$

In the same procedure we employ for

$$\frac{d\hat{p}_1}{dt} = -i/\hbar[\hat{p}_1, \hat{H}] - \gamma_1\hat{p}_1 + \xi_1, \tag{3.8}$$

$$\begin{aligned}\dot{\hat{p}}_1 = -i\Big(& \triangle_1 [\hat{p}_1, \hat{a}_1^\dagger \hat{a}_1] + \triangle_2 [\hat{p}_1, \hat{a}_2^\dagger \hat{a}_2] + Gm_1 \hat{a}_1^\dagger \hat{a}_1 [\hat{p}_1, \hat{q}_1] + Gm_2 \hat{a}_2^\dagger \hat{a}_2 [\hat{p}_1, \hat{q}_2] \\ & + \frac{1}{2}\omega_{m1} [\hat{p}_1, \hat{q}_1^2 + \hat{p}_1^2] + \frac{1}{2}\omega_{m2} [\hat{p}_1, \hat{q}_2^2 + \hat{p}_2^2] + iE_1 [\hat{p}_1, \hat{a}_1^\dagger - \hat{a}_1] + iE_2 [\hat{p}_1, \hat{a}_2^\dagger - \hat{a}_2] \\ & + J[\hat{p}_1, \hat{a}_1^\dagger \hat{a}_2] + J[\hat{p}_1, \hat{a}_2^\dagger \hat{a}_1] + i\Omega e^{i\theta} [\hat{p}_1, \hat{a}^{\dagger 2}_1] - i\Omega e^{-i\theta} [\hat{p}_1, \hat{a}_1^2] + i\Omega e^{i\theta} [\hat{p}_1, \hat{a}^{\dagger 2}_2] \\ & - i\Omega e^{-i\theta} [\hat{p}_1, \hat{a}_2^2] \Big) - \gamma_1 \hat{p}_1 + \xi_1, \end{aligned} \tag{3.9}$$

$$\dot{\hat{p}}_1 = -Gm_1 \hat{a}_1^\dagger \hat{a}_1 - \omega_{m1} \hat{q}_1 - \gamma_1 \hat{p}_1 + \xi_1. \tag{3.10}$$

Similarly

$$\frac{d\hat{p}_2}{dt} = -i/\hbar [\hat{p}_2, \hat{H}] - \gamma_2 \hat{p}_2 + \xi_2, \tag{3.11}$$

$$\begin{aligned}\dot{\hat{p}}_2 = -i\Big(& \triangle_1 [\hat{p}_2, \hat{a}_1^\dagger \hat{a}_1] + \triangle_2 [\hat{p}_2, \hat{a}_2^\dagger \hat{a}_2] + Gm_1 \hat{a}_1^\dagger \hat{a}_1 [\hat{p}_2, \hat{q}_1] + Gm_2 \hat{a}_2^\dagger \hat{a}_2 [\hat{p}_2, \hat{q}_2] \\ & + \frac{1}{2}\omega_{m1} [\hat{p}_2, \hat{q}_1^2 + \hat{p}_1^2] + \frac{1}{2}\omega_{m2} [\hat{p}_2, \hat{q}_2^2 + \hat{p}_2^2] + iE_1 [\hat{p}_2, \hat{a}_1^\dagger - \hat{a}_1] + iE_2 [\hat{p}_2, \hat{a}_2^\dagger - \hat{a}_2] \\ & + J[\hat{p}_2, \hat{a}_1^\dagger \hat{a}_2] + J[\hat{p}_2, \hat{a}_2^\dagger \hat{a}_1] + i\Omega e^{i\theta} [\hat{p}_2, \hat{a}^{\dagger 2}_1] - i\Omega e^{-i\theta} [\hat{p}_2, \hat{a}_1^2] + i\Omega e^{i\theta} [\hat{p}_2, \hat{a}^{\dagger 2}_2] \\ & - i\Omega e^{-i\theta} [\hat{p}_2, \hat{a}_2^2] \Big) - \gamma_2 \hat{p}_2 + \xi_2, \end{aligned} \tag{3.12}$$

$$\dot{\hat{p}}_2 = -Gm_2 \hat{a}_2^\dagger \hat{a}_2 - \omega_{m2} \hat{q}_2 - \gamma_2 \hat{p}_2 + \xi_2. \tag{3.13}$$

In the same procedure we can find

$$\frac{d\hat{a}_1}{dt} = -i/\hbar [\hat{a}_1, \hat{H}] - \beta_1 \hat{a}_1 + \sqrt{2\beta_1} \hat{a}_1^{in}, \tag{3.14}$$

$$\begin{aligned}\dot{\hat{a}}_1 = -i\Big(& \triangle_1 [\hat{a}_1, \hat{a}_1^\dagger \hat{a}_1] + \triangle_2 [\hat{a}_1, \hat{a}_2^\dagger \hat{a}_2] + Gm_1 \hat{a}_1^\dagger \hat{a}_1 [\hat{a}_1, \hat{q}_1] + Gm_2 \hat{a}_2^\dagger \hat{a}_2 [\hat{a}_1, \hat{q}_2] \\ & + \frac{1}{2}\omega_{m1} [\hat{a}_1, \hat{q}_1^2 + \hat{p}_1^2] + \frac{1}{2}\omega_{m2} [\hat{a}_1, \hat{q}_2^2 + \hat{p}_2^2] + iE_1 [\hat{a}_1, \hat{a}_1^\dagger - \hat{a}_1] + iE_2 [\hat{a}_1, \hat{a}_2^\dagger - \hat{a}_2] \\ & + J[\hat{a}_1, \hat{a}_1^\dagger \hat{a}_2] + J[\hat{a}_1, \hat{a}_2^\dagger \hat{a}_1] + i\Omega e^{i\theta} [\hat{a}_1, \hat{a}^{\dagger 2}_1] - i\Omega e^{-i\theta} [\hat{a}_1, \hat{a}_1^2] + i\Omega e^{i\theta} [\hat{a}_1, \hat{a}^{\dagger 2}_2] \\ & - i\Omega e^{-i\theta} [\hat{a}_1, \hat{a}_2^2] \Big), \end{aligned} \tag{3.15}$$

$$\dot{\hat{a}}_1 = -(i\triangle_1 + \beta_1)\hat{a}_1 - iGm_1 \hat{q}_1 \hat{a}_1 + E_1 - iJ\hat{a}_2 + 2\Omega e^{i\theta} \hat{a}_1^\dagger + \sqrt{2\beta_1} \hat{a}_1^{in}, \tag{3.16}$$

Similarly

$$\frac{d\hat{a}_2}{dt} = -i/\hbar[\hat{a}_2, \hat{H}] - \beta_2\hat{a}_2 + \sqrt{2\beta_2}\hat{a}_2^{in}, \tag{3.17}$$

$$\begin{aligned}
\dot{\hat{a}}_2 = -i\Bigg(& \triangle_1 [\hat{a}_2, \hat{a}_1^\dagger \hat{a}_1] + \triangle_2[\hat{a}_2, \hat{a}_2^\dagger \hat{a}_2] + Gm_1\hat{a}_1^\dagger \hat{a}_1[\hat{a}_2, \hat{q}_1] + Gm_2\hat{a}_2^\dagger \hat{a}_2[\hat{a}_2, \hat{q}_2] \\
& + \frac{1}{2}\omega_{m1}[\hat{a}_2, \hat{q}_1^2 + \hat{p}_1^2] + \frac{1}{2}\omega_{m2}[\hat{a}_2, \hat{q}_2^2 + \hat{p}_2^2] + iE_1[\hat{a}_2, \hat{a}_1^\dagger - \hat{a}_1] + iE_2[\hat{a}_2, \hat{a}_2^\dagger - \hat{a}_2] \\
& + J[\hat{a}_2, \hat{a}_1^\dagger \hat{a}_2] + J[\hat{a}_2, \hat{a}_2^\dagger \hat{a}_1] + iGe^{i\theta}[\hat{a}_2, \hat{a}^{\dagger 2}_1] - iGe^{-i\theta}[\hat{a}_2, \hat{a}_1^2] + iGe^{i\theta}[\hat{a}_2, \hat{a}^{\dagger 2}_2] \\
& - iGe^{-i\theta}[\hat{a}_2, \hat{a}_2^2]\Bigg) - \beta_2\hat{a}_2 + \sqrt{2\beta_2}\hat{a}_2^{in},
\end{aligned} \tag{3.18}$$

$$\dot{\hat{a}}_2 = -(i\triangle_2 + \beta_2)\hat{a}_2 - iGm_2\hat{q}_2\hat{a}_2 + E_2 - iJ\hat{a}_1 + 2\Omega e^{i\theta}\hat{a}_2^\dagger + \sqrt{2\beta_2}\hat{a}_2^{in}, \tag{3.19}$$

Thus, the time evolution of the system is obtained following nonlinear quantum Langevin equations:

$$\begin{aligned}
&\dot{\hat{q}}_1 = \omega_{m1}\hat{p}_1, \\
&\dot{\hat{p}}_1 = -\gamma_1\hat{p}_1 - G_{m1}\hat{a}_1^\dagger \hat{a}_1 - \omega_{m1}\hat{q}_1 + \xi_1, \\
&\dot{\hat{q}}_2 = \omega_{m2}\hat{p}_2, \\
&\dot{\hat{p}}_2 = -\gamma_2\hat{p}_2 - G_{m2}\hat{a}_2^\dagger \hat{a}_2 - \omega_{m2}\hat{q}_2 + \xi_2, \\
&\dot{\hat{a}}_1 = -(i\triangle_1 + \beta_1)\hat{a}_1 - iG_{m1}\hat{q}_1\hat{a}_1 + E_1 - iJ\hat{a}_2 + 2\Omega e^{i\theta}\hat{a}_1^\dagger + \sqrt{2\beta_1}\hat{a}_1^{in}, \\
&\dot{\hat{a}}_2 = -(i\triangle_2 + \beta_2)\hat{a}_2 - iG_{m2}\hat{q}_2\hat{a}_2 + E_2 - iJ\hat{a}_1 + 2\Omega e^{i\theta}\hat{a}_2^\dagger + \sqrt{2\beta_2}\hat{a}_2^{in},
\end{aligned} \tag{3.20}$$

where β_j and γ_j represent the dissipation of optical and mechanical modes. The thermal Langevin force is resulting from the coupling of the oscillating mirror to the environment, which is auto-correlated, as (Giovannetti and Vitali, 2001)

$$\langle \xi_j(t)\xi_j(t')\rangle = \frac{\gamma_j}{\omega_{mj}} \int \frac{d\omega}{2\pi} e^{-i\omega(t-t')}\omega\left[\coth\left(\frac{\hbar\omega}{2k_\beta T}\right) + 1\right], \tag{3.21}$$

where k_β is the Boltzmann constant and T is the temperature of the environment. $\hat{a}_j^{in}$ is the vacuum noise operator for the cavity operator, in which the nonzero correlation function is

$$\langle \hat{a}_j^{in}(t)\hat{a}_{j'}^{\dagger,in}(t)\rangle = \delta(t-t'). \tag{3.22}$$

3.4. Steady-state and linearized Langevin equations

In the hope of reducing the involved rigor, we opt to restrict the case when $\omega_{m1} = \omega_{m2}$. We assume that the optical cavity fields are intense, $\alpha_{js} \gg 1$. In this case, we seek to apply the linearization approach (Tesfa, 2008) by expanding each field operator as a sum of its steady-state mean values and fluctuation operator with zero-mean value, which can be treated separately as

$$\hat{a}_j = \alpha_{js} + \delta\hat{a}_j, \hat{p}_j = \hat{p}_{js} + \delta\hat{p}_j, \hat{q}_j = \hat{q}_{js} + \delta\hat{q}_j. \tag{3.23}$$

The steady-state mean values of $\hat{p_1}s$ and $\hat{p_2}s$ can be derived from the third and fifth lines of Eq. (3.20)

$$\hat{p_1}s = \hat{p_2}s = 0. \tag{3.24}$$

In the same manner, from the fourth and sixth lines of Eq. (3.20), we see that

$$\hat{q}_1 s = \frac{-Gm_1|\alpha_1 s|^2}{\omega_{m1}}, \tag{3.25}$$

$$\hat{q}_2 s = \frac{-Gm_2|\alpha_2 s|^2}{\omega_{m2}}. \tag{3.26}$$

Therefore, using the same procedure, one can easily obtain

$$\alpha_{1s} = \frac{E_1 J}{(\beta_1 - 2\Omega\cos\theta) + i(\triangle^{01} - 2\Omega\sin\theta) + J^2}, \tag{3.27}$$

$$\alpha_{2s} = \frac{E_2 J}{(\beta_2 - 2\Omega\cos\theta) + i(\triangle^{02} - 2\Omega\sin\theta) + J^2}, \tag{3.28}$$

Therefore, the steady-state mean values of the system can be rewritten as:

$$\begin{aligned}
\hat{p}_{js} &= 0, \\
\hat{q}_{js} &= -G_{mj}|\alpha_{js}|^2/\omega_{mj}, \\
\alpha_{js} &= \frac{E_j J}{(\beta_j - 2\Omega\cos\theta) + i(\triangle^{0j} - 2\Omega\sin\theta) + J^2},
\end{aligned} \tag{3.29}$$

where $\triangle^{0j} = \triangle_j - G_{mj}\hat{q}_{js}$, are the effective cavity detunings including the frequency shift due to the interaction with the mechanical resonator. It is straightforward to see that the OPAs lead to two effects: it modifies the cavity decay rate $\beta_j \Rightarrow \beta_j - 2\Omega\cos\theta$ and also the effective detunings $\triangle^j \Rightarrow \triangle^j - 2\Omega\sin\theta$.

We have also defined the quadrature fluctuation operators of the cavity modes.

$$\delta\hat{x}_j = (\delta\hat{a}_j + \delta\hat{a}_j^\dagger)/\sqrt{2}, \delta\hat{y}_j = i(\delta\hat{a}_j^\dagger - \delta\hat{a}_j)/\sqrt{2}, \tag{3.30}$$

and the corresponding input noise operators

$$\hat{x}_j^{in} = (\hat{a}_j^{in} + \hat{a}_j^{in,\dagger})/\sqrt{2}, \hat{y}_j^{in} = i(\hat{a}_j^{in,\dagger} - \hat{a}_j^{in})/\sqrt{2}. \tag{3.31}$$

Furthermore, let us proceed to get linearized Langevin equations as follows: The fourth line of Eq. (3.20) can be rewritten as

$$\delta\dot{\hat{p}}_1 = -\gamma_1\delta\hat{p}_1 - Gm_1\alpha_s(\delta\hat{a}_1^\dagger + \delta\hat{a}_1) - \omega_{m1}\delta\hat{q}_1 + \xi_1, \tag{3.32}$$

but we have

$$\delta\hat{x}_1 = \frac{(\delta\hat{a}_1^\dagger + \delta\hat{a}_1)}{\sqrt{2}}, \tag{3.33}$$

$$\delta\dot{\hat{p}}_1 = -\gamma_1\delta\hat{p}_1 - g_1\delta\hat{x}_1 - \omega_{m1}\delta\hat{q}_1 + \xi_1, \tag{3.34}$$

where

$$g_1 = Gm_1\sqrt{2}\alpha_s. \tag{3.35}$$

Similarly, one can easily obtain that

$$\delta\dot{\hat{p}}_2 = -\gamma_2\delta\hat{p}_2 - g_2\delta\hat{x}_2 - \omega_{m2}\delta\hat{q}_2 + \xi_2, \tag{3.36}$$

where

$$g_2 = Gm_2\sqrt{2}\alpha_s. \tag{3.37}$$

Furthermore, from the first line of Eq. (3.20), we have

$$\delta\dot{\hat{a}}_1 = -(i\triangle_1 + \beta_1)\delta\hat{a}_1 - iGm_1\hat{q}_{1s}\delta\hat{a}_1 - iJ\delta\hat{a}_2 + 2\Omega e^{i\theta}\delta\hat{a}_1^\dagger + \sqrt{2\beta_1}\delta\hat{a}_1^{in}, \tag{3.38}$$

from this one can obtain that

$$\delta\dot{\hat{a}}_1^\dagger = -(-i\triangle_1 + \beta_1)\delta\hat{a}_1^\dagger + iGm_1\hat{q}_{1s}\delta\hat{a}_1^\dagger + iJ\delta\hat{a}_2^\dagger + 2\Omega e^{-i\theta}\delta\hat{a}_1 + \sqrt{2\beta_1}\delta\hat{a}_1^{\dagger,in}, \tag{3.39}$$

by taking

$$\delta\dot{\hat{x}}_1 = \delta\dot{\hat{a}}_1^\dagger + \delta\dot{\hat{a}}_1, \tag{3.40}$$

on account of the last line of Eq. (3.25) with Eqs. (3.38) and (3.39) into Eq. (3.40) we see that

$$\delta\dot{\hat{x}}_1 = -(\beta_1 - 2\Omega\cos)\delta\hat{x}_1 + (\triangle^{01} + 2\Omega\sin)\delta\hat{y}_1 + J\delta\hat{y}_2 + \sqrt{2\beta_1}\delta\hat{x}_1^{in}. \tag{3.41}$$

In the same procedure, one can easily obtain for $\delta\dot{\hat{y}}_1$, $\delta\dot{\hat{x}}_2$, and $\delta\dot{\hat{y}}_2$. Therefore, the following linearized Langevin equations can be obtained:

$$\begin{aligned}
&\delta\dot{\hat{q}}_1 = \omega_{m1}\delta\hat{p}_1,\\
&\delta\dot{\hat{p}}_1 = -\gamma_1\delta\hat{p}_1 - g_1\delta\hat{x}_1 - \omega_{m1}\delta\hat{q}_1 + \xi_1,\\
&\delta\dot{\hat{q}}_2 = \omega_{m2}\delta\hat{p}_2,\\
&\delta\dot{\hat{p}}_2 = -\gamma_2\delta\hat{p}_2 - g_2\delta\hat{x}_2 - \omega_{m2}\delta\hat{q}_2 + \xi_2,\\
&\delta\dot{\hat{a}}_1 = -(\beta_1 - 2\Omega\cos\theta)\delta\hat{x}_1 + (\triangle^{01} + 2\Omega\sin\theta)\delta\hat{y}_1 + J\delta\hat{y}_2 + \sqrt{2\beta_1}\delta\hat{x}_1^{in},\\
&\delta\dot{\hat{y}}_1 = -(\beta_1 + 2\Omega\cos\theta)\delta\hat{y}_1 + (\triangle^{01} - 2\Omega\sin\theta)\delta\hat{x}_1 + g_1\delta\hat{q}_1 - J\delta\hat{x}_2 + \sqrt{2\beta_1}\delta\hat{y}_1^{in},\\
&\delta\dot{\hat{x}}_2 = -(\beta_2 - 2\Omega\cos\theta)\delta\hat{x}_2 + (\triangle^{02} + 2\Omega\sin\theta)\delta\hat{y}_2 + J\delta\hat{y}_1 + \sqrt{2\beta_2}\delta\hat{x}_2^{in},\\
&\delta\dot{\hat{y}}_2 = -(\beta_2 + 2\Omega\cos\theta)\delta\hat{y}_2 + (\triangle^{02} - 2\Omega\sin\theta)\delta\hat{x}_2 + g_2\delta\hat{q}_2 - J\delta\hat{x}_1 + \sqrt{2\beta_2}\delta\hat{y}_2^{in},
\end{aligned} \tag{3.42}$$

where $g_j = \sqrt{2}G_{mj}\alpha_{js}$ is the effective optomechanical coupling strength, where we have taken α_{js} real by properly choosing the phase reference of the cavity fields.
With the above conditions, we express Eq. (3.42) in a more compact form

$$\dot{S}(t) = AS(t) + \Theta(t), \tag{3.43}$$

with setting $S(t)$ as the column vector of the quantum fluctuations and $\Theta(t)$ being the column vector of the noise sources. Their transposed elements are given by;

$$\begin{aligned}
&S(t)^T = (\delta\hat{q}_1, \delta\hat{p}_1, \delta\hat{q}_2, \delta\hat{p}_2, \delta\hat{x}_1, \delta\hat{y}_1, \delta\hat{x}_2, \delta\hat{y}_2),\\
&\Theta(t)^T = (0, \xi_1, 0, \xi_2, \sqrt{2\beta_1}\delta\hat{x}_1^{in}, \sqrt{2\beta_1}\delta\hat{y}_1^{in}, \sqrt{2\beta_2}\delta\hat{x}_2^{in}, \sqrt{2\beta_2}\delta\hat{y}_2^{in}).
\end{aligned} \tag{3.44}$$

The corresponding drift matrix A takes the form

$$A = \begin{pmatrix} 0 & \omega_{m1} & 0 & 0 & 0 & 0 & 0 & 0 \\ -\omega_{m1} & -\gamma_1 & 0 & 0 & -g_1 & 0 & 0 & 0 \\ 0 & 0 & 0 & \omega_{m2} & 0 & 0 & 0 & 0 \\ 0 & 0 & -\omega_{m2} & -\gamma_2 & 0 & 0 & -g_2 & 0 \\ 0 & 0 & 0 & 0 & \vartheta & \phi & 0 & J \\ g_1 & 0 & 0 & 0 & \varphi & \varsigma & -J & 0 \\ 0 & 0 & 0 & 0 & 0 & J & \Psi & \sigma \\ 0 & 0 & g_2 & 0 & -J & 0 & \chi & \zeta \end{pmatrix}, \tag{3.45}$$

where $\vartheta = -\beta_1 + \rho$, $\phi = \triangle^{01} + \eta$, $\varphi = \triangle^{01} - \eta$, $\varsigma = -\beta_1 - \rho$, $\Psi = -\beta_2 + \rho$, $\sigma = \triangle^{02} + \eta$, $\chi = \triangle^{02} - \eta$, $\zeta = -\beta_2 - \rho$, $\rho = 2\Omega\cos\theta$, and $\eta = 2\Omega\sin\theta$. The system would be stable and reach a steady-state when the real parts of all eigenvalues of matrix A are negative. Due to the Gaussian nature of the quantum noise terms in Eq. (3.44) and the linearized dynamics, the steady-state quantum fluctuations of the system are fully characterized by 8×8 covariance matrix. In light of this, a steady-state covariance matrix can be obtained by solving the corresponding Lyapunov equation (Vitali et al., 2007)

$$AV + VA^T = -D, \tag{3.46}$$

in Eq. (3.46) V with its entries defined as

$$V_{ij} = (\langle u_i(\infty)u_j(\infty) + u_j(\infty)u_i(\infty)\rangle)/2, \tag{3.47}$$

where $(i, j = 1, 2)$ and

$$u^T(\infty) = (\delta\hat{q}_1(\infty), \delta\hat{p}_1(\infty), \delta\hat{q}_2(\infty), \delta\hat{p}_2(\infty), \delta\hat{x}_1(\infty), \delta\hat{y}_1(\infty), \delta\hat{x}_2(\infty), \delta\hat{y}_2(\infty)), \tag{3.48}$$

is the vector of the fluctuation operators at the steady-state $(t \to \infty)$.

$$D = Diag[0, \gamma_1(2\bar{n}+1), 0, \gamma_2(2\bar{n}+1), \beta, \beta, \beta, \beta] \tag{3.49}$$

is the diffusion matrix. The physical meaning of diffusion matrix encodes the influence of quantum noise and can represent the coupling between the system and its environment, which leads to decoherence and dissipation. It is derived from the correlation functions of the noise operators in the linearized form of the Langevin equation. We have supposed the mechanical resonator is of high quality factor $Q = \omega_{mj}/\gamma_j \gg 1$, which is satisfied under the experiment (Gröblacher et al., 2009). The correlation function of the noise $\xi(t)$ can be obtained as

$$\langle \xi_j(t)\xi_j(t') + \xi_j(t')\xi_j(t)\rangle/2 \backsimeq \gamma_j(2\bar{n}+1)\delta(t-t'), \tag{3.50}$$

where $\bar{n} = [exp(\hbar\omega_{mj}/k_B T) - 1]^{-1}$ is the mean thermal phonon number of the resonator, and T is the environmental temperature. The covariance matrix (CM) can also be written in the form of a block matrix:

$$V = \begin{pmatrix} R_{a1} & K_{a1a2} & K_{a1a3} & K_{ma1} \\ K_{a1a2}^T & R_{a2} & K_{ma3} & K_{ma2} \\ K_{a1a3}^T & K_{ma3}^T & R_{a3} & K_{ma3} \\ K_{ma1}^T & K_{ma2}^T & K_{ma3}^T & R_m \end{pmatrix}, \tag{3.51}$$

where each element of this matrix is a 2×2 matrix.
R_{a1}, R_{a2} R_{a3}, and R_m stand for the variances of the mechanical oscillator mode 1, the mechanical oscillator mode 2, the cavity field mode 1, and the cavity field mode 2 with optical parametric amplifier respectively. $K_{a_1a_2}$, $K_{a_1a_3}$, K_{ma_2}, K_{ma_3}, and K_{ma_1} represent the correlation between the mechanical oscillator modes 1 and 2, mechanical oscillator mode 1 and the cavity mode 1, mechanical oscillator mode 2 and the cavity mode 2, the cavity mode 2 and the cavity mode 1, and mechanical oscillator mode 1 and the cavity mode 2, respectively. To compute the bipartite entanglement between the sub-systems in a hybrid optomechanical system, we reduce the 4×4 covariance matrix V to a 2×2 sub-matrix V_s. For instance, if the indices i and j for the element V_{ij} are confined to the set $1,2,3,4$, the sub-matrix $V_s = V_{ij}$ is molded by the first four rows and columns of the correlation matrix V, and this represents the covariance between the mechanical oscillators 1 and 2 as

$$V_s = \begin{pmatrix} R_{a1} & K_{a1a2} \\ K_{a1a2}^T & R_{a2} \end{pmatrix}. \tag{3.52}$$

If the indices $1,2,5$, and 6 are the first, second, fifth, and sixth rows and columns of V, respectively, they represent the covariance between the mechanical oscillator 1 and the cavity mode 1 with an optical parametric amplifier, and the sub matrix v_s is given as

$$v_s = \begin{pmatrix} R_{a1} & K_{a_1a_3} \\ K_{a_1a_3}^T & R_{a3} \end{pmatrix}. \tag{3.53}$$

The covariance between the mechanical oscillator 2 and the cavity mode 2 with an optical parametric amplifier is represented by indices $3,4,7,8$, which are the third, fourth, seventh, and eighth rows and columns of V, respectively, and the sub matrix v_s is given as

$$v_s = \begin{pmatrix} R_{a_2} & K_{ma_2} \\ K_{ma_2}^T & R_m \end{pmatrix}. \tag{3.54}$$

And the covariance between the cavity mode 1 and 2 with an optical parametric amplifier is represented by indices $5,6,7,8$, which are the fifth, sixth, seventh, and eighth rows and columns of V, respectively, and the sub matrix v_s is given as

$$v_s = \begin{pmatrix} R_{a_3} & K_{ma_3} \\ K_{ma_3}^T & R_m \end{pmatrix}. \tag{3.55}$$

Logarithmic negativity is a convenient entanglement measure because it is the only one that can always be explicitly computed, and it is also additive. Once the covariance matrix V is obtained, we can then calculate the steady-state bipartite entanglement. To compute the bipartite entanglement, we choose logarithmic negativity (Vidal and Werner, 2002). Results and discussions of steady-state bipartite entanglement are presented in chapter 4 (4.1).

3.5. Generation of stationary entanglement and quantum discord in an optomechanical system through three-level atoms

3.5.1 Model and Hamiltonian of the system

We consider an optomechanical cavity wherein an atomic medium with a cascade configuration is injected into the cavity (Zhou et al., 2011; Li et al., 2020). We designate the levels of a three-level atom as follows: the top, intermediate, and bottom levels as $|a\rangle$, $|b\rangle$, and $|c\rangle$, respectively, are introduced into the cavity and engage in interactions with the cavity field. These atoms are initially prepared in a coherent superposition of their ground and upper excited levels. They are then injected into the cavity at a constant rate, denoted by γ_a. The cavity field with frequency ω_c is excited by the external driving laser with frequency ω_0. As illustrated in Figure 5, a Fabry-Pérot cavity with one cavity mirror is fixed, and the other one is a perfectly reflective movable mirror. Thus, a mechanical resonator can be described by a harmonic oscillator of frequency ω_m and decay rate κ, which is one side coupled to the optical cavity.

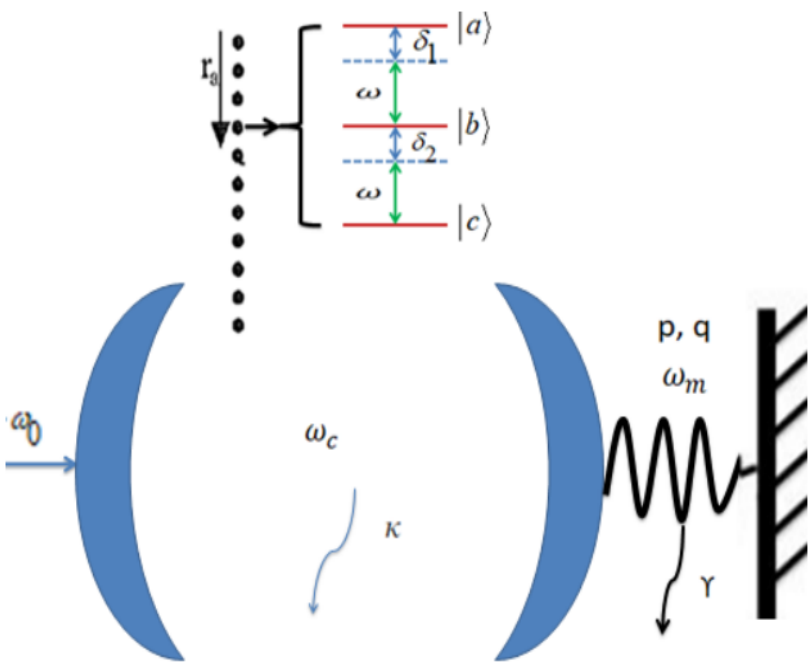

Figure 5: The schematic model of an optomechanical system whose cavity is injected by a three-level atomic ensemble with detunings δ_1 and δ_2. The fixed mirror is driven by a laser frequency of ω_0, and the other symbols are defined in the main text.

The total Hamiltonian of the system can be written as (Kibret et al., 2024)

$$\hat{H} = \hbar\omega_c\hat{a}^\dagger\hat{a} + \hbar G\hat{a}^\dagger\hat{a}\hat{q} + \hbar\frac{1}{2}\omega_m(\hat{q}^2 + \hat{p}^2) + i\hbar E(\hat{a}^\dagger e^{-i\omega_0 t} - \hat{a}e^{i\omega_0 t})$$
$$+ \hbar(E_a\hat{\sigma}_{aa} + E_b\hat{\sigma}_{bb} + E_c\hat{\sigma}_{cc}) + \hbar(g_1\hat{\sigma}_{ba}\hat{a}^\dagger + g_2\hat{\sigma}_{cb}\hat{a}^\dagger + H.c.), \tag{3.56}$$

where the first term describes the energy of the optical cavity modes, with operators $\hat{a}$ or $\hat{a}^\dagger$, the second term characterizes the energy due to radiation-pressure with the coupling rate $G = (\omega_c/L)\sqrt{\hbar/m\omega_m}$, where L is cavity length and m is effective mass. The third term represents the energy of the mechanical resonator in terms of position and momentum operators $\hat{p}$ and $\hat{q}$, respectively; the fourth term describes the energy of the input laser with the amplitude $|E| = \sqrt{2P\kappa/\hbar\omega_0}$, where $\kappa = \pi c/FL$ with F is the cavity finesse, c is the speed of light, and P is driving power. The fifth term describes the free Hamiltonian of the atomic medium, where each atom is modeled by a three-level system. We describe each atom in the medium using the spin operators. $\hat{\sigma}_{jj'} = |j\rangle j'\langle|[j(j') = a,b,c]$. The last term describes the interactions of the atomic medium with the driven cavity fields. Furthermore, we apply the Holstein Primakoff approximation to characterize the collective behavior of atomic systems as harmonic oscillators (Holstein and Primakoff, 1940). So, through proper linearization, the effective coupling strength is given by $g_k = \sqrt{N}$, where k = 1, 2 represents the averaged atom-field coupling strength (Zhou et al., 2011). The Hamiltonian of the whole system after a frame rotates can be rewritten as follows:

$$\hat{H} = \hbar\triangle\hat{a}^\dagger\hat{a} + \hbar G\hat{a}^\dagger\hat{a}\hat{q} + \hbar\frac{1}{2}\omega_m(\hat{q}^2+\hat{p}^2) + i\hbar E(\hat{a}^\dagger - \hat{a})$$
$$+\hbar(g_1\hat{\sigma}_{ba}\hat{a}^\dagger + g_2\hat{\sigma}_{cb}\hat{a}^\dagger + H.c.) + \hbar\phi^{'}\hat{\sigma}_{aa} - \hbar\phi^{''}\hat{\sigma}_{cc}, \tag{3.57}$$

where $\phi^{'} = E_a - E_b - \omega_0$, $\phi^{''} = E_b - E_c - \omega_0$, $\delta_1 = E_a - E_b - \omega$, $\delta_2 = E_b - E_c - \omega$. Thus, $\triangle = \phi^{'} - \delta_1 = \phi^{''} - \delta_2 = \omega - \omega_0$ denotes detuning between the cavity and the classical driving field, where $\omega_c = \omega$. $\hat{\sigma}_{ab} = |a\rangle\langle b|$, $\hat{\sigma}_{ba} = |b\rangle\langle a|$, and $\hat{\sigma}_{bc} = |b\rangle\langle c|$ denote operators of the atoms.

3.5.2 Quantum Langevin equations

In order to describe the complete dynamics of the system, the dissipation and fluctuation terms are added to the Heisenberg equations of motion to obtain the optomechanical system's dynamics from the quantum Langevin equations. From Eq. (3.57), we have

$$\hat{H} = \hbar\triangle\hat{a}^\dagger\hat{a} + \hbar G\hat{a}^\dagger\hat{a}\hat{q} + \hbar\frac{1}{2}\omega_m(\hat{q}^2+\hat{p}^2) + i\hbar E(\hat{a}^\dagger - \hat{a})$$
$$+\hbar(g_1\hat{\sigma}_{ba}\hat{a}^\dagger + g_2\hat{\sigma}_{cb}\hat{a}^\dagger + H.c.) + \hbar\phi^{'}\hat{\sigma}_{aa} - \hbar\phi^{''}\sigma_{cc}, \tag{3.58}$$

where $H.c.$ is a hermtian conjugate. On account of Eqs. (2.15) and (3.58), we see that

$$\frac{d\hat{q}}{dt} = -i\Big([\hat{q},\triangle\hat{a}^\dagger\hat{a}] + [\hat{q},G\hat{a}^\dagger\hat{a}\hat{q}] + [\hat{q},\frac{1}{2}\omega_m(\hat{q}^2+\hat{p}^2)] + [\hat{q},iE(\hat{a}^\dagger-\hat{a})]$$
$$+[\hat{q},g_1\hat{\sigma}_{ba}\hat{a}^\dagger + g_2\hat{\sigma}_{cb}\hat{a}^\dagger + H.c.] + \phi^{'}[\hat{q},\hat{\sigma}_{aa}] - \phi^{''}[\hat{q},\sigma_{cc}]\Big), \tag{3.59}$$

$$\dot{\hat{q}} = \omega_m\hat{p}. \tag{3.60}$$

Similarly,

$$\frac{d\hat{p}}{dt} = -i\Big([\hat{p},\triangle\hat{a}^\dagger\hat{a}] + [\hat{p},G\hat{a}^\dagger\hat{a}\hat{q}] + [\hat{p},\frac{1}{2}\omega_m(\hat{q}^2+\hat{p}^2)] + [\hat{p},iE(\hat{a}^\dagger-\hat{a})]$$
$$+[\hat{p},g_1\hat{\sigma}_{ba}\hat{a}^\dagger + g_2\hat{\sigma}_{cb}\hat{a}^\dagger + H.c.] + \phi^{'}[\hat{p},\hat{\sigma}_{aa}] - \phi^{''}[\hat{p},\sigma_{cc}]\Big) - \gamma\hat{p} + \xi, \tag{3.61}$$

$$\dot{\hat{p}} = -\omega_m\hat{q} - \gamma\hat{p} - G\hat{a}^\dagger\hat{a} + \xi. \tag{3.62}$$

Furthermore,

$$\frac{d\hat{a}}{dt} = -i\bigg([\hat{a}, \triangle\hat{a}^\dagger\hat{a}] + [\hat{a}, G\hat{a}^\dagger\hat{a}\hat{q}] + [\hat{a}, \frac{1}{2}\omega_m(\hat{q}^2+\hat{p}^2)] + [\hat{a}, iE(\hat{a}^\dagger - \hat{a})]$$
$$+ [\hat{a}, g_1\hat{\sigma}_{ba}\hat{a}^\dagger + g_2\hat{\sigma}_{cb}\hat{a}^\dagger + H.c.] + \phi^{'}[\hat{a}, \hat{\sigma}_{aa}] - \phi^{''}[\hat{a}, \sigma_{cc}]\bigg) - \kappa a + \sqrt{2k}\hat{a}^{in}, \qquad (3.63)$$

$$\dot{\hat{a}} = -(i\Delta + k)\hat{a} - iG\hat{q}\hat{a} - i(g_1\hat{\sigma}_{ba} + g_2\hat{\sigma}_{cb}) + E + \sqrt{2k}\hat{a}^{in}. \qquad (3.64)$$

With the same procedure, one can easily obtain the expressions $\dot{\hat{\sigma}}_{ba}$ and $\dot{\hat{\sigma}}_{cb}$ as follows:

$$\frac{d\hat{\sigma}_{ba}}{dt} = -i/\hbar[\hat{\sigma}_{ba}, \hat{H}] - \Gamma^{'}\hat{\sigma}_{ba}, \qquad (3.65)$$

$$\dot{\hat{\sigma}}_{ba} = -i\bigg(\triangle^{'}[\hat{\sigma}_{ba}, \hat{a}^\dagger\hat{a}] + G\hat{a}^\dagger\hat{a}[\hat{\sigma}_{ba}, \hat{q}] + \frac{1}{2}\omega_m[\hat{\sigma}_{ba}, \hat{q}^2 + \hat{p}^2] +$$
$$+ iE[\hat{\sigma}_{ba}, \hat{a}^\dagger - \hat{a}] + g_1[\hat{\sigma}_{ba}, \hat{\sigma}_{ba}\hat{a}^\dagger] + g_1[\hat{\sigma}_{ba}, \hat{\sigma}_{ab}\hat{a}]$$
$$+ g_2[\hat{\sigma}_{ba}, \hat{\sigma}_{cb}\hat{a}^\dagger] + g_2[\hat{\sigma}_{ba}, \hat{\sigma}_{bc}a] + \phi^{'}[\hat{\sigma}_{ba}, \hat{\sigma}_{aa}] - \phi^{''}[\hat{\sigma}_{ba}, \hat{\sigma}_{cc}]\bigg) - \Gamma^{'}\hat{\sigma}_{ba}, \qquad (3.66)$$

$$\dot{\hat{\sigma}}_{ba} = -(\Gamma^{'} + i\phi^{'})\hat{\sigma}_{ba} - ig_1\hat{a}(\hat{\sigma}_{bb} - \hat{\sigma}_{aa}) + ig_2\hat{a}^\dagger\hat{\sigma}_{ba}. \qquad (3.67)$$

Similarly

$$\frac{d\hat{\sigma}_{cb}}{dt} = -i/\hbar[\hat{\sigma}_{cb}, \hat{H}] - \Gamma^{''}\hat{\sigma}_{cb}, \qquad (3.68)$$

$$\dot{\hat{\sigma}}_{cb} = -i\bigg(\triangle^{''}[\hat{\sigma}_{cb}, \hat{a}^\dagger\hat{a}] + G\hat{a}^\dagger\hat{a}[\hat{\sigma}_{cb}, \hat{q}] + \frac{1}{2}\omega_m[\hat{\sigma}_{cb}, \hat{q}^2 + \hat{p}^2] +$$
$$+ iE[\hat{\sigma}_{cb}, \hat{a}^\dagger - \hat{a}] + g_1[\hat{\sigma}_{cb}, \hat{\sigma}_{ba}\hat{a}^\dagger] + g_1[\hat{\sigma}_{cb}, \hat{\sigma}_{ab}\hat{a}]$$
$$+ g_2[\hat{\sigma}_{cb}, \hat{\sigma}_{cb}\hat{a}^\dagger] + g_2[\hat{\sigma}_{cb}, \hat{\sigma}_{bc}\hat{a}] + \phi^{'}[\hat{\sigma}_{cb}, \hat{\sigma}_{aa}] - \phi^{''}[\hat{\sigma}_{cb}, \hat{\sigma}_{cc}]\bigg) - \Gamma^{''}\hat{\sigma}_{cb}, \qquad (3.69)$$

$$\dot{\hat{\sigma}}_{cb} = -(\Gamma^{''} + i\phi^{''})\hat{\sigma}_{cb} - ig_2\hat{a}(\hat{\sigma}_{cc} - \hat{\sigma}_{bb}) - ig_1\hat{a}^\dagger\hat{\sigma}_{ca}. \qquad (3.70)$$

Therefore, from Eqs. (3.60), (3.62), (3.64), (3.67), and (3.70) the non-linear quantum Langevin equations for operators $\dot{\hat{q}}$, $\dot{\hat{p}}$, $\dot{\hat{a}}$, $\dot{\hat{\sigma}}_{ba}$, and $\dot{\hat{\sigma}}_{cb}$, is given by

$$\begin{aligned}
&\dot{\hat{q}} = \omega_m \hat{p}, \\
&\dot{\hat{p}} = -\omega_m \hat{q} - G\hat{a}^{\dagger}\hat{a} - \gamma\hat{p} + \xi, \\
&\dot{\hat{a}} = -(i\Delta + k)\hat{a} - iG\hat{q}\hat{a} - i(g_1\hat{\sigma}_{ba} + g_2\hat{\sigma}_{cb}) + E + \sqrt{2k}\hat{a}^{in}, \\
&\dot{\hat{\sigma}}_{ba} = -(\Gamma^{'} + i\phi^{'})\hat{\sigma}_{ba} - ig_1\hat{a}(\hat{\sigma}_{bb} - \hat{\sigma}_{aa}) + ig_2\hat{a}^{\dagger}\hat{\sigma}_{ca}, \\
&\dot{\hat{\sigma}}_{cb} = -(\Gamma^{''} + i\phi^{''})\hat{\sigma}_{cb} - ig_2\hat{a}(\hat{\sigma}_{cc} - \hat{\sigma}_{bb}) - ig_1\hat{a}^{\dagger}\hat{\sigma}_{ca},
\end{aligned} \tag{3.71}$$

where γ damping rate of the mechanical oscillator, each three-level atom is decayed by the decay rate $\Gamma^{'}$ and $\Gamma^{''}$. The resonator is affected by the quantum Brownian noise ξ (t), leading to the damping of its oscillation with a rate γ possessing the correlation function (Giovannetti and Vitali, 2001).

$$\langle \xi(t)\xi(t')\rangle = \frac{\gamma}{\omega_m}\int \frac{d\omega}{2\pi} e^{-i\omega(t-t^{'})}\omega\left[coth(\frac{\hbar\omega}{2k_B T}) + 1\right], \tag{3.72}$$

where k_B is the Boltzmann constant and T is the temperature of the environment. In order to obtain the steady-state solution of the system, we use the linear approximation theory (Scully and Zubairy, 1997) to solve the last two Eqs. (3.71) to the first order in g_k. That is, $\hat{\sigma}_{jj'}$ is substituted by $\langle\hat{\sigma}_{jj'}\rangle$ for the terms in which the $\hat{\sigma}_{jj'}$ multiply $\hat{a}(\hat{a}^{\dagger})$. We assume that the atoms are injected into the cavity with the state

$$\hat{\rho}(0) = \rho^0_{aa}|a\rangle\langle a| + \rho^0_{cc}|c\rangle\langle c| + \rho^0_{ca}(|c\rangle\langle a| + |a\rangle\langle c|) \tag{3.73}$$

and the atoms are injected into the cavity at a constant rate γ_a, where $\rho^0_{cc}|c\rangle\langle c|$ and $\rho^0_{aa}|a\rangle\langle a|$ are the probabilities of the atom to be initially in the level $|c\rangle$ and $|a\rangle$, respectively. In this respect, the last two Eq.(3.71) can be rewritten as

$$\dot{\hat{\sigma}}_{ba} = -\left(\Gamma^{'} + i\phi^{'}\right)\hat{\sigma}_{ba} + ig_1\gamma_a\rho^0_{aa}\hat{a} + ig_2\gamma_a\rho^0_{ca}\hat{a}^{\dagger}, \tag{3.74}$$

$$\dot{\hat{\sigma}}_{cb} = -\left(\Gamma^{''} + i\phi^{''}\right)\hat{\sigma}_{cb} - ig_2\gamma_a\rho^0_{cc}\hat{a} - ig_1\gamma_a\rho^0_{ca}\hat{a}^{\dagger}. \tag{3.75}$$

By combining Eqs. (3.74) and (3.75) with Eq. (3.71), it is possible to derive the steady-state mean values as:

$$\hat{p}_s = 0, \hat{q}_s = -G|\alpha_s|^2/\omega_m, \alpha_s = \frac{S_2^*E + E^*V_1}{V_1V_2^* + S_1S_2^*}, \tag{3.76}$$

with

$$S_1 = \kappa + i\triangle - \frac{g_1^2\gamma_a\rho_{aa}^0}{\Gamma' + i\phi'}, S_2 = \kappa + i\triangle + \frac{g_2^2\gamma_a\rho_{cc}^0}{\Gamma'' + i\phi''}, V_1 = \frac{g_1g_2\gamma_a\rho_{ca}^0}{\Gamma' + i\phi'},$$
$$V_2 = \frac{g_1g_2\gamma_a\rho_{ca}^0}{\Gamma'' + i\phi''}, \tag{3.77}$$

where the effective cavity detuning, including radiation pressure effects, can be expressed as $\triangle^1 = \triangle - \frac{G|\alpha_s|^2}{\omega_m}$. $G_1 = \sqrt{2}G\alpha_s$ is the effective optomechanical coupling strength, where we have taken α_s real by properly choosing the phase reference of the cavity fields. It is evident that the system's steady-state values are highly dependent on the atomic medium's parameters, including the upper level's ρ_{aa}^0 initial population, the lower level's ρ_{cc}^0 initial population, and their coherence ρ_{ca}^0. The linearized dynamics of the quantum fluctuation around the semiclassical fixed points are the subject of our next discussion. In these scenarios, the cavity's steady-state photon number should be large, i.e., $|\alpha_s| \gg 1$. In this case, one splits the operators in Eq. (3.71) with Eqs. (3.74) and (3.75) into their steady-state values and quantum fluctuations, e.g., $O = O_s + \delta O(O = \hat{q}, \hat{p}, \hat{a}, \hat{\sigma}_{ab}, \hat{\sigma}_{cb})$. By inserting the ansatz $O = O_s + \delta O$ into Eq.(3.71) with Eqs. (3.74) and (3.75) and neglecting all the terms higher than linear order in the fluctuation δO, the quantum Langevin equations for the fluctuations can be written as

$$\begin{aligned}
&\delta\dot{\hat{q}} = \omega_m\delta\hat{p},\\
&\delta\dot{\hat{p}} = -\omega_m\delta\hat{q} - G\delta\hat{x} - \gamma\delta\hat{p} + \xi,\\
&\delta\dot{\hat{a}} = -(i\Delta + k)\delta\hat{a} - iG\hat{a}\delta\hat{x} - i(g_1\delta\hat{\sigma}_{ba} + g_2\delta\hat{\sigma}_{cb}) + \sqrt{2k}\delta\hat{a}^{in},\\
&\delta\dot{\hat{\sigma}}_{ba} = -\left(\Gamma' + i\phi'\right)\delta\hat{\sigma}_{ba} + ig_1\gamma_a\rho_{aa}^0\delta\hat{a} + ig_2\gamma_a\rho_{ca}^0\delta\hat{a}^\dagger,\\
&\delta\dot{\hat{\sigma}}_{cb} = -\left(\Gamma'' + i\phi''\right)\delta\hat{\sigma}_{cb} - ig_2\gamma_a\rho_{cc}^0\delta\hat{a} - ig_1\gamma_a\rho_{ca}^0\delta\hat{a}^\dagger.
\end{aligned} \tag{3.78}$$

We have defined the quadrature fluctuation operators of the cavity mode, the corresponding input noise operators, and the atom quadratures as (Ma and Zhou, 2012; Zhou et al., 2011; Li et al., 2020):

$$\delta\hat{x} = \left(\delta\hat{a} + \delta\hat{a}^\dagger\right)/\sqrt{2}, \delta\hat{y} = i\left(\delta\hat{a}^\dagger - \delta\hat{a}\right)/\sqrt{2}, \delta\hat{x}^{in} = \left(\delta\hat{a}^{in} + \delta\hat{a}^{in,\dagger}\right)/\sqrt{2},$$
$$\delta\hat{y}^{in} = i\left(\delta\hat{a}^{in,\dagger} - \delta\hat{a}^{in}\right)/\sqrt{2}, \tag{3.79}$$

and atom quadrature satisfies the relation.

$$\delta\hat{r} = \left(\delta\hat{\sigma}_{ab} + \delta\hat{\sigma}_{ba}\right)/\sqrt{2}, \delta\hat{s} = i\left(\delta\hat{\sigma}_{ab} - \delta\hat{\sigma}_{ba}\right)/\sqrt{2}, \delta\hat{u} = \left(\delta\hat{\sigma}_{bc} + \delta\hat{\sigma}_{cb}\right)/\sqrt{2},$$
$$\delta\hat{v} = i\left(\delta\hat{\sigma}_{bc} - \delta\hat{\sigma}_{cb}\right)/\sqrt{2}. \tag{3.80}$$

With this consideration, we get the following linearized quantum Langevin equations:

$$
\begin{aligned}
&\delta\dot{\hat{q}} = \omega_m \delta\hat{p},\\
&\delta\dot{\hat{p}} = -\omega_m \delta\hat{q} - \gamma\delta\hat{p} - G\delta\hat{x} + \xi,\\
&\delta\dot{\hat{x}} = -\kappa\delta\hat{x} + \triangle^{'}\delta\hat{y} + g_1\delta\hat{s} + g_2\delta\hat{v} + \sqrt{2\kappa}\delta\hat{x}^{in},\\
&\delta\dot{\hat{y}} = -\kappa\delta\hat{y} - \triangle^{'}\delta\hat{x} + G_1\delta\hat{q} - g_1\delta\hat{r} - g_2\delta\hat{u} + \sqrt{2\kappa}\delta\hat{y}^{in},\\
&\delta\dot{\hat{r}} = -\Gamma^{'}\delta\hat{r} + \phi^{'}\delta\hat{s} - (g_1\gamma_a\rho^0_{aa} - g_2\gamma_a\rho^0_{ac})\delta\hat{y},\\
&\delta\dot{\hat{s}} = -\Gamma^{'}\delta\hat{s} - \phi^{'}\delta\hat{r} + (g_1\gamma_a\rho^0_{aa} + g_2\gamma_a\rho^0_{ac})\delta\hat{x},\\
&\delta\dot{\hat{u}} = -\Gamma^{''}\delta\hat{u} + \phi^{''}\delta\hat{v} + (g_2\gamma_a\rho^0_{cc} - g_1\gamma_a\rho^0_{ca})\delta\hat{y},\\
&\delta\dot{\hat{v}} = -\Gamma^{''}\delta\hat{v} - \phi^{''}\delta\hat{u} - (g_2\gamma_a\rho^0_{cc} + g_1\gamma_a\rho^0_{ca})\delta\hat{x}.
\end{aligned}
\tag{3.81}
$$

We express Eq. (3.81) in a more compact form.

$$
\dot{\eta}(t) = B\eta(t) + \chi(t), \tag{3.82}
$$

with setting $\eta(t)$ as the column vector of the quantum fluctuations and $\chi(t)$ being the column vector of the noise sources. The corresponding drift matrix B which takes the form

$$
B = \begin{pmatrix}
0 & \omega_m & 0 & 0 & 0 & 0 & 0 & 0\\
-\omega_m & -\gamma & -G_1 & 0 & 0 & 0 & 0 & 0\\
0 & 0 & -\kappa & \triangle^{'} & 0 & g_1 & 0 & g_2\\
G_1 & 0 & -\triangle^{'} & -\kappa & -g_1 & 0 & -g_2 & 0\\
0 & 0 & 0 & -\zeta & -\Gamma^{'} & \phi^{'} & 0 & 0\\
0 & 0 & \varsigma & 0 & -\phi^{'} & -\Gamma^{'} & 0 & 0\\
0 & 0 & 0 & \Omega & 0 & 0 & -\Gamma^{''} & \phi^{''}\\
0 & 0 & -\tau & 0 & 0 & 0 & -\phi^{''} & -\Gamma^{''}
\end{pmatrix}, \tag{3.83}
$$

$\zeta = g_1\gamma_a\rho^0_{aa} - g_2\gamma_a\rho^0_{ac}$, $\varsigma = g_1\gamma_a\rho^0_{aa} + g_2\gamma_a\rho^0_{ac}$, $\Omega = g_2\gamma_a\rho^0_{cc} - g_1\gamma_a\rho^0_{ca}$, $\tau = g_2\gamma_a\rho^0_{cc} + g_1\gamma_a\rho^0_{ca}$, and $G_1 = \sqrt{2}G\alpha_s$. Their transposed elements are given by:

$$
\eta(t)^T = (\delta\hat{q}, \delta\hat{p}, \delta\hat{x}, \delta\hat{y}, \delta\hat{r}, \delta\hat{s}, \delta\hat{u}, \delta\hat{v}), \tag{3.84}
$$

$$
\chi(t)^T = (0, \xi, \sqrt{2\kappa}\delta\hat{x}^{in}, \sqrt{2\kappa}\delta\hat{y}^{in}, 0, 0, 0, 0), \tag{3.85}
$$

The system is stable and reaches a steady-state; the drift matrix B possesses negative real eigenvalues. The steady-state covariance matrix R can be obtained by solving the Lyapunov equation.

$$BR + RB^T = -D, \tag{3.86}$$

where R is the system covariance matrix, which contains all information about the steady-state and

$$D = Diag[0, \gamma(2n+1), k, k, 0, 0, 0, 0)], \tag{3.87}$$

$n = \left[exp\left(\hbar\omega_c/K_B T\right)^{-1} \right]^{-1}$ is the diffusion matrix stemming from the noise correlations. Based on the model of the system shown above, the dynamics of an optomechanical system approved by three-level atoms, particularly the two-mode steady-state entanglement in the subsystems, can be computed numerically using the correlation matrix (CM) 8×8 of the entanglement. The covariance matrix R can be written in the form of a block matrix:

$$R = \begin{pmatrix} V_{a1} & N_{a1a2} & N_{a1a3} & N_{ma1} \\ N^T_{a1a2} & V_{a2} & N_{ma3} & N_{ma2} \\ N^T_{a1a3} & N^T_{ma3} & V_{a3} & N_{ma3} \\ N^T_{ma1} & N^T_{ma2} & N^T_{ma3} & V_m \end{pmatrix}, \tag{3.88}$$

in Eq.(3.88) R with its entries defined as $R_{ij} = (\langle u_i(\infty)u_j(\infty) + u_j(\infty)u_i(\infty)\rangle)/2$ and

$$u^T(\infty) = (\delta\hat{q}(\infty), \delta\hat{p}(\infty), \delta\hat{x}(\infty), \delta\hat{y}(\infty), \delta\hat{r}(\infty), \delta\hat{s}(\infty), \delta\hat{u}(\infty), \delta\hat{v}(\infty)), \tag{3.89}$$

is the vector of the fluctuation operators at the steady-state $(t \to \infty)$. R_{ij} is describing the local properties of mode j, whereas N_{ij} is referring to the intermode correlations (i, j, a_1, a_2, a_3, m).

When a two-level atom is injected into the cavity, we also express Eq. (3.81) in a more compact form as:

$$\dot{\eta}'(t) = C\eta(t) + \chi'(t), \tag{3.90}$$

with setting $\eta'(t)$ as the column vector of the quantum fluctuations and $\chi'(t)$ being the column vector of the noise sources. The corresponding drift matrix C which takes the form

$$C = \begin{pmatrix} 0 & \omega_m & 0 & 0 & 0 & 0 \\ -\omega_m & -\gamma & -G_1 & 0 & 0 & 0 \\ 0 & 0 & -\kappa & \triangle' & 0 & g_1 \\ G_1 & 0 & -\triangle' & -\kappa & -g_1 & 0 \\ 0 & 0 & 0 & -\zeta & -\Gamma' & \phi' \\ 0 & 0 & \varsigma & 0 & -\phi' & -\Gamma' \end{pmatrix}, \tag{3.91}$$

$\zeta = g_1\gamma_a\rho^0_{aa} - g_2\gamma_a\rho^0_{ac}$, $\varsigma = g_1\gamma_a\rho^0_{aa} + g_2\gamma_a\rho^0_{ac}$, and $G_1 = \sqrt{2}G\alpha_s$. Their transposed elements are given by:

$$\eta^{'}(t)^T = (\delta\hat{q}, \delta\hat{p}, \delta\hat{x}, \delta\hat{y}, \delta\hat{r}, \delta\hat{s}), \tag{3.92}$$

$$\chi^{'}(t)^T = (0, \xi, \sqrt{2\kappa}\delta\hat{x}^{in}, \sqrt{2\kappa}\delta\hat{y}^{in}, 0, 0). \tag{3.93}$$

The results of the generation of stationary entanglement and Gaussian quantum discord are discussed under chapter four (4.2).

3.6. Generation of Quantum Correlations through Optical Parametric Amplifcation in a Hybrid Optomechanical System

3.6.1 Model and dynamics of the system

We consider a model of a hybrid optomechanical system (Maquedano and Costa, 2024; Liao et al., 2020) in which a single cavity is coupled to a degenerate optical parametric amplifier via a cavity-cavity coupling parameter. In this setup, we incorporate a quantum mechanical harmonic oscillator with an effective mass m, where two cavity mirrors are fixed and the other is movable. Each cavity mode is driven by a laser, interacting with the movable mirrors through radiation pressure interaction, as depicted in Figure 6.

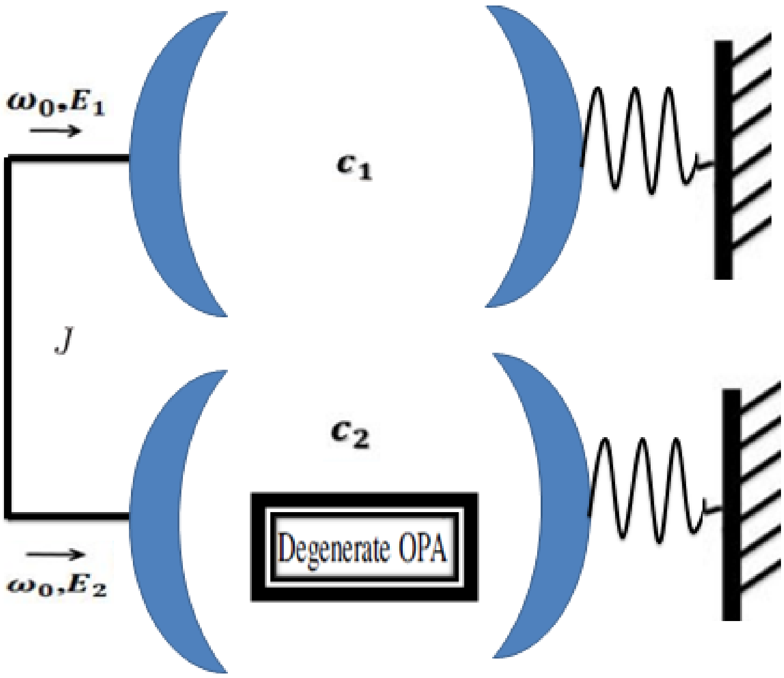

Figure 6: Schematic diagram of two distant Fabry-Pérot cavities coupled via cavity-cavity coupling with J. While the other symbols are defined in the main text.

Now it is convenient to transform the optical mode description by applying the unitary transformation $\hat{U} = \exp\left(\hat{c}_1^{+}\hat{c}_1 - \hat{c}_2^{+}\hat{c}_2\right)t$ and the Hamiltonian that characterizes this system is (Ma and Wu, 2015)

$$\hat{H} = \sum_{k=1}^{2}\left(\omega_{ck}\hat{c}_k^{\dagger}\hat{c}_k + g_k\hat{c}_k^{\dagger}\hat{c}_k\hat{Q}_k + \frac{1}{2}\omega_m\left(\hat{Q}_k^2 + \hat{P}_k^2\right) + iE_k\left(\hat{c}_k^{\dagger}e^{-i\omega_0 t} - \hat{c}_k e^{i\omega_0 t}\right)\right)$$
$$+ i\Sigma\left(e^{i\theta}\hat{c}_2^{\dagger 2}e^{-i\omega_0 t} - e^{-i\theta}\hat{c}_2^2 e^{i\omega_0 t}\right) + J\left(\hat{c}_1^{\dagger}\hat{c}_2 + \hat{c}_2^{\dagger}\hat{c}_1\right). \tag{3.94}$$

Switching to a frame rotating with respect to the frequency ω_o, and the total Hamiltonian of the whole system can be rewritten;

$$\hat{H} = \sum_{k=1}^{2}\left(\triangle_k\hat{c}_k^{\dagger}\hat{c}_k + g_k\hat{c}_k^{\dagger}\hat{c}_k\hat{Q}_k + \frac{1}{2}\omega_m\left(\hat{Q}_k^2 + \hat{P}_k^2\right) + iE_k\left(\hat{c}_k^{\dagger} - \hat{c}_k\right)\right)$$
$$+ i\Sigma\left(e^{i\theta}\hat{c}_2^{\dagger 2} - e^{-i\theta}\hat{c}_2^2\right) + J\left(\hat{c}_1^{\dagger}\hat{c}_2 + \hat{c}_2^{\dagger}\hat{c}_1\right), \tag{3.95}$$

where $\triangle_k = \omega_{ck} - \omega_0$ is detuning frequency of the cavity. Here, the first term describes the free Hamiltonian of two cavities, with $\hat{c}_k^{\dagger}$ and $\hat{c}_k$ being the creation and annihilation operators of the cavity modes. The second term describes the interaction of two cavity modes with a radiation pressure force with a coupling rate of g_k. The third term represents the free Hamiltonian for the two mechanical systems with dimensionless position and momentum operators $\hat{Q}_k$ and $\hat{P}_k$ ($k = 1,2$). The fourth term represents the two input driving lasers with frequencies ω_0 and $|E_k|$ is the driving amplitude related to driving power P_k and the cavity decay rate κ_k by $|E_k| = \sqrt{2P_k\kappa_k/\hbar\omega_0}$ in which $\kappa_1 = \kappa_2 = \kappa = \pi c/2FL$ and F is the cavity finesse. In addition, $g_k = \left(\omega_{ck}/L\right)\sqrt{\hbar/m\omega_m}$ (L is the cavity length and m is the effective mass) is the single-photon optomechanical coupling associated with the cavity mode with frequency ω_{ck}. The fifth term is the driving laser from the nonlinear parametric gain. While Σ is the nonlinear gain of OPA, which is proportional to the pump driving the OPA. The last term denotes the coupling between two distant cavities by a cavity-cavity coupling strength with an inter-mode coupling constant J (Gebremariam et al., 2017).

3.6.2 Dynamics of the System

The dynamics of a coupled optomechanical system can be examined by employing the standard quantum Langevin method (Mekonnen et al., 2024). Since the system dynamics include fluctuation and dissipation processes and the corresponding effects of damping and noises, Therefore, using Eq. (3.95), we can obtain the following array time evolution of the system, which describes the dynamics of the coupled systems as

$$\begin{aligned}
&\dot{\hat{Q}}_1 = \omega_m \hat{P}_1, \\
&\dot{\hat{P}}_1 = -\gamma_m \hat{P}_1 - g_1 \hat{c}_1^\dagger \hat{c}_1 - \omega_m \hat{Q}_1 + \xi_1, \\
&\dot{\hat{Q}}_2 = \omega_m \hat{P}_2, \\
&\dot{\hat{P}}_2 = -\gamma_m \hat{P}_2 - g_2 \hat{c}_2^\dagger \hat{c}_2 - \omega_m \hat{Q}_2 + \xi_2, \\
&\dot{\hat{c}}_1 = -\Big(i\triangle_1 + \kappa_1\Big)\hat{c}_1 - ig_1 \hat{Q}_1 \hat{c}_1 + E_1 - iJ\hat{c}_2 + \sqrt{2\kappa_1}\hat{c}_1^{in}, \\
&\dot{\hat{c}}_2 = -\Big(i\triangle_2 + \kappa_2\Big)\hat{c}_2 - ig_2 \hat{Q}_2 \hat{c}_2 + E_2 - iJ\hat{c}_1 + 2\Sigma e^{i\theta}\hat{c}_2^\dagger + \sqrt{2\kappa_2}\hat{c}_2^{in},
\end{aligned} \tag{3.96}$$

where κ_k, γ_m represents the dissipation of optical and mechanical modes, $\triangle_k^{'} = \triangle_k - g_k \alpha_{ks}$ are the effective cavity detunings, including the frequency shift due to the interaction with the mechanical resonator. While, $\gamma_1 = \gamma_2 = \gamma_m$ and $\omega_{m1} = \omega_{m2} = \omega_m$.
It is straightforward to see that the OPA leads to two effects: it modifies the cavity decay rate $\kappa_k \Rightarrow \kappa_k - 2\Sigma\cos\theta$ and also the effective detunings $\triangle_k^{'} \Rightarrow \triangle_k^{'} - 2\Sigma\sin\theta$. The mechanical resonator is affected by the quantum Brownian noise $\xi_k(t)$ leading a mechanical oscillator with a correlation function (Gardiner and Zoller, 2004)

$$\Big\langle \xi_k(t)\xi_k(t^{'}) \Big\rangle = \frac{\gamma_m}{\omega_m}\int \frac{d\omega}{2\pi} e^{-i\omega}\big(t-t^{'}\big)\omega\left[1 + \coth\big(\frac{\hbar\omega}{2\,k_B T}\big)\right], \tag{3.97}$$

where $\hat{c}_k^{in}$ is the zero-mean vacuum cavity input noise, which obeys the following correlation function, $\Big\langle \hat{c}_k^{in}(t)\hat{c}_k^{\dagger,in}(t) \Big\rangle = \delta\big(t-t^{'}\big)$, where $n = \Big[exp\big(\omega_m/k_B T\big) - 1\Big]^{-1}$ is the mean thermal photon number in the optical mode, which is assumed to be at the same environmental temperature (Yin et al., 2013).

3.6.3 Linearization of Langevin equations

Now, it is important to mention that the dynamical equations of the system can be linearized in order to study the statistical properties of the system. To this aim, we assume that the cavity is intensively driven with a very large response power. Thus, in the steady state, the intracavity fields have a large amplitude. Accordingly, the nonlinear quantum Langevin equations of the system can be linearized by re-writing each Heisenberg operator as a sum of its coherent amplitudes of steady-state value and an additional fluctuation operator with zero-mean value as (Gebremariam et al., 2017) $\alpha_{sk} + \delta\hat{c}_k$ and $\hat{Q}_{sk} + \delta\hat{P}_k$, where (k = 1, 2) represents the subsystem. $\hat{\alpha}_{sk}$ and $\hat{Q}_{sk}$ characterize the steady-state averages of the operators. While $\delta\hat{c}_k$ and $\delta\hat{P}_k$ describe the fluctuations of the system, respectively. By setting the time derivatives to zero and the steady-state average

$$
\begin{aligned}
&\hat{Q}_{1s} = -g_1|\alpha_{1s}|^2/\omega_m, \\
&\hat{P}_{1s} = 0, \\
&\hat{\alpha}_{s1} = \frac{E_1 J}{\kappa_1 + i\triangle_1' + J^2}, \\
&\hat{Q}_{2s} = -g_2|\alpha_{2s}|^2/\omega_m, \\
&\hat{P}_{s2} = 0, \\
&\alpha_{2s} = \frac{E_2 J}{\left(\kappa_2 - 2\Sigma\cos\theta\right) + i\left(\triangle_2' - 2\Sigma\sin\theta\right) + J^2}.
\end{aligned} \tag{3.98}
$$

As for the fluctuations, their dynamics are given by the linearized quantum Langevin Eq. (3.96). After linearizing the operators within the subsystem, its linearized QLEs can be obtained by neglecting the small value quantities, and the steady-state fluctuation state of the dynamics can be established.

Specifically, the statistical properties of bipartite entanglement and its correlations with the system can be characterized by analyzing the variance between these quadrature components of the fields. Now we define the dimensionless quadrature operators for the optical and mechanical parts of the system, respectively, as:

$$
\delta\hat{X}_k = \left(\delta\hat{c}_k + \delta\hat{c}_k^\dagger\right)/\sqrt{2}, \delta\hat{Y}_k = i\left(\delta\hat{c}_k^\dagger - \delta\hat{c}_k\right)/\sqrt{2},
$$

and the corresponding quadrature components of Hermitian input noise operators

$$
\hat{X}_k^{in} = \left(\hat{c}_k^{in} + \hat{c}_k^{in,\dagger}\right)/\sqrt{2}, \hat{Y}_k^{in} = i\left(\hat{c}_k^{in,\dagger} - \hat{c}_k^{in}\right)/\sqrt{2}.
$$

Consequently, by incorporating these quadratures into rewriting Eq. (3.96), we can obtain the quantum fluctuation dynamics as:

$$
\begin{aligned}
&\delta\dot{\hat{Q}}_1 = \omega_m \delta\hat{P}_1, \\
&\delta\dot{\hat{P}}_1 = -\gamma_m \delta\hat{P}_1 - g_1 \delta\hat{X}_1 - \omega_m \delta\hat{Q}_1 + \xi_1, \\
&\delta\dot{\hat{Q}}_2 = \omega_m \delta\hat{P}_2, \\
&\delta\dot{\hat{P}}_2 = -\gamma_m \delta\hat{P}_2 - g_2 \delta\hat{X}_2 - \omega_m \delta\hat{Q}_2 + \xi_2, \\
&\delta\dot{\hat{X}}_1 = -\kappa_1 \delta\hat{X}_1 + \triangle_1^{'} \delta\hat{Y}_1 + J\delta\hat{Y}_2 + \sqrt{2\kappa_1}\delta\hat{X}_1^{in}, \\
&\delta\dot{\hat{Y}}_1 = -\kappa_1 \delta\hat{Y}_1 + \triangle_1^{'} \delta\hat{X}_1 - g_1 \delta\hat{Q}_1 + J\delta\hat{X}_2 + \sqrt{2\kappa_1}\delta\hat{Y}_1^{in}, \\
&\delta\dot{\hat{X}}_2 = -\left(\kappa_2 - 2\Sigma\cos\theta\right)\delta\hat{X}_2 + \left(\triangle_2^{'} + 2\Sigma\sin\theta\right)\delta y_2 + J\delta\hat{Y}_1 + \sqrt{2\kappa_2}\delta\hat{X}_2^{in}, \\
&\delta\dot{\hat{Y}}_2 = -\left(\kappa_2 + 2\Sigma\cos\theta\right)\delta\hat{Y}_2 + \left(\triangle_2^{'} - 2\Sigma\sin\theta\right)\delta\hat{X}_2 + g_2 \delta\hat{Q}_2 - J\delta\hat{X}_1 + \sqrt{2\kappa_2}\delta\hat{Y}_2^{in},
\end{aligned}
\tag{3.99}
$$

where $G_{sk} = \sqrt{2}g_k\alpha_{ks}$ is the effective optomechanical coupling strength. where we have taken α_{ks} real by properly choosing the phase reference of the cavity fields. Thus, we can rewrite Eq. (3.99) in a more compact form as

$$
\dot{\mathbb{W}}(t) = \mathbb{M}\mathbb{W}(t) + \mathbb{N}(t), \tag{3.100}
$$

with setting $\mathbb{W}(t)$ as the column vector of the quantum fluctuations and $\mathbb{N}(t)$ as the input noise vectors, respectively. Their transposed elements thus turn out to be

$$
\mathbb{W}(t) = \left(\delta\hat{Q}_1, \delta\hat{P}_1, \delta\hat{Q}_2, \delta\hat{P}_2, \delta\hat{X}_1, \delta\hat{Y}_1, \delta\hat{X}_2, \delta\hat{Y}_2\right)^T, \tag{3.101}
$$

$$
\mathbb{N}(t) = \left(0, \xi_1, 0, \xi_2, \sqrt{2\kappa}\hat{X}_1^{in}, \sqrt{2\kappa}\hat{Y}_1^{in}, \sqrt{2\kappa_2}\hat{X}_2^{in}, \sqrt{2\kappa}\hat{Y}_2^{in}\right)^T. \tag{3.102}
$$

Therefore, the corresponding drift matrix $\mathbb{M}$ takes the form

$$\mathbb{M}=\begin{pmatrix} 0 & \omega_m & 0 & 0 & 0 & 0 & 0 & 0 \\ -\omega_m & -\gamma_m & 0 & 0 & -G_{s1} & 0 & 0 & 0 \\ 0 & 0 & 0 & \omega_m & 0 & 0 & 0 & 0 \\ 0 & 0 & -\omega_m & -\gamma_m & 0 & 0 & -G_{s2} & 0 \\ 0 & 0 & 0 & 0 & -\kappa & \triangle_1^{'} & 0 & J \\ G_{s1} & 0 & 0 & 0 & \triangle_1^{'} & -\kappa & -J & 0 \\ 0 & 0 & 0 & 0 & 0 & J & -\kappa+2\Sigma\cos\theta & \triangle_2^{'}+2\Sigma\sin\theta \\ 0 & 0 & G_{s2} & 0 & -J & 0 & \triangle_2^{'}-2\Sigma\sin\theta & -\kappa-2\Sigma\cos\theta \end{pmatrix}. \tag{3.103}$$

To measure the bipartite quantum correlations and entanglement properties between the subsystems, the stability of the system is guaranteed and a prerequisite for a feasible and realizable system. Furthermore, the drift matrix $\mathbb{M}$ contains information about the system. Particularly, the criteria to be stable for the drift matrix $\mathbb{M}$ are satisfied by the Routh-Hurwitz criterion (Leng et al., 2009), i.e., if the eigenvalues of the drift matrix must be negative real parts. Consequentially, the system is stable and reaches a steady state, which is fully characterized by the correlation matrix with corresponding components (Walls et al., 1994)

$$\mathbb{V}_{ij}(t)=\frac{1}{2n}(\langle\mathbb{W}_i(t)\mathbb{W}_j(t)+\mathbb{W}_j(t)\mathbb{W}_i(t)\rangle). \tag{3.104}$$

Thus, the stability criteria (Leng et al., 2009) are satisfied, and the steady-state correlation matrix of the quantum fluctuation can be derived by the following Lyapunov equation (Li et al., 2016; Wang et al., 2014a)

$$\mathbb{M}\mathbb{V}+\mathbb{V}\mathbb{M}^T=-\mathbb{D}, \tag{3.105}$$

where, $\mathbb{D}$=*Diag* (0, $\gamma_m(2n+1)$, 0, $\gamma_m(2n+1)$, κ, κ, κ, κ) is the matrix of the stationary noise correlations; it characterizes the noise correlations, i.e., the diffusion matrix. Eq. (3.105) is a linear equation in $\mathbb{V}$ that can be straightforwardly solved; however, the exact analytical expression is too cumbersome and will not be reported. Specifically, the block matrix off-diagonal represents the correlations between two components, i.e., the covariance across various subsystems. While the block elements of the main diagonal characterize the variance between each subsystem. Note that results and discussion of stationary entanglement, quantum discord, and steering are presented under chapter four (4.3).

4. RESULTS AND DISCUSSION

4.1. Steady-state entanglement of an optomechanical system with OPA

4.1.1 Steady-state bipartite entanglement

In this section, we discussed the nature of steady-state bipartite entanglement, such as the entanglement between the first cavity-mechanical oscillator modes and the second cavity-mechanical oscillator modes, and the two cavity modes. For such a system without OPA, the entanglement properties of bipartite modes have been studied (Tesfahannes, 2020; Huang and Agarwal, 2009c; Kuzyk et al., 2013; Wang and Clerk, 2013). We opt to focus on the effects of the nonlinear gain of OPA and cavity-cavity coupling strength on logarithmic negativity. In doing so, we choose experimental parameters and the parameters of the two optomechanical cavities to be the same: $\beta_1 = \beta_2 = \beta$, $\gamma_1 = \gamma_2 = \gamma$, and $\omega_{m1} = \omega_{m2} = \omega_m$ (Kippenberg and Vahala, 2008; Mari and Eisert, 2009). Besides, the results are obtained by adopting the parameters analogous to Refs. Firstly, we investigate steady-state

Table 1: List of experimental parameters for the system (Eichenfield et al., 2009; Cho et al., 2008; Schmidt et al., 2015)

Parameters	Symbol	Value
Frequency of mechanical oscillator	ω_m	$2\pi\times$ 10 MHz
Mechanical quality factor	Q	10^5
Optical laser wavelength	λ	810nm
Length of the cavity	L	1mm
Mass of mechanical oscillator	m	$5 \times 10^{-12} kg$
Driven laser power	P_1	100 mW
	P_2	50 mW
Cavity finesse	F	1.07×10^4
Mechanical damping rate	γ	$2\pi \times 100 Hz$

bipartite entanglement between the cavity-mechanical oscillating modes, the second cavity-mechanical modes, and the two cavity modes as a function of the phase θ

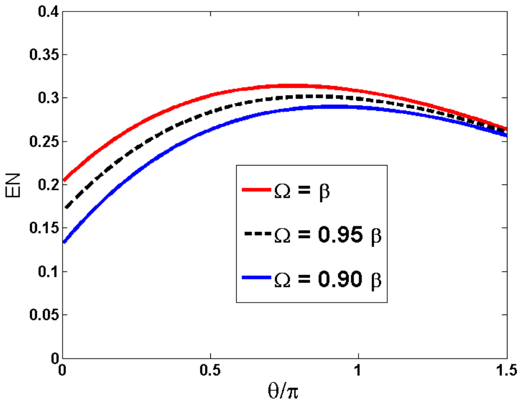

(a)

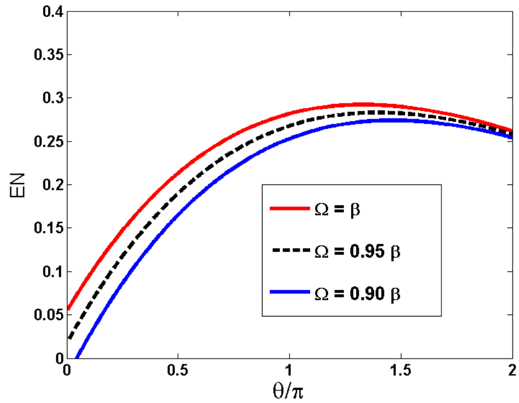

,(b)

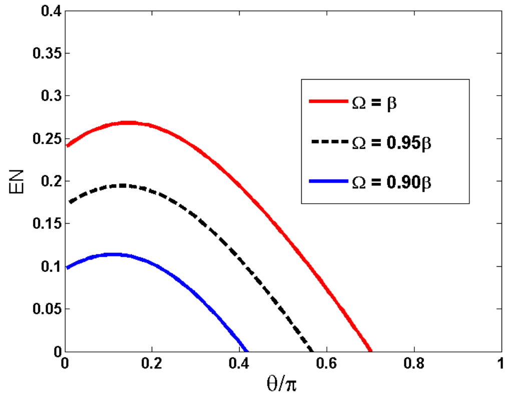

(c) ,

Figure 7: Plots of EN between (a) $C1-M1$, (b) $C2-M2$, and (c) $C1-C2$ at $\Omega=\beta$ (red solid curve), $\Omega=0.95\beta$ (black dashed curve), and $\Omega=0.9\beta$ (blue solid curve) as a function of the phase θ for various optimal values of nonlinear gain at temperature $T=400mk$, $\beta=44MHz$, and coupling strength $J=0.5\omega_m$. The rest of the parameters are given in Table 1.

In Figure 7(a), the entanglement of the first cavity-mechanical oscillator modes as a function of the phase θ for various optimal values of nonlinear gain is plotted. We observe that the steady-state entanglement generated and the nature of entanglement significantly vary with the value of the nonlinear gain of the OPA. Specifically, from Figure 7(a), we see that when the nonlinear gain of OPA medium increases, the entanglement measurement also increases. In Figure 7(b), we also plot the entanglement of the second cavity-mechanical oscillator modes as a function of the phase θ for various values of the nonlinear gain of OPA, and the other parameters that have been used are the same as in Figure 7. Similarly, from this figure, we can see that the entanglement increases with increasing nonlinear gain in the OPA medium. But, comparing Figures 7(a) and (b), the maximum entanglement between the first cavity-mechanical oscillating modes is greater than the maximum entanglement between the second cavity-mechanical modes. The reason is that increasing the input laser power increases the parametric gain, and this causes a stronger coupling between the movable mirror and the cavity field, leading to an increase in entanglement. Furthermore, Figure 7(c) illustrates the entanglement between two cavity modes as a function of phase θ, and the other parameters are the same as in Figure 7. We also observe that the entanglement between two cavity modes is generated in a steady state. Specifically, the entanglement increases with the nonlinear gain of the OPA medium until certain θ, then it decreases. The minimum value of entanglement between the two cavity modes at a reasonable temperature is non-zero; this shows that there is an entanglement transfer in the system due to cavity-cavity coupling strength. From the three Figures 7(a), (b), and c, we observe that the steady-state entanglement generated and the entanglement measurement increase with increasing the value of nonlinear gain Ω. The fact is that increasing the nonlinear gain of the medium causes a stronger coupling between the cavity and mechanical oscillator modes. Furthermore, the minimum value of entanglement at a reasonable temperature is non-zero; this shows that there is an entanglement transfer in the system. More importantly, from Figures 7 (a), (b), and c, we can see that the generation of steady-state entanglement and entanglement transfer strongly depends on cavity-cavity coupling strength and OPA medium. In light of the observed result, it is worth noting that the emerging entanglement is induced due to the coupling of degenerate OPA with their cavity and the presence of cavity-cavity coupling strength. Comparing the behavior of entanglement measurement in a Fabry-Perot cavity without the OPA of an oscillating micro-mirror driven by coherent light [28] with the presence of the OPA, the entanglement is more enhanced. Additionally, in the present paper, the system is different from the standard optomechanical system reported in Refs. (Tesfahannes, 2020; Mi et al., 2013; Yang et al., 2017). Therefore, such a hybrid optomechanical system can utilize immediate practical interest in the investigation of remote entanglement measurements and is suitable for future information processing applications.

Secondly, we discuss the steady-state bipartite entanglement as a function of the normalized detuning $\triangle/\omega$ for different values of the coupling parameter J. The main reason for the choice of the parameter is to see an evident difference in the entanglement in a coupled system and to determine in what way the nature of the entanglement would be influenced by the strength of the cavity-cavity coupling parameter. With this respect, we plot the bipartite entanglement as a function of the normalized detuning for different values of J.

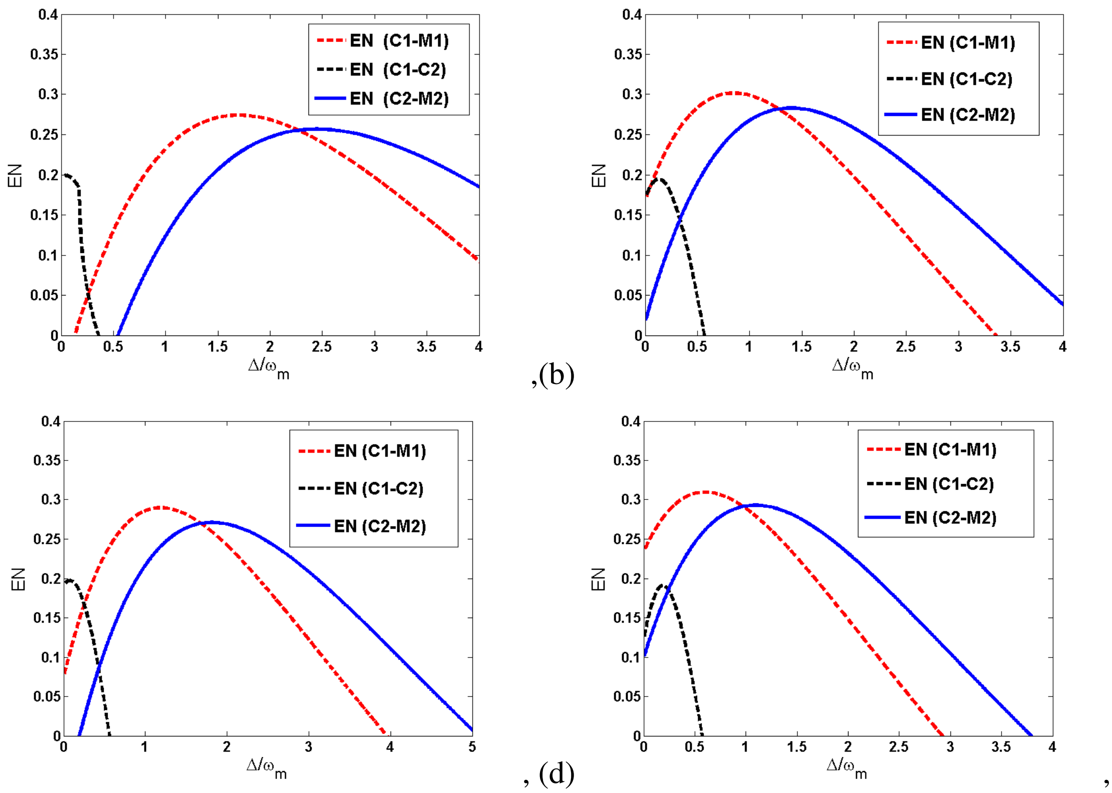

Figure 8: Plots of *EN* of the first cavity-mechanical oscillator modes (red dashed curve), the second cavity-mechanical oscillator modes (blue solid curve), and the two cavity modes (black dashed curve) as a function of the normalized detuning $\triangle/\omega$ for coupling strength (a) $J = 0.3\omega_m$, (b) $J = 0.4\omega_m$, (c) $J = 0.5\omega_m$, and (d) $J = 0.6\omega_m$, with fixed value of $\Omega = 0.95\beta$, where the other parameters are taken to be the same as in Figure 7.

Specifically, in Figure 8(a), we plot the entanglement of the first cavity-mechanical oscillator modes, the second cavity-mechanical oscillator modes, and the two cavity modes as a function of $\triangle/\omega$ with coupling strength $J = 0.3\omega_m$, and the other parameters are the same as in Figure 7. We can see that the entanglement of the first cavity-mechanical oscillator modes and second cavity-mechanical oscillator modes increases with normalized detuning until a certain range, and then it decreases. In Figure 8(b), we also plot the bipartite entanglement as a function of the normalized detuning for coupling strength $J = 0.4\omega_m$, and the other parameters are taken to be the same as in Figure 7. The logarithmic negativity that accounts for the entanglement of cavity-mechanical oscillator modes also increases until a certain detuning, and then it decreases. But the entanglement between the two cavity modes almost decreases from a certain maximum entanglement. It is possible to see from Figures 8(a),(b), and(d) that continuous variable entanglement witnessed for the parameter $\triangle/\omega$ ranging from 0 to 4. Similarly, in Figures 8(c) and (d), we plot the entanglement of the first cavity-mechanical oscillator modes, the second cavity-mechanical oscillator modes, and the two cavity modes as a function of $\triangle/\omega$ for coupling strengths J = 0.5m and J= $0.6\omega_m$, respectively. We also observe the same behavior as in Figures 8(a) and (b). We see from Figure 8(c) that continuous variable entanglement is witnessed for the parameter

$\triangle/\omega$ ranging from 0 to 5, which entails that the greater possibility of entanglement can be easily realized in an experiment. This shows the behavior of the generation of our bipartite entanglement consistent with the photonic-crystal optomechanical cavity (Eichenfield et al., 2009).

Additionally, we observe the effect of coupling rate J on the bipartite entanglement from Table below. In Table 2, we see that the entanglement of the first cavity-mechanical oscillator

Table 2: The maximum value of EN concerning the strength of the coupling parameter from Figure 8

The strength of coupling rate J	**EN (C1-M1)**	**EN (C1-C2)**	**EN (C2-M2)**
$0.3\omega_m$	0.27	0.19	0.26
$0.4\omega_m$	0.29	0.194	0.27
$0.5\omega_m$	0.30	0.19	0.28
$0.6\omega_m$	0.31	0.19	0.29

modes and second cavity-mechanical oscillator coupled modes increases with increasing the value of cavity-cavity coupling strength J. However, the entanglement between the two cavity modes is almost consistent with increasing the strength of the coupling parameter. In addition, these results can be compared with the situation discussed in Ref. (Tesfahannes, 2020). From this point of view, the bipartite entanglement with our model can be generated and significantly enhanced by a variation in the cavity-cavity coupling strength process. The generation of entanglement between the two cavity modes can be transferred entirely due to the coupling strengths. It might then be possible to deduce that the strength of the coupling rate J would be very crucial in transferring quantum features in a hybrid optomechanical system.

Thirdly, we examine the effect of the coupling rate on the entanglement. Figure 9 exhibits the EN of optomechanical systems for different input laser power when the nonlinear gain of OPA $\Omega = 0.95\beta$.

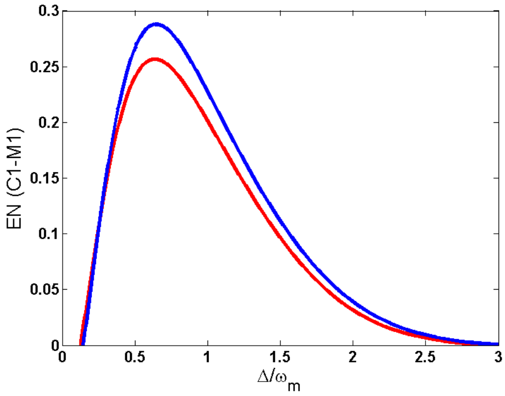

(a)

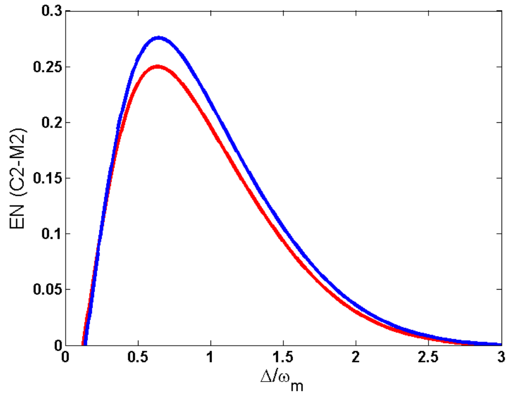

,(b) ,

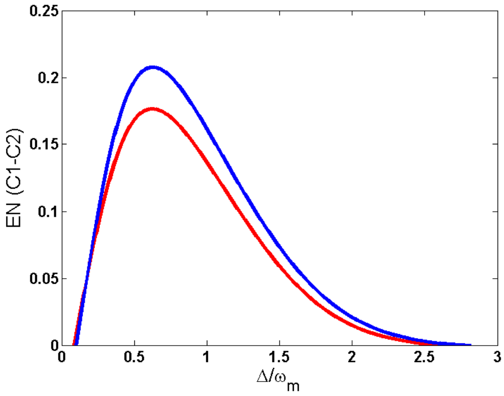

(c)

Figure 9: Plots of EN between (a) the first cavity-mechanical oscillator modes, (b) the second cavity-mechanical oscillator modes, and (c) the two cavity modes as a function of the normalized detuning $\triangle/\omega$, $\Omega = 0.95\beta$, blue solid and red solid lines correspond to the parameters $P_1 = 100mW$ and $P_2 = 50mW$, respectively. The rest of the parameters are taken to be the same as in Figure 7.

From Figures 9 (a), (b), and (c), we observe that the entanglement of the coupled cavity optomechanical systems increases when the laser power is increased. That means increasing the input laser power increases the mean photon number, leading to increase the coupling rate g_j. The reason is that the real part of the effective coupling rate is given by $g_j = \sqrt{2}G_{mj}\alpha_s$. Since the steady-state amplitudes α_{1s} of the cavity fields are proportional to the laser driving amplitude E_J, it should be realized that the g_j factor in the drift matrix A is essentially determined by $g_j \propto G_m E_j$. This shows that the behavior of the coupling rate g_j on the entanglement is consistent with a recent experiment (Thompson et al., 2008). Therefore, one can show that our discussion of steady-state entanglement is actually experimentally realistic.

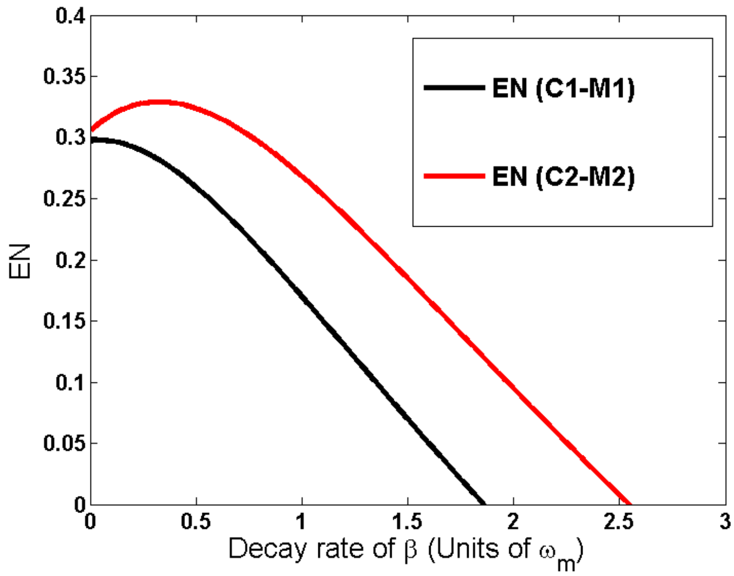

Figure 10: Plots of EN of the first cavity-mechanical oscillator modes (red solid line) and the second cavity-mechanical oscillator modes (black solid line) as a function of the decay rate β, for $T = 100mK$, $\Omega = 6 \times 10^6 s^{-1}$, where the other parameters are taken to be the same as in Figure 7.

In Figure 10, we observe that the bipartite entanglement between the cavity-mechanical oscillator modes increases as the cavity field decay rate decreases. In other worlds, when the decay rate increases, the bipartite entanglement degrades. In fact, from Figure 10, we also see that the optical cavity losses destroy entanglement. Therefore, decay rates decrease the bipartite entanglement and produce different amounts of bipartite entanglement in the subsystem. Additionally, the bipartite entanglement between the mechanical oscillators is not a monotonic function of the decay rate. In fact, external factors like temperature variations in the surrounding environment can contribute to thermal noise in sensitive measurements. Thus, we prefer cryogenic temperature $T = 100mK$ since, the system requires very low temperatures.

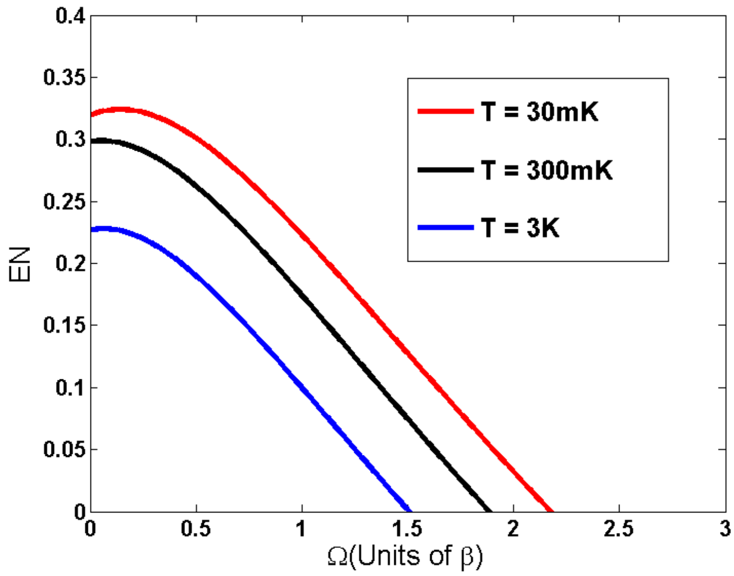

Figure 11: Plots of *EN* as a function of the nonlinear gain of Ω for various temperatures and the other parameters are taken to be the same as in Figure 7.

Moreover, we plot the entanglement versus the nonlinear gain of Ω for various temperatures. From Figure 11, we observe that as the temperature of the environment increases, the bipartite entanglement between the subsystems decreases. This implies that at the moderate value of nonlinear gain, the bipartite entanglement increases. Furthermore, at a large value of nonlinear gain, the entanglement decreases. This shows that our system would prefer to work at cryogenic temperatures. Furthermore, from our theoretical point of view, we investigated the entanglement between the cavity and mechanical oscillator modes, and the two cavity modes are analyzed through the applicable choice of nonlinear gain of OPA, optical cavity detuning, and cavity-cavity coupling strength. However, it is possible to generate the entanglement for the optomechanical subsystem between the two mechanical modes. To achieve this, we have to fix the cavity-laser detuning associated with the mechanical resonator. Therefore, under this regime and by switching the roles of the cavity modes and the mechanical mode, comparable techniques were utilized to generate entanglement between the subsystems, such as two mechanical resonators (Yang et al., 2017; Li et al., 2015a). Subsequently, there is a state transfer between the mechanical resonator and the cavity mode. This confirms that there is still a possibility of generating entanglement between subsystems. Such entanglement between the two mechanical oscillators is very sensitive to the choice of cavity-cavity coupling strength. Since, in our model, there is no direct interaction between two mechanical oscillators, and the entanglement is entirely transferred due to cavity-cavity coupling strength. This confirms we can generate the entanglement by fixing the value of cavity-cavity coupling strength, and one can measure the optomechanical entanglement between two oscillators. From the above, we can conclude that by exchanging the roles of the cavity modes, the mechanical modes, and cavity-cavity coupling strength, a similar mechanism can be used to prepare the entanglement between the two mechanical oscillators interacting with the cavity modes.

4.2. Correlations in an optomechanical system with three-level atoms

4.2.1 Generation of stationary entanglement

Stationary entanglement is a convenient entanglement measure because it is the only one that can always be explicitly computed. To compute the steady-state entanglement, we choose the stationary entanglement (Adesso et al., 2004), which is defined as

$$E_N = max[0, -\ln 2\bar{\Sigma}], \tag{4.1}$$

where $\bar{\Sigma}$ is the minimum symplectic eigenvalue of partial transposed CM corresponding to the bipartite system of interest, which is given by

$$\bar{\Sigma} = \sqrt{\frac{\Sigma(Z) - \sqrt{\Sigma(Z)^2 - 4detZ}}{2}},$$

where Z can be expressed in a form of block matrix extracted from the covariance matrix. R as as

$$Z = \begin{pmatrix} Z_A & Z_C \\ Z_C^T & Z_B \end{pmatrix} \tag{4.2}$$

and $\sum(Z)$ = $detZ_A + detZ_B - 2detZ_C$, where each element of the block plays as a 2×2 of the correlation matrix. Once the covariance matrix is obtained, we then reduce the 8×8 CM to a 4×4 sub-matrix. The CM characterizes the system since the blocks Z_A and Z_B are associated with the oscillating mirror and cavity modes, respectively. The block matrix Z_C describes the optomechanical correlation in the presence of atoms. If the partially transposed density matrix has no negative eigenvalues (i.e., it is positive semi-definite), the logarithmic negativity will be zero, meaning it does not detect entanglement.

In this section, we discuss and study the nature of steady-state entanglement and quantum correlation between the cavity and mechanical oscillator modes by concentrating on the presence and absence of atoms' effects on stationary entanglement and Gaussian quantum discord, respectively. We begin our discussion of the stationary entanglement and Gaussian quantum discord for an optomechanical cavity approved by the presence of three-level atoms, two-level atoms, and in the absence of atoms. Besides, the results are obtained by adopting the following experimental parameters analogous to Refs.

With this consideration, we get stationary entanglement as a function of normalized detuning $\triangle/\omega_m$.

Table 3: List of experimental parameters for the system (Gigan et al., 2006; Barzanjeh et al., 2019; Ma and Zhou, 2012; Lai et al., 2021; Gut et al., 2020; Kleckner and Bouwmeester, 2006)

Symbol	Value
ω_m	$2\pi\times$ 10 MHz
Q	10^5
λ	810nm
L	1mm
m	$5\times10^{-12}kg$
P	50 mW
F	1.07×10^4
γ	$2\pi\times100Hz$
κ	$88MHz$
ω_0	7.8×10^{14}
G	$700Hz$
γ_a	2000
$\Gamma^{'}$	$\pi\times10^6$
$\Gamma^{''}$	$1.4\pi\times10^6$
$g_1=g_2$	$3\pi\times10^5$
$\phi^{'}$	$1.8\pi\times10^7$
$\phi^{''}$	$3.2\pi\times10^7$

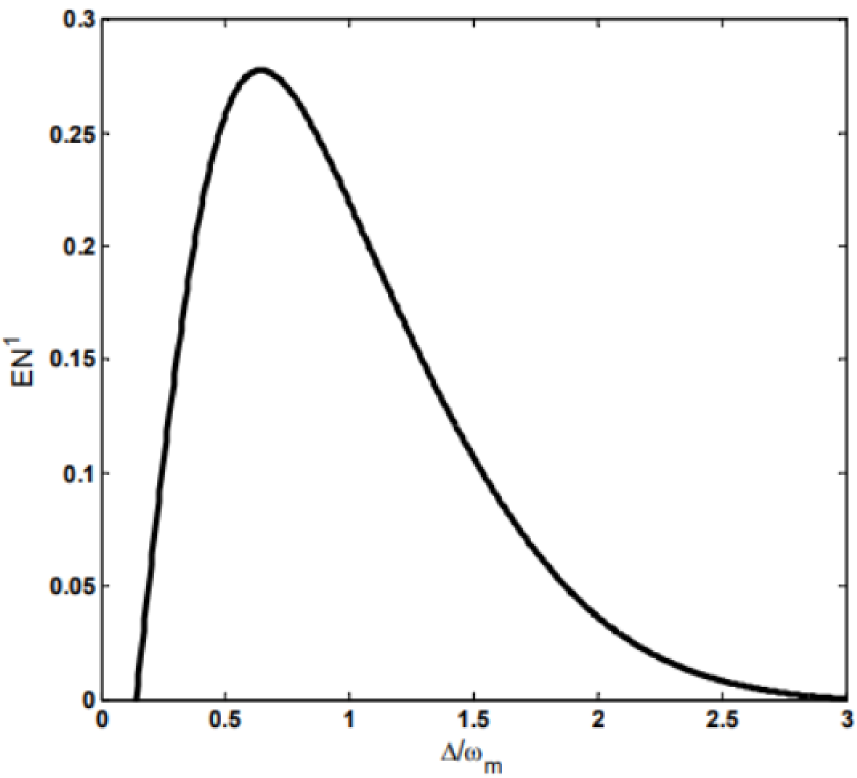

Figure 12: Plots of EN^1 as a function of the normalized detuning $\triangle/\omega_m$ of cavity-mechanical oscillator mode in the absence of atoms. The parameters are given in the Table 3.

The stationary entanglement between the cavity and mechanical oscillator modes in the absence of atoms is plotted against the normalized detuning in Figure 12. The graph's curve indicates that, for a certain parameter range, continuous variable entanglement is present. Keep in mind that the maximum entanglement happens close to the resonance case, and the value of entanglement in the absence of an atom reaches its maximum value, which is similar to a Fabry-Pérot experiment that can be used to determine the degree of entanglement between the cavity and mechanical oscillator modes of an optomechamical cavity without atoms. Therefore, the degree of entanglement between the cavity and mechanical oscillator modes of an optomechamical cavity without atoms is consistent with a Fabry-Pérot experiment.

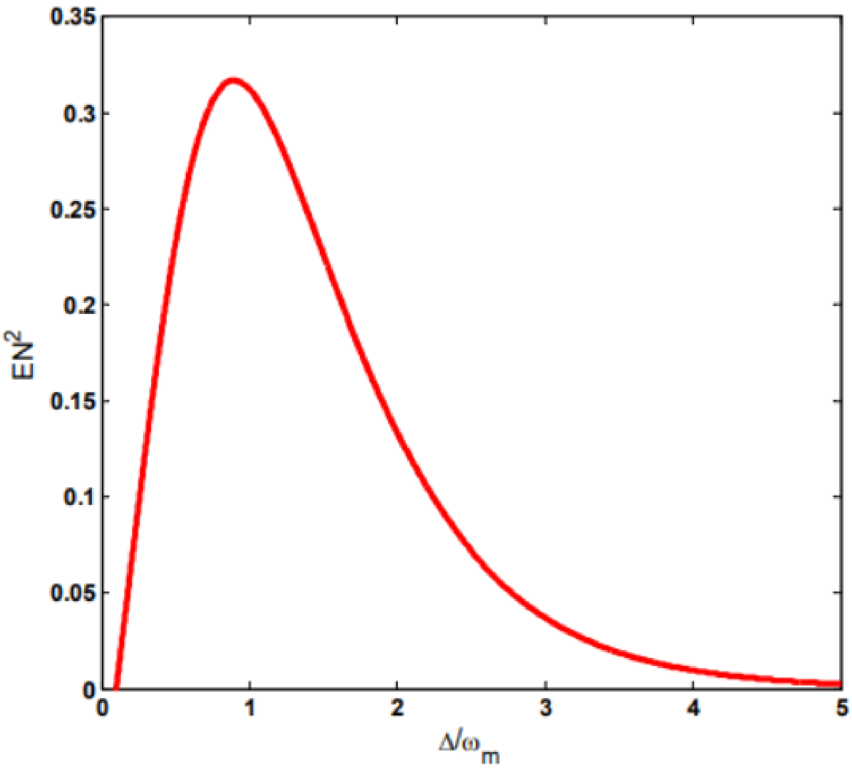

Figure 13: Plots of EN^2 versus the normalized detuning $\triangle/\omega_m$ for cavity-mechanical oscillator mode in the presence of two-level atoms and the parameters are the same as in Figure 12.

Moreover, Figure 13 shows the stationary entanglement of cavity-mechanical oscillator mode in the presence of two-level atoms as a function of the normalized detuning $\triangle/\omega_m$. The curve indicates the same behavior as Figure 12, which is that continuous variable entanglement persists for the parameter $\triangle/\omega_m$. Specifically, the value of entanglement in the presence of two-level atoms is increased, and similarly, the maximum entanglement occurs near the ringing case. Therefore, the degree of entanglement between the cavity and mechanical oscillator mode for the optomechanical cavity in the presence of two-level atoms can be increased when we compare it with the steady-state entanglement of a Fabry-Pérot experiment without atoms.

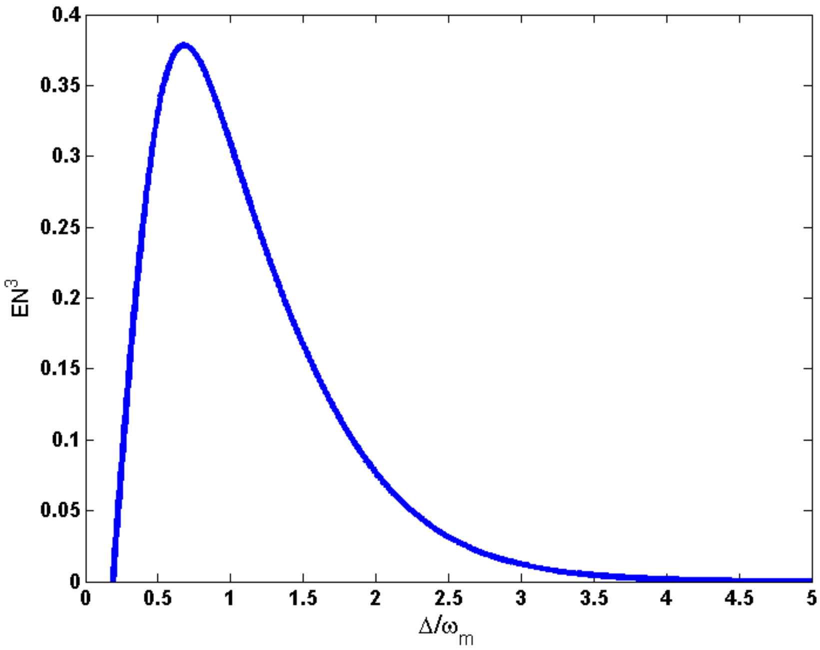

Figure 14: Plots of EN^3 versus the normalized detuning $\triangle/\omega_m$ for cavity-mechanical oscillator mode in the presence of three-level atoms, and the parameters are the same as in Figure 12.

In addition, Figure 14 shows the stationary entanglement as a function of the normalized detuning $\triangle/\omega_m$ between the cavity and mechanical oscillator modes when three-level atoms are present. The entanglement between the cavity and mechanical oscillator mode is generated in the steady state. With normalized detuning, the generated steady-state entanglement increases up to a certain range and then decreases. Furthermore, the behavior of the curve explains why the entanglement persists as a continuous variable. In particular, the value of entanglement in the presence of three-level atoms is enhanced and dramatically decreases when normalized detuning increases. The maximum entanglement also occurs near the resonance case.

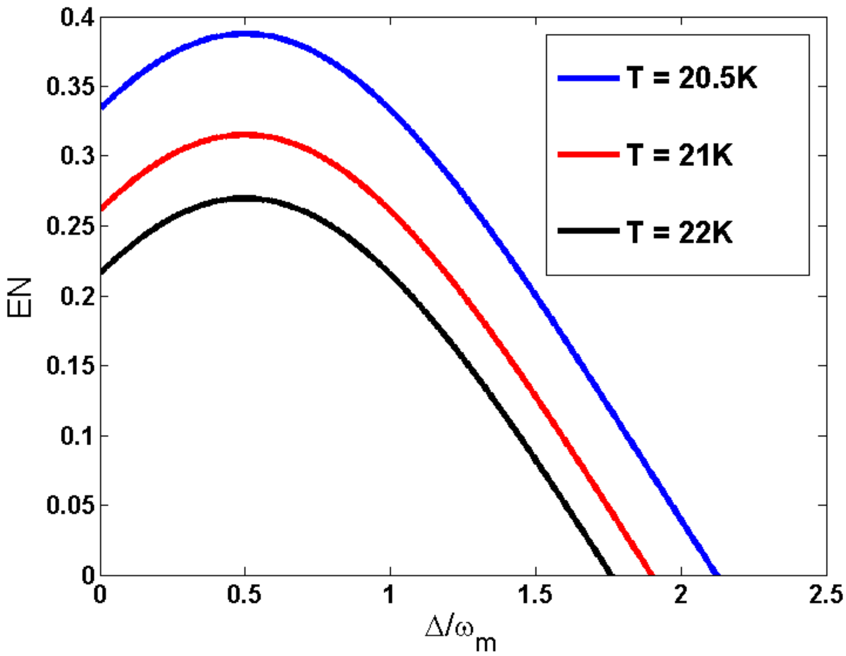

Figure 15: Plots of (a) stationary entanglement between cavity-mechanical oscillator modes in the presence of three-level atoms for various temperatures $T = 20.5K$ (blue solid curve), $T = 21K$ (red solid curve), and $T = 22K$ (black solid curve) of the atoms as a function of the normalized detuning $\triangle/\omega_m$. The other parameters are the same as in Figure 12.

In particular, we saw in Figure 15 that when the environment's temperature drops, the degree of entanglement produced by three-level atoms injected into a Fabry-Pérot cavity increases. Additionally, the injected three-level atoms can help to improve the degree of steady-state entanglement between the cavity and the mechanical oscillator mode compared to the value without the injection of atoms. Therefore, the entanglement is temperature-dependent, exhibiting the same behavior as an entanglement measurement using a Fabry-Pérot cavity injected with two-level atoms (Ma and Zhou, 2012).

Finally, we investigate how the steady-state entanglement is affected by the coupling rate for varying input laser power. The stationary entanglement of a three-level atom-injected optomechanical cavity as a function of normalized detuning is shown in Figure 16.

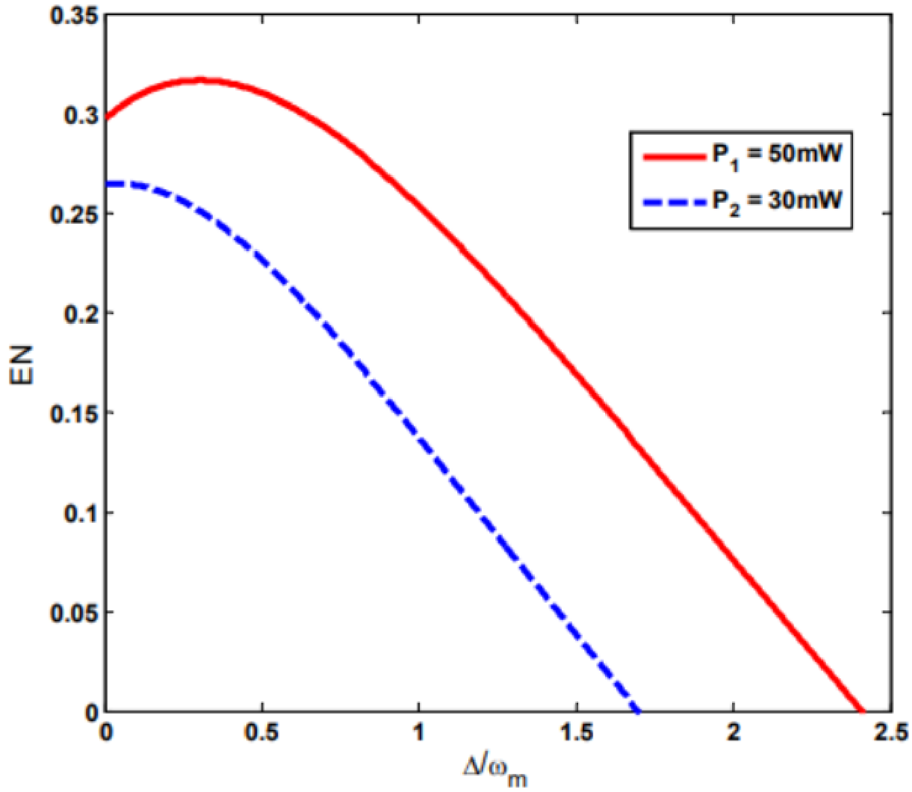

Figure 16: Plots of stationary entanglement between cavity-mechanical oscillator mode in the presence of three-level atoms as a function of the normalized detuning, blue dashed and red solid lines correspond to the parameters $P = 30mW$ and $P = 50mW$, respectively. The other parameters are the same as in Figure 12.

We can see that the entanglement rises with input laser power in this output figure. That shows that increasing the input laser power increases the mean photon number, leading to an increase the coupling rate. The mean photon number and the effective coupling rate are directly correlated, which explains the reason. This suggests that the coupling rate's behavior on the entanglement is in line with the findings of a recent experiment (Thompson et al., 2008). Thus, one can show that our discussion of steady-state entanglement is actually experimentally realistic.

4.2.2 Generation of Gaussian quantum discord

Furthermore, it has been proposed that in certain models of quantum computing and quantum communication, quantum discord plays an important role (Datta and Gharibian, 2009; Cui and Fan, 2010). More broadly, the quantum discord quantifies the nonclassical correlations of a more fundamental type, since separable mixed states can have a nonzero quantum discord. This implies that quantum correlations in classical communication may arise from the existence of nonorthogonal quantum states. Quantum discord, the fundamental building block of quantum information, is realized through bipartite systems of continuous variables, which are defined by Gaussian states with two modes. Therefore, it is acknowledged that a quantum correlation offers a broader approach to measuring the separation between quantum systems. In particular, Gaussian quantum discord is a useful class of correlation measures for continuous variables. We study quantum discord as two manifestations of mutual information. The covariance matrix is actually an 8×8 dimensional matrix. Specifically, to use Gaussian quantum discord to study quantum correlation. We illustrate the entire Z from Eq. (4.2) covariance matrix is 4×4 sub-matrices. In this way, a bipartite Gaussian state that is described by its two-mode covariance matrix. The Gaussian quantum discord is defined as (Yang et al., 2015; Giorda and Paris, 2010).

$$D = U(\sqrt{Z_2}) - U(\gamma^-) - U(\gamma^+) - U(\frac{\sqrt{Z_1 + 2\sqrt{Z_1 Z_2} + 2\Psi}}{1 + 2\sqrt{Z_2}}), \tag{4.3}$$

where for any Θ,

$$U(\Theta) = (\Theta + \frac{1}{2}) log(\Theta + \frac{1}{2}) - (\Theta - \frac{1}{2}) log(\Theta - \frac{1}{2}), \gamma^{\pm} = \frac{1}{2}\sqrt{\Lambda \pm \sqrt{\Lambda^2} - 4Z_4},$$
$$\Lambda = Z_1 + Z_2 + 2\Psi, Z_1 = det(Z_A), Z_2 = det(Z_B), Z_3 = det(Z_C), and Z_4 = det(Z). \tag{4.4}$$

In this section, we also discuss the nature of the quantum correlation between the cavity and mechanical oscillator modes by concentrating on the presence and absence of atoms' effects. Gaussian quantum discord. We assume the Gaussian quantum discord, represented by D_1, D_2, and D_3, between the cavity and mechanical oscillator modes in the absence of atoms and the presence of two-level and three-level atoms, respectively.

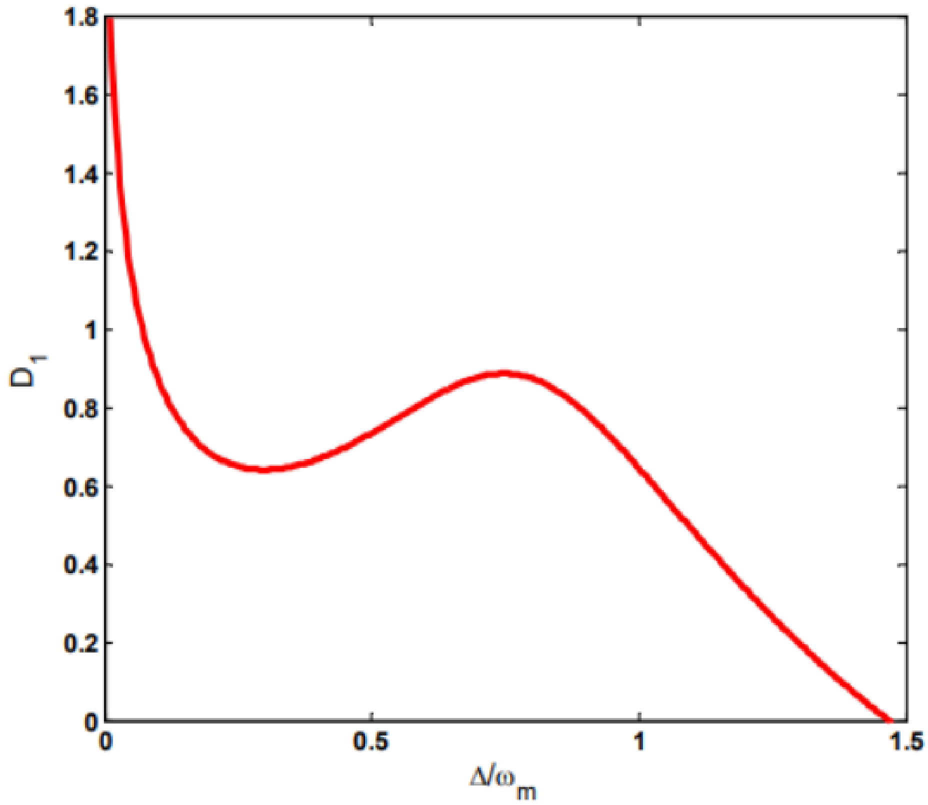

Figure 17: Plots of D_1 as a function of the normalized detuning $\triangle/\omega_m$ of cavity-mechanical oscillator mode in the absence of atoms. The other parameters are the same as in Figure 12.

Figure 17 presents the results of the Gaussian quantum discord as a function of the normalized detuning $\triangle/\omega_m$ parameter. It is evident from Figure 17 that there is a Gaussian quantum discord between the cavity and mechanical oscillator mode in the absence of atoms, which reaches a maximum when the normalized detuning value approaches zero. Furthermore, the Gaussian quantum discord decreases when the value of normalized detuning increases. Conversely, when the normalized detuning value lies between some intervals, the Gaussian quantum discord is entangled $(D > 1)$. On the other hand, the covariance matrix can be correlated or unentangled $(D < 1)$ for the values of $\triangle/\omega_m$ increased.

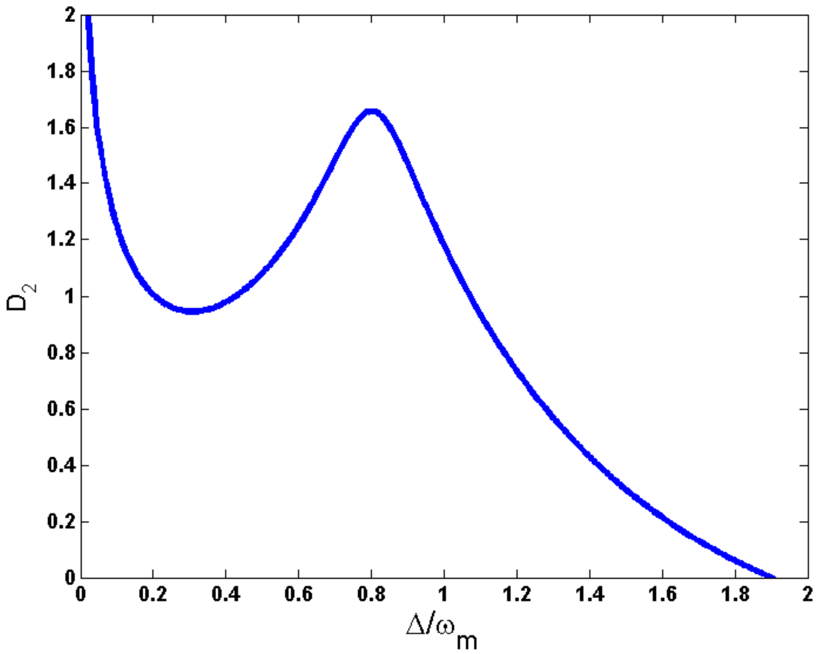

Figure 18: Plots of D_2 versus the normalized detuning $\triangle/\omega_m$ of cavity-mechanical oscillator mode in the presence of two-level atoms, and the parameters are the same as in Figure 12.

The dynamical Gaussian quantum discord is plotted against the normalized detuning parameter in Figure 18. The Gaussian quantum discord reaches a maximum value when the normalized detuning value approaches zero. The figure makes it evident that there is an increase in the Gaussian quantum discord between the cavity and mechanical oscillator when two-level atoms exist. However, the Gaussian quantum discord decreases when the value of normalized detuning increases. Additionally, when the values of normalized detuning increase to a certain range, the Gaussian quantum discord is entangled $(D > 1)$. Conversely, the covariance matrix can be correlated or not entangled $(D < 1)$ for some interval of $\triangle/\omega_m$.

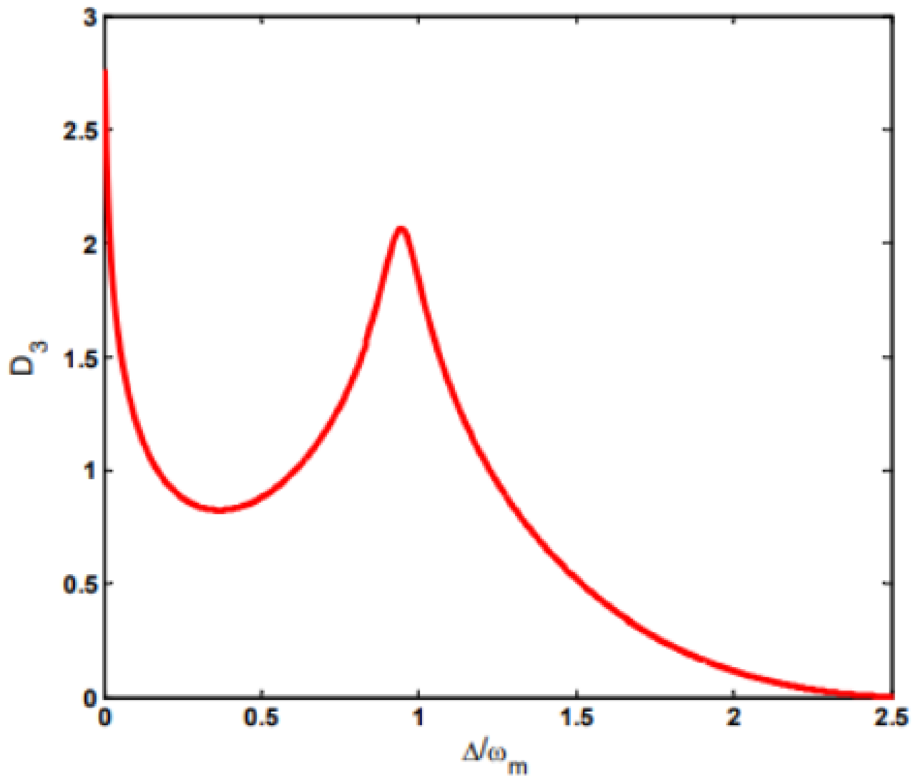

Figure 19: Plots of D_3 versus the normalized detuning $\triangle/\omega_m$ of cavity-mechanical oscillator mode in the presence of three-level atoms, and the parameters are the same as in Figure 12.

The findings displayed in Figure 19 make it abundantly evident that, in the presence of three-level atoms, there is a Gaussian quantum discord between the cavity and the mechanical oscillator against the normalized detuning parameter. The Gaussian quantum discord increases and reaches its maximum value when the value of normalized detuning disappears. Additionally, as the value of normalized detuning increases, the Gaussian quantum discord monotonically decreases. The Gaussian quantum discord is entangled $(D > 1)$ when the value of normalized detuning $\triangle/\omega_m$ increases. While, for a certain range of normalized detuning $\triangle/\omega_m$, the Gaussian quantum discord can be correlated or not entangled $(D < 1)$.

Additionally, we plotted the quantum discord for different system temperatures as a function of the normalized detuning. The quantum discord D is plotted against the normalized detuning for a range of temperature values in Figure 20.

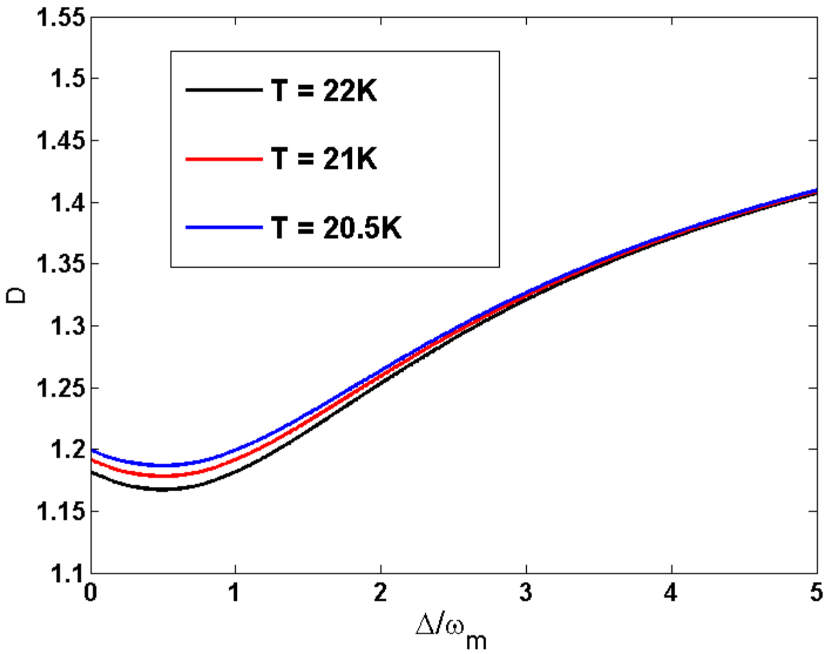

Figure 20: Plots of Gaussian quantum discord between cavity-mechanical oscillator modes in the presence of three-level atoms for various temperatures $T = 20.5K$ (blue solid curve), $T = 21K$ (red solid curve), and $T = 22K$ (black solid curve) of the atoms as a function of the normalized detuning $\triangle/\omega_m$. The other parameters are the same as in Figure 12.

Furthermore, quantum effects such as entanglement and discord can be generated under cryogenic temperatures, typically in the range of millikelvins (mK) to a few kelvins (K), in order to achieve and observe quantum effects. Moreover, those temperature regimes provide quantum dominance, where thermal noise is greatly suppressed, allowing for the observation of delicate quantum phenomena and the study of quantum behavior with minimal thermal disturbances.

More importantly, from the above results, we observed that the atoms injected into the cavity have a strong influence on the enhanced steady-state entanglement and Gaussian quantum discord. Through a comparison of the three curves, we found that the three-level atoms injecting an optomechanical cavity exhibit more enhanced steady-state entanglement and quantum discord than the two-level atoms. Similarly, when two-level atoms are injected into an optomechanical cavity, they also become more entangled or correlated than they would be in an optomechanical cavity without atoms. It is important to note that the emergence of quantum entanglement and correlation is caused by the presence of atoms, especially in light of the observed result. Thus, by contrasting this entanglement measurement's behavior with previous studies of a Fabry-Pérot cavity driven by coherent light and devoid of atoms of an oscillating micro-mirror (Vitali et al., 2007), and in the case of two or three-level atoms, the steady-state entanglement between the cavity field and the movable mirror is highly increased.

4.3. Quantum correlations through OPA in an optomechanical system

4.3.1 Generation of Stationary Entanglement

To quantitatively measure the stationary entanglement between different modes, we utilized E_N (Vidal and Werner, 2002), which defined as

$$E_N = max[0, -\ln 2\bar{\zeta}], \tag{4.5}$$

where $\bar{\zeta}$ is the minimum symplectic eigenvalue of partial transposed *CM* corresponding to the bipartite system of interest, which is given by

$$\bar{\zeta} = \sqrt{\frac{\sum(A) - \sqrt{\sum(A)^2 - 4detA}}{2}},$$

where A can be expressed in a form of block matrix extracted from covariance matrix as as

$$A = \begin{pmatrix} R_A & R_C \\ R_C^T & R_B \end{pmatrix} \tag{4.6}$$

and $\sum(A) = detR_A + detR_B - 2detR_C$, where R_A, R_C, and R_B are being 2×2 blocks matrices and can be extracted from the correlation matrix $\mathbb{V}$. Specifically, the correlation matrix associated with the selected bipartite can be obtained by neglecting the rows and columns in the uninteresting mode in the 8×8 correlation matrix $\mathbb{V}$.

We trace over the remaining degrees of freedom to obtain the entanglement of the possible bipartite subsystems, i.e., between cavity-mechanical oscillator modes and cavity-cavity modes, from which we can study the bipartite entanglement in our system. For example, when the bipartite entanglement between the mechanical oscillator mode 1 and the cavity mode 1 is evaluated, we have

$$R_A = \begin{pmatrix} \mathbb{V}_{11} & \mathbb{V}_{12} \\ \mathbb{V}_{21} & \mathbb{V}_{22} \end{pmatrix}, \tag{4.7}$$

$$R_B = \begin{pmatrix} \mathbb{V}_{33} & \mathbb{V}_{34} \\ \mathbb{V}_{43} & \mathbb{V}_{44} \end{pmatrix}, \tag{4.8}$$

and

$$R_C = \begin{pmatrix} \mathbb{V}_{13} & \mathbb{V}_{14} \\ \mathbb{V}_{23} & \mathbb{V}_{24} \end{pmatrix}. \tag{4.9}$$

Logarithmic negativity will be used to quantify this bipartite entanglement. We choose all the following experimental parameters by setting the cavities and mechanical oscillators to be the same, for example: $P_1 = P_2 = P$, $E_1 = E_2 = E$, and $g_1 = g_2 = g$. The results are obtained by adopting the parameters analogous to those in Refs. (Vitali et al., 2007; Schmidt et al., 2015; Giorda and Paris, 2010; Vidal and Werner, 2002).

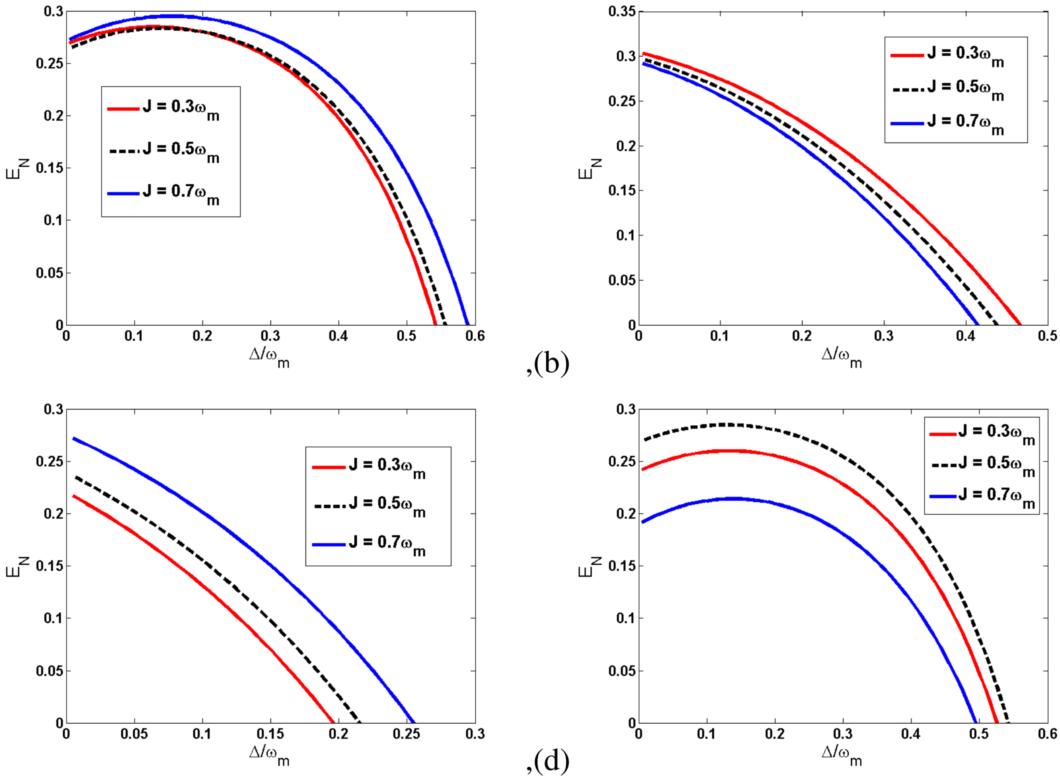

(a) ,(b)

(c) ,(d)

Figure 21: Plots of logarithmic negativity between (a) $C1-M1$, (b) $C2-M2$, (c) $C1-C2$, and (d) $M1-M2$ as a function of the normalized function $\triangle/\omega$ for various values of the cavity-cavity coupling parameter using $\Sigma = 1.4\kappa$ and temperature $T = 100mk$. The other parameters are given in Table 4.

Table 4: List of experimental parameters

Parameters	**Symbol**	**Value**
Frequency of mechanical oscillator	ω_m	$2\pi\times$ 10 MHz
Mass of mechanical oscillator	m	$5\times10^{-12}kg$
Length of the cavity	L	1mm
Optical laser wavelength	λ	810nm
Mechanical quality factor	Q	10^5
Driven laser power	P	60mW
Cavity finesse	F	1.07×10^4
Mechanical damping rate	γ	$2\pi\times\ 100Hz$

First, we generate the steady-state bipartite entanglement between subsystems as a function of the normalized detuning for various values of the cavity-cavity coupling parameter J. Using realistic values of the parameters for which a significant amount of entanglement is achievable, we observed steady-state entanglement as a function of the normalized detuning for various values of the cavity-cavity coupling between cavity-mirrors, two cavity modes, and two mirrors, as shown in Figure 21. Figures 21 (a), (b), (c), and (d) show the logarithmic negativity between the first cavity-mirror, second cavity-mirror, two cavity modes, and between the two mirrors as a function of the normalized detuning, respectively. As indicated above in our model of the system, a degenerate OPA is placed in the second cavity, while the first cavity is without a degenerate OPA coupled through a coupling parameter. Under this circumstance, one can easily observe from Figure 21 (a) that the logarithmic negativity, which accounts for the entanglement of the first cavity-mirror modes, increases with the coupling parameter to a certain range of parameter J. While, in Figure 21 (b), the entanglement between the second cavity-mirror modes decreased as the cavity-cavity coupling parameter increased. On the other hand, from Figure 21 (c), we see that the entanglement between two cavity modes increases with the coupling parameter. Similarly, the result of Figure 21 (d) shows the entanglement between the modes of two mirrors increases with the value of the coupling parameter. The value of the cavity-cavity coupling parameter increases the entanglement between the two cavity modes and the modes of the two mirrors. Furthermore, we found that the range of entanglement between the first cavity - mirrors and between the two mirrors can be expanded by increasing the coupling parameter, which implies that a greater possibility of entanglement can be readily realized in an experiment. This demonstrates how our bipartite entanglement is generated in a way that is consistent with an optomechanical cavity with photonic crystals (Vitali et al., 2007). Then, one could infer that the cavity-cavity coupling parameter can modify the entanglement considerably, meaning that the transfer of quantum features in a hybrid optomechanical cavity would depend greatly on the strength of the coupling. A significant advantage for the practical implementation of remote entanglement preparation in quantum information processing is the observed transfer of entanglement from the two cavities to mechanical mirrors, between the two cavities, and between the two mirrors (Riedinger et al., 2018).

Secondly, another aspect of interest is the influence of the phase of the OPA on the distribution of entanglement between different modes.

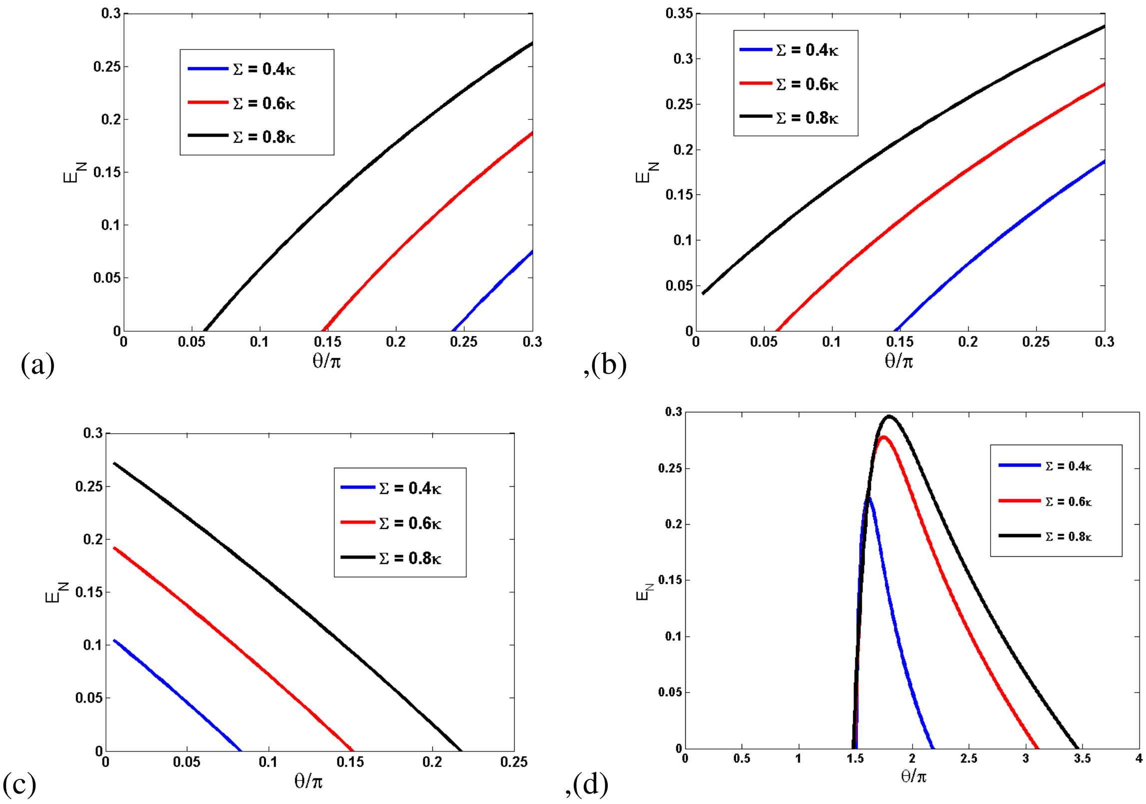

Figure 22: Plots of logarithmic negativity between (a) $C1-M1$, (b) $C2-M2$, (c) $C1-C2$, and (d) $M1-M2$ as a function of the phase with various values of nonlinear gain with the values of cavity-cavity coupling parameter $J = 0.6\omega_m$ and the rest parameters are the same as Figure 21.

Figures 22 (a), (b), (c), and (d) illustrate the logarithmic negativity between the first cavity-mirror and the second cavity-mirror, the two cavity modes, and the modes of the two mirrors as a function of the phase with various values of nonlinear gain. We examine the impact of OPA in hybrid optomechanical systems by varying the nonlinear gain of OPA while maintaining all other parameters constant. It is interesting to note that, entanglement greatly depends upon the choice of Σ. In this respect, we also show the plot of logarithmic negativity as a function of the phase with various values of three different choices of nonlinear gain. For instance, in Figure 22 (a), the value of entanglement increases with the value of the nonlinear gain of the OPA medium. Similarly, in Figure 22 (b), the value of entanglement also increases with increasing the value of nonlinear gain. Furthermore, Figure 22 (c) shows the plot of the logarithmic negativity between two cavity modes as a function of the phase with various values of nonlinear gain. Particularly, it indicates that a large value of nonlinear gain generates a large value of entanglement, while a small value of entanglement generates a small value of nonlinear gain in the in the OPA medium. Figure 22 (d) shows plots of the logarithmic negativity between the two mirrors as a function of the phase with various values of nonlinear gain. From these results, we see that the presence of OPA enhances the generation of entanglement between two mirrors. It may not be difficult to see from Figure 22 that the logarithmic negativity is enhanced with the value of the nonlinear gain of OPA medium. It is important to note in light of the observed result that the hybrid optomechanical cavity's cavity-cavity coupling parameter, in addition to the presence of degenerate OPA in the second cavity, is what's responsible for the emerging enhanced entanglement between subsystems. Consequently, it can be observed that this entanglement measurement is strengthened by OPA when compared to previous studies of a Fabry-Perot cavity driven by coherent light and lacking degenerate OPA of an oscillating micro mirror (Vidal and Werner, 2002). These findings help optimize system performance and offer valuable insights into underlying quantum mechanical interactions, with potential applications in quantum technologies.

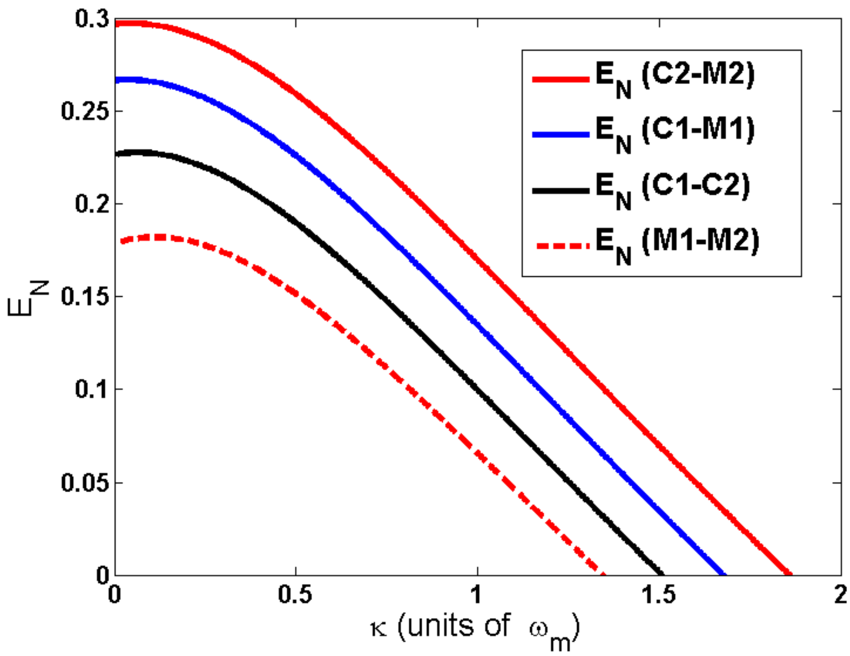

Figure 23: Plots of logarithmic negativity between $C1-M1$, $C2-M2$, $C1-C2$, and $M1-M2$ as a function of decay rates and the other parameters are taken to be the same as Figure 21.

Next, we discuss the effect of the decay rate on bipartite entanglement. In Figure 23, we plot entanglement as a function of decay rate values. Our results show that as the cavity field decay rate decreases, entanglement increases. This implies that while higher nonlinear gain enhances entanglement, decay rates significantly impact its sustainability. Consequently, different decay rates lead to varying levels of bipartite entanglement in the subsystem, generally reducing entanglement as decay rates increase. Therefore, balancing gain and decay rates is essential for maintaining robust entanglement, with high decay rates diminishing entanglement unless countered by sufficiently high OPA gain.

4.3.2 Generation of Quantum Correlations via Quantum Discord

Furthermore, we use another quantum correlation quantifier, which is a fundamental notion allowing for the description of the quantumness of the correlations present in the state of a quantum system. In our case, the Gaussian quantum discord denotes non-classical correlations if the two distant cavity fields mirror and a distant cavity field and two distant mirrors are separable or not. Employing Eq. (4.6) on Eqs. (2.40) and (2.43), the Gaussian quantum discord for the subsystem can be obtained (Giorda and Paris, 2010; Mekonnen et al., 2023). In this way, we used the quantum quantifier of quantum discord to quantify the correlations between the subsystems. In particular, Gaussian quantum discord offers a way to detect and measure non-classical correlations between different modes, like whether or not optical-to-mechanical correlations are separable.

Thus, from our theoretical perspective, we looked into the Gaussian quantum discord between two distant mirrors, two cavity fields, and a mirror and a cavity field by selecting the appropriate parameters for the cavity-cavity coupling parameter, optical cavity detuning, and parametric gain of OPA.

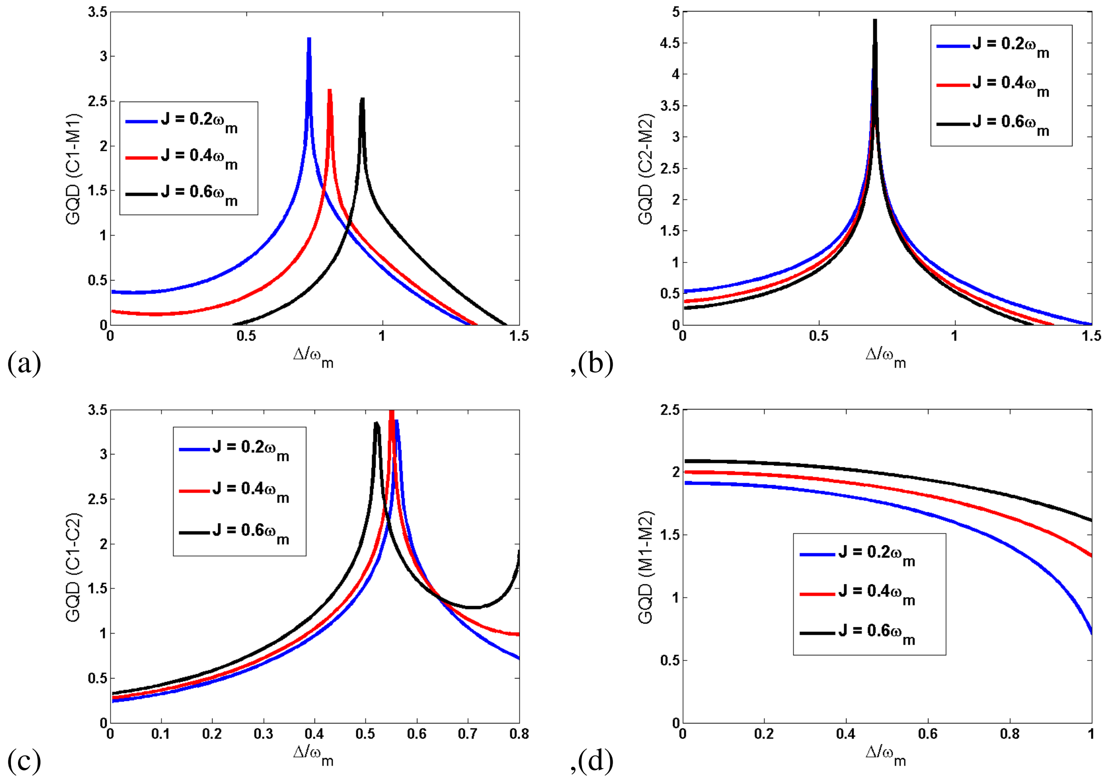

Figure 24: The plot of GQD between (a) $C1-M1$, (b) $C2-M2$, (c) $C1-C2$, and (d) $M1-M2$ as function of normalized detuning $\triangle/\omega$ for various values of cavity-cavity coupling parameter. The other parameters are the same as in Figure 21.

Figure 24 (a) demonstrates that when the cavity-cavity coupling increases, the Gaussian quantum discord between the first cavity-mirror decreases to a certain range. It is enhanced with the value of $J = 0.2\omega_m$ (green solid curve) and reaches its maximum value at the critical point of the normalized detuning. Conversely, the Gaussian quantum discord decreases as the normalized detuning increases after increasing to a certain range. Furthermore, Figure 24 (b) shows the Gaussian quantum discord between the second cavity-mirror as a function of normalized detuning for various values of the cavity-cavity coupling parameter. The *GQD* increases with the normalized detuning, and the maximum value is reached with $J = 0.6\omega_m$ (black solid curve) at the critical point. While after the critical point, the *GQD* decreases, normalized detuning. Specifically, the *GQD* decreases when the coupling parameter increases. In both cases, we observed that the covariance matrix can be correlated or not entangled when it is less than one, whereas the *GQD* is entangled when Gaussian quantum discord is greater than one. Furthermore, Figure 24 (c) shows the plot of the Gaussian quantum discord between two cavity fields as a function of normalized detuning for various values of cavity-cavity coupling strength. When the normalized detuning number is gradually increased, we observe that the Gaussian quantum discord amount varies between its maximum and minimum bounds. This makes it evident that in Figure 24 (c), the Gaussian quantum discord value rises, reaches its maximum at the normalized detuning critical value, and then dramatically falls to a specific range. On the other hand, in Figure 24 (c), the quantum discord value increases with the coupling parameter value. Conversely, the cavity-cavity coupling parameter $J = 0.4\omega_m$ yielded the maximum value (red-solid curve). Furthermore, Figure 24 (d) clearly indicates that the Gaussian quantum discord between two distant mirrors against the normalized detuning parameter for various values of coupling parameter $J = 0.2\omega_m$ (green-solid curve), $J = 0.4\omega_m$ (red-solid curve), and $J = 0.6\omega_m$ (black-solid curve). The *GQD* is generated and increases as the coupling parameter increases. It is possible to generate *GQD* for the hybrid optomechanical subsystem between the two mechanical modes. The two cavity modes work together with the mechanical oscillator to exchange the roles of the cavity and mechanical modes to fix the effective detuning value, choose the cavity-laser detuning properly by fixing the value of the OPA's nonlinear gain, and prepare the *GQD* between the two mechanical oscillators interacting with the cavity modes. In general, from Figure 24, we can see that the enhanced Gaussian quantum discord strongly depends on the coupling strength. Furthermore, from our point of view, it is evident to us that the covariance matrix exhibits either entangled or unentangled within specific detuning parameter intervals, as indicated by the Gaussian quantum discord, which shows a midpoint value between zero and unity. Consequently, an entangled covariance matrix can be created from the interaction of an interacting optical parametric amplifier in a hybrid optomechanical system. Numerous applications in secure communication and quantum information theory can benefit from these findings, both analytically and experimentally. A similar interpretation using distinct systems was documented in Refs. (Liu et al., 2015; Zhao et al., 2017). Consequently, we can enumerate the prerequisites required to assess the quality of correlations between the coupled hybrid optomechanical cavities based on the results above. In fact, we can draw the conclusion that different optomechanical parameters are controllable. In general, by maintaining different initial settings of parametric gain of OPA and strength of coupling between cavity parameters, the corresponding covariance matrices are correlated, especially when the Gaussian quantum discord is plotted with respect to changes in the normalized detuning parameter. Therefore, the study of GQD contributes to a deeper understanding of broader quantum correlations beyond entanglement within such systems. It highlights potential pathways for enhancing quantum coherence and advancing applications in quantum technology.

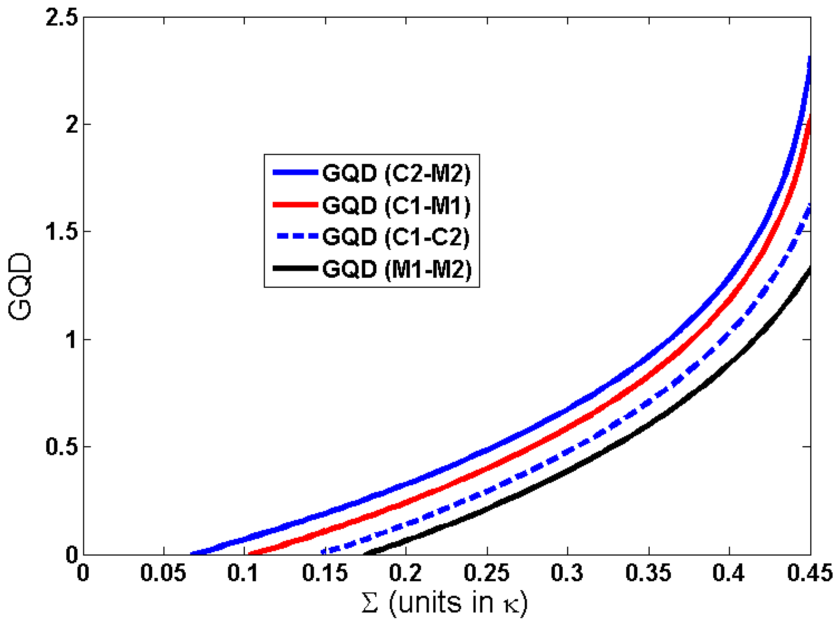

Figure 25: The plot of *GQD* between the C1-M1 (red-solid line), $C2-M2$ (blue-solid line), $C1-C2$ (blue-dashed line), and $M1-M2$ (black-solid line) as a function of parametric gain Σ with the values of cavity-cavity coupling parameter $J = 0.4\omega_m$, the other parameters are taken to be the same as Figure 21.

Furthermore, we discuss the Gaussian quantum discord between cavity-mirrors, two cavity fields, and two mirrors as shown in Figure 25 as a function of parametric nonlinear gain (Σ). The choice of parametric gain has a significant impact on the quantum discord. The Gaussian quantum discord of the system increases with the parametric gain at the given environmental temperature. The decrease in parametric nonlinear gain Σ reduces the enhancement of quantum discord between two mirrors, and two cavity fields, as well as between a mirror and a cavity field. In this instance, the OPA can greatly improve quantum discord. Within the hybrid optomechanical system, *GQD* quantifies the quantum correlations between subsystems that go beyond entanglement. It takes into account more general types of Gaussian state quantum correlations. The figures show how the parametric gain affects *GQD*. The optical and mechanical modes' coherence characteristics and interaction strengths are influenced by this parameter. The larger parametric nonlinear gain usually results in stronger nonlinear interactions inside the system, which impacts the quantum correlations that *GQD* captures. For various values of the cavity-cavity coupling parameter, *GQD* is displayed in each plot. The interaction between the optical modes in various cavities is enhanced by higher coupling strengths. Indirect optical coupling effects may influence correlations between two mirrors and result in greater quantum correlations between two cavity fields when there is enhanced coupling.

4.3.3 Generation of quantum steering

A basic asymmetry in the characteristics of quantum systems is demonstrated by steering, a type of quantum correlation. The relationships between subsystems of a composite quantum system, such as quantum entanglement, quantum discord, steerability, and Bell nonlocality, are referred to as quantum correlations. Put another way, suppose Alice tries to convince Bob, who doesn't believe her, that she is involved with him in a complicated way. Let's say Bob wants to convince Alice, so he asks Alice to remotely prepare a set of states for his subsystems. Imagine that Alice notified Bob of the results after taking the necessary measurements covertly. Given the nature of quantum measurement and an analysis of Alice's prepared conditional states, it is interesting to notice that Bob can certify using the concept of quantum steering regardless of whether the measurements originate from an entangled state or not. The roles R_A and R_B could be exchanged in order to achieve steerability. It is important to note at this time that the quantum guidance shown in this form is comparable to quantum discord and logarithmic negativity-quantifiable bipartite entanglement. The ability to change the state of the remote system without necessarily interacting with it is represented by the higher degree of steerability, which could be useful for reliably teleporting quantum information. It is also a measure of the asymmetry between two subsystems' entangled observers. It also offers a means of measuring the degree of steerability that each of the two independent modes possesses. The steerability of $R_A \to R_B$ is defined as (Kogias et al., 2015) if we utilize the covariance matrix of mechanical oscillators of Eq. (2.39) to analyze the information flow between Alice R_A and Bob R_B. From the above, there are two possibilities for quantum steering between R_A and R_B: If $S^{R_A \to R_B} = S^{R_B \to R_A} = 0$, there is no-way steering, which means Alice cannot steer Bob and vice versa even if they are not separable, and two-way steering if $S^{R_A \to R_B} = S^{R_B \to R_A} > 0$. In actuality, a non-separable state is not always a steerable state, while a steerable state is always not separable (Mekonnen et al., 2023; Kogias et al., 2015).

In light of this, we generate the steering between subsystems as a function of the normalized $\triangle/\omega_m$ for various values of the cavity-cavity coupling parameter J.

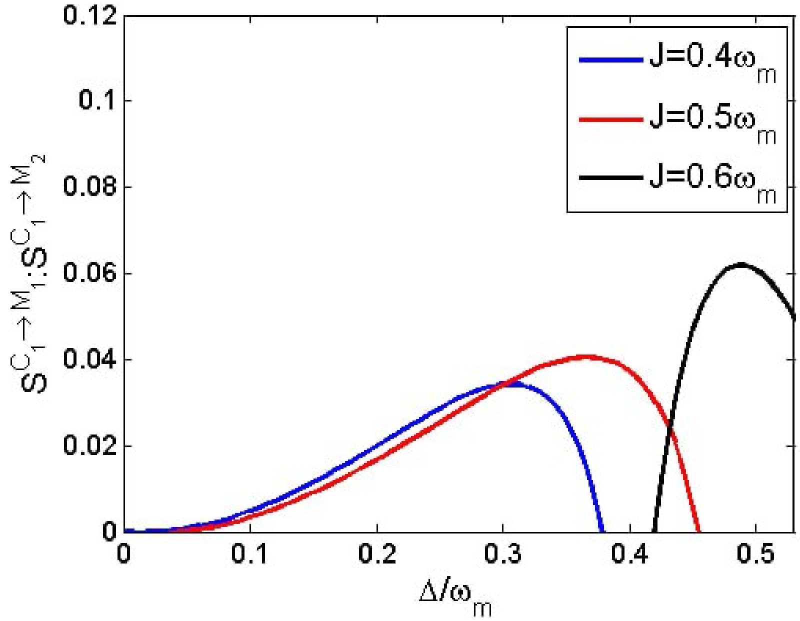

Figure 26: The plot of the steering between the first cavity and the two mirrors as a function of normalized detuning $\triangle/\omega_m$ for various values of cavity-cavity coupling strength $J = 0.4\omega_m$ (blue-solid curve), $J = 0.5\omega_m$ (red-solid curve), and $J = 0.6\omega_m$ (black-solid curve). The other parameters are the same as in Figure 21.

Using realistic values of the parameters, a significant amount of steering is achievable. We observed steering as a function of the normalized detuning for various values of the coupling between the first cavity and the two mirrors, as shown in Figure 26. As indicated above in our model of the system, a degenerate OPA is placed in the second cavity coupled to the first cavity without OPA through the cavity-cavity coupling parameter. Under this circumstance, one can easily observe from Figure 26 that the steering of the first cavity to the two mirrors increases with the coupling parameter to a certain range. Furthermore, we found that the range of steering between the first cavity to the two mirrors can be expanded by increasing the cavity-cavity coupling, which implies that a greater possibility of steering can be readily realized in an experiment.

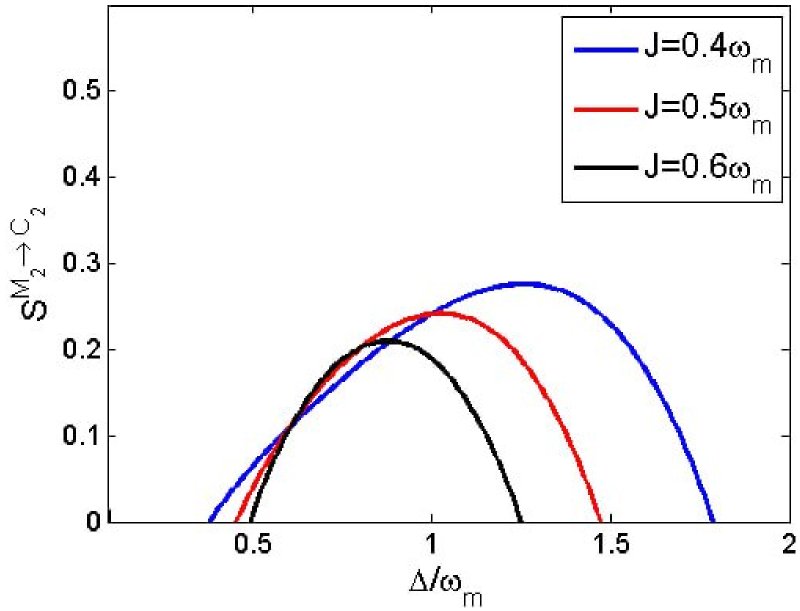

Figure 27: The plot of the steering between the second mirror to cavity field as a function of normalized detuning $\triangle/\omega_m$ for various values of cavity-cavity coupling strength $J = 0.4\omega_m$ (blue-solid curve), $J = 0.5\omega_m$ (red-solid curve), and $J = 0.6\omega_m$ (black-solid curve). The other parameters are the same as in Figure 26.

While, in Figure 27, the steering between the second mirror to cavity field decreased as the coupling parameter increased. However, from this result, we see that the presence of OPA enhances the generation of steering between the second mirror to cavity field.

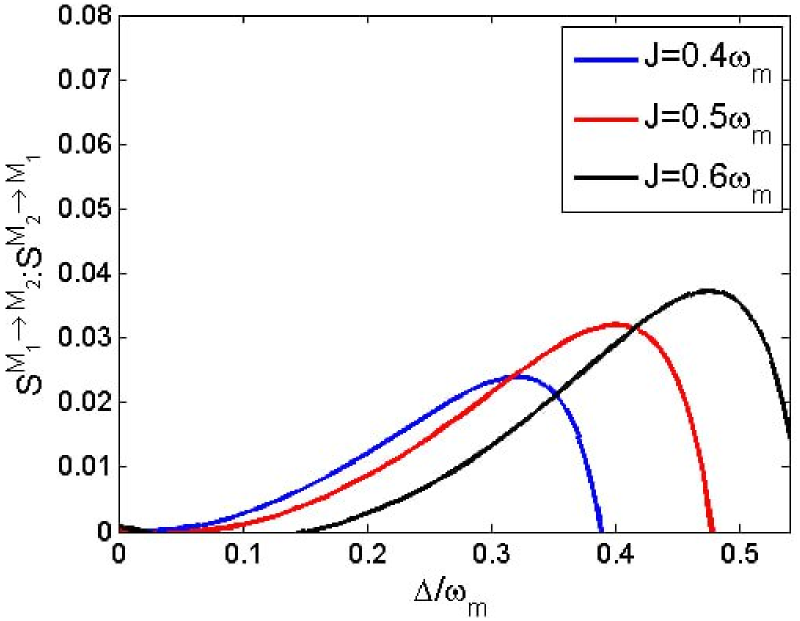

Figure 28: The plot of the steering between the two mirrors as a function of normalized detuning $\triangle/\omega_m$ for various values of cavity-cavity coupling strength $J = 0.4\omega_m$ (blue-solid curve), $J = 0.5\omega_m$ (red-solid curve), and $J = 0.6\omega_m$ (black-solid curve). The other parameters are the same as in Figure 26.

Similarly, the result of Figure 28 shows the steering between the modes of two mirrors increases with the value of the coupling parameter. A significant advantage for the practical implementation of remote steering preparation in quantum information processing is the observed transfer of steering from the two mirrors.

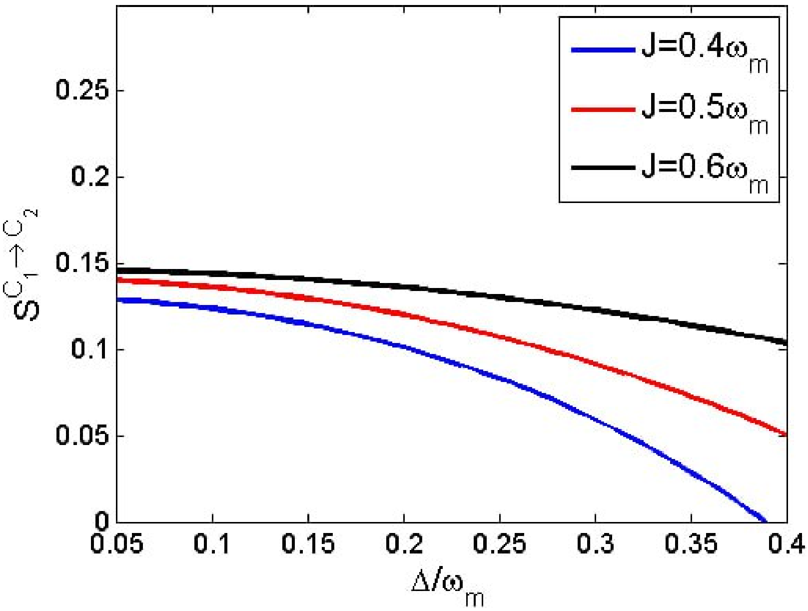

Figure 29: The plot of the steering between the first cavity to the second cavity field as a function of normalized detuning $\triangle/\omega_m$ for various values of coupling strength J = 0.4ω_m (blue-solid curve), J = 0.5ω_m (red-solid curve), and J = 0.6ω_m (black-solid curve). The other parameters are the same as in Figure 26.

Furthermore, Figure 29 shows the plot of the steering between the first cavity to the second cavity field as a function of normalized detuning $\triangle/\omega_m$ for various values of coupling strength. In Figure 29, the quantum steering value increases with the coupling parameter value. These show, in general, how our steering is generated in a manner consistent with steady-state entanglement in a hybrid optomechanical system improved by optical parametric amplifiers (Kibret et al., 2023) and entanglement in an optomechanical cavity containing photonic crystals (Eichenfield et al., 2009). Then, one could infer that the cavity-cavity coupling can modify the steering considerably, meaning that the transfer of quantum features in a hybrid optomechanical cavity would depend greatly on the strength of the coupling.

5. CONCLUSIONS AND RECOMMENDATIONS

5.1. CONCLUSIONS

We have investigated the generation of bipartite quantum features and transfer of quantum states in hybrid optomechanical system with an optical parametric amplifier and three-level atoms. In particularly, we primarily focused on the steady-state entanglement between the two cavity modes, the second cavity-mechanical modes, and the first cavity-mechanical oscillator modes in a hybrid optomechanical system. The cavities in the system, which contain two distinct degenerate OPAs, are externally connected. Because of the measure of logarithmic negativity, we were able to construct the linearized quantum Langevin equations in the steady-state regime and quantify the steady-state entanglement. In this way, at steady-state, the bipartite entanglement is generated by the degenerate OPA. It is discovered that the entanglement rises as the OPA medium's nonlinear gain does. It has also been demonstrated that the type of entanglement between cavity-mechanical oscillator modes is strongly dependent on the strength of cavity-cavity coupling. Furthermore, we have demonstrated that, at an acceptable temperature, the lowest value of entanglement between the two cavity modes is non-zero. This is because the system exhibits entanglement transfer, which has experimental significance. Hopefully, the possibility of entangling the modes of mechanical oscillators externally coupled via sharing the quantum properties of the accompanying OPA may have potential applications in the realization of continuous-variable quantum information processing applications.

Furthermore, we have investigated the impact of atoms on the generation of stationary entanglement and quantum discord between the cavity and mechanical oscillator mode using an optomechanical cavity injected with three-level atoms. Specifically, we quantified steady-state entanglement and quantum correlations using Gaussian quantum discord and stationary entanglement, respectively.

We have demonstrated the existence of an entangled state in the quantum discord and entanglement generated between the cavity and mechanical oscillator mode, both with and without atoms. We observed that the atoms injected into the cavity have a strong influence on the generation of stationary entanglement and quantum discord. Besides, the injected three-level atoms enhanced the degree of entanglement and quantum discord compared to without the injection of atoms. Furthermore, the we indicates that, for a certain parameter range, continuous variable entanglement is present and the resonance case is close to the point of maximum entanglement. Moreover, the curve's width is increased, and this is important for the probability of finding the existence of entanglement in the experimental realization. Furthermore, we have demonstrated a direct correlation between the effective coupling rate and the mean photon number. This implies that the behavior of the coupling rate on the entanglement is in fact consistent with experimental reality. Consequently, we think that our findings could provide a basis for a practical instrument in the implementation of continuous variable quantum information processing.

In addition, in this dissertation, we have also studied the generation of quantum correlations in a hybrid optomechanical system with OPA, where the two cavity modes are coupled via the cavity-cavity coupling process. We characterized the quantum correlations among the subsystems using various quantum correlation measures. Specifically, we utilized logarithmic negativity to quantify bipartite entanglement and assess state transfer among the subsystems. Quantum steering was used to measure the steerability of the two entangled bipartite states, and Gaussian quantum discord was employed to evaluate the correlation between two Gaussian states, extending our analysis beyond entanglement. Our results show that higher nonlinear gain under OPA strengthens quantum correlations, leading to stronger entanglement. However, the sustainability of these correlations is significantly impacted by the decay rates. Furthermore, we demonstrate that Gaussian quantum discord plays a role in more general quantum correlations beyond entanglement. Finally, by analyzing the steerability between subsystems, we found that, strong coupling under OPA increases quantum steering between cavity modes. Therefore, our model can be useful for building long-distance quantum communication networks.

5.2. RECOMMENDATIONS

The current study can be switched to different direction of optomechanics. The influence of the characteristics of quantum harmonically oscillating mirrors (masses, frequencies, mechanical mode of damping rate, cavity finnese) on the nonclassical behaviors of mechanical modes has not been discussed from an overall perspective due to time constraints. The other area of concentration will be on using quantum information science by changing the input quantum resource. We propose that researchers studying quantum information processing take into consideration the problem of quantum communication and metrology since changes in the OPA, atomic, cavity, and parameters impact the features of different nonclassical correlations. We will continue to study more nonclassical correlations in the future, including fidelity, quantum monogamy, bistability of mechanical modes, magnon, and others, both theoretically and experimentally using different means.

List of Publications

1. A. A. Kibret, T. Y. Derge, and T. G. Tesfahannes, “Steady-state entanglement in a hybrid optomechanical system enhanced by optical parametric amplifiers,” Opt. Continuum 2, 2131–2143 (2023),
https://doi.org/10.1364/OPTCON.502349

2. A. A. Kibret, T. Y. Derge, and T. G. Tesfahannes, “Generation of stationary entanglement and quantum discord in an optomechanical system through three-level atoms,” J. Opt. Soc. Am. B 41, 3131–2143 (2024),
https://doi.org/10.1364/JOSAB.516660

3. A. A. Kibret, E. A. Beisie, H. D. Mekonnen, T. Y. Darge, and T. G. Tesfahannes (2024). Generation of quantum correlations through optical parametric amplification in a hybrid optomechanical system. The European Physical Journal Plus, 139(8), 1-12.
https://doi.org/10.1140/epjp/s13360-024-05511-6

4. Two different manuscripts are being prepared for publication in the near future.

LIST OF CONFERENCE PARTICIPATION

I have been participating in different national and international conferences, such as
1. The 13th National Conference of the Ethiopian Physical Society was held at Adama Science and Technology University in February 2019. (Participant)
2. National Conference on Science, Technology, and Innovations Application and Transfer for Development Endeavors June 2018 was held at Wollega University. (Chaired and Participant)
3. The National Conference of Physics Laboratory Curriculum Review was held at Wollega University in May 2018. (Reviewer)
4. USAID HIV presentation program (FHI360) in collaboration with the Ministry of Education in response to the fight against HIV/AIDS 2021–2022. (Leader)
5. Ethiopian Physical Society 14th annual conference February 7-8 2020 at Arbaminch University, Arbaminch. (Participant)
6. In addition, the findings of this research were presented at international conferences in 2024.

REFERENCES

Adamyan, H. and Kryuchkyan, G. Y. (2004). Continuous-variable entanglement of phase-locked light beams. *Physical Review A*, 69(5):053814.

Adesso, G. and Datta, A. (2010). Quantum versus classical correlations in gaussian states. *Physical review letters*, 105(3):030501.

Agarwal, G. S. and Huang, S. (2010). Electromagnetically induced transparency in mechanical effects of light. *Physical Review A*, 81(4):041803.

Alebachew, E. (2007). Continuous-variable entanglement in a nondegenerate three-level laser with a parametric oscillator. *Physical Review A*, 76(2):023808.

Amazioug, M., Jebli, L., Nassik, M., and Habiballah, N. (2020a). Quantifying non-classical correlations under thermal effects in a double cavity optomechanical system. *Chinese Physics B*, 29(2):020304.

Amazioug, M., Maroufi, B., and Daoud, M. (2020b). Creating mirror–mirror quantum correlations in optomechanics. *The European Physical Journal D*, 74:1–9.

Amazioug, M., Nassik, M., and Habiballah, N. (2018). Entanglement, epr steering and gaussian geometric discord in a double cavity optomechanical systems. *The European Physical Journal D*, 72:1–9.

Anetsberger, G., Arcizet, O., Unterreithmeier, Q. P., Rivière, R., Schliesser, A., Weig, E. M., Kotthaus, J. P., and Kippenberg, T. J. (2009). Near-field cavity optomechanics with nanomechanical oscillators. *Nature Physics*, 5(12):909–914.

Artigas, D., Reid, D. T., Fejer, M. M., and Torner, L. (2002). Pulse compression and gain enhancement in a degenerate optical parametric amplifier based on aperiodically poled crystals. *Optics letters*, 27(6):442–444.

Aspelmeyer, M., Kippenberg, T. J., and Marquardt, F. (2014). Cavity optomechanics. *Reviews of Modern Physics*, 86(4):1391.

Ayehu, D. (2021). Squeezing and entanglement properties of the cavity light with decoherence in a cascade three-level laser. *Journal of Russian Laser Research*, 42:136–145.

Bai, C.-H., Wang, D.-Y., Wang, H.-F., Zhu, A.-D., and Zhang, S. (2016). Robust entanglement between a movable mirror and atomic ensemble and entanglement transfer in coupled optomechanical system. *Scientific reports*, 6(1):33404.

Bariani, F., Singh, S., Buchmann, L., Vengalattore, M., and Meystre, P. (2014). Hybrid optomechanical cooling by atomic λ systems. *Physical Review A*, 90(3):033838.

Barzanjeh, S., Redchenko, E., Peruzzo, M., Wulf, M., Lewis, D., Arnold, G., and Fink, J. M. (2019). Stationary entangled radiation from micromechanical motion. *Nature*, 570(7762):480–483.

Bennett, C. H., Grudka, A., Horodecki, M., Horodecki, P., and Horodecki, R. (2011). Postulates for measures of genuine multipartite correlations. *Physical Review A*, 83(1):012312.

Berkley, A., Xu, H., Ramos, R., Gubrud, M., Strauch, F., Johnson, P., Anderson, J., Dragt, A., Lobb, C., and Wellstood, F. (2003). Entangled macroscopic quantum states in two superconducting qubits. *Science*, 300(5625):1548–1550.

Berrada, K., Chafik, A., Eleuch, H., and Hassouni, Y. (2010). Concurrence in the framework of coherent states. *Quantum Information Processing*, 9:13–26.

Berrada, K., Eleuch, H., and Hassouni, Y. (2011). Asymptotic dynamics of quantum discord in open quantum systems. *Journal of Physics B: Atomic, Molecular and Optical Physics*, 44(14):145503.

Beth, R. A. (1936). Mechanical detection and measurement of the angular momentum of light. *Physical Review*, 50(2):115.

Bub, J. (2014). Quantum correlations and the measurement problem. *International Journal of Theoretical Physics*, 53:3346–3369.

Budriūnas, R., Kučinskas, D., Valiulis, G., and Varanavičius, A. (2021). Increasing the efficiency of optical parametric amplifiers with polarization-based idler elimination. In *Nonlinear Optics*, pages NF2A–3. Optica Publishing Group.

Carmon, T., Rokhsari, H., Yang, L., Kippenberg, T. J., and Vahala, K. J. (2005). Temporal behavior of radiation-pressure-induced vibrations of an optical microcavity phonon mode. *Physical review letters*, 94(22):223902.

Chakraborty, S. and Sarma, A. K. Enhancing quantum correlations in an optomechanical system via cross-kerr nonlinearity. *JOSA B*, 34.

Chen, Y. (2013). Macroscopic quantum mechanics: theory and experimental concepts of optomechanics. *Journal of Physics B: Atomic, Molecular and Optical Physics*, 46(10):104001.

Cho, J., Angelakis, D. G., and Bose, S. (2008). Heralded generation of entanglement with coupled cavities. *Physical Review A*, 78(2):022323.

Cui, J. and Fan, H. (2010). Correlations in the grover search. *Journal of Physics A: Mathematical and Theoretical*, 43(4):045305.

Datta, A. and Gharibian, S. (2009). Signatures of nonclassicality in mixed-state quantum computation. *Physical Review A*, 79(4):042325.

Datta, A., Shaji, A., and Caves, C. M. (2008). Quantum discord and the power of one qubit. *Physical review letters*, 100(5):050502.

Dobrindt, J. M., Wilson-Rae, I., and Kippenberg, T. J. (2008). Parametric normal-mode splitting in cavity optomechanics. *Physical Review Letters*, 101(26):263602.

Dodonov, V. and Dodonov, A. (2006). The heisenberg-langevin model of a quantum damped harmonic oscillator with time-dependent frequency and damping coefficients. *Journal of Russian Laser Research*, 27:379–388.

Eichenfield, M., Camacho, R., Chan, J., Vahala, K. J., and Painter, O. (2009). A picogram- and nanometre-scale photonic-crystal optomechanical cavity. *nature*, 459(7246):550–555.

Einstein, A. (1909). On the development of our understanding of the nature and composition of radiation. *Physikalische Zeitschrift*, 10(22):817–826.

Elsaesser, T., Fujimoto, J. G., Wiersma, D. A., Zinth, W., Lochbrunner, S., Wilhelm, T., Piel, J., Huppmann, P., Spörlein, S., and Riedle, E. (1998). Tunable visible and nir parametric amplifiers at 1 khz and pulse lengths down to 10 fs. In *Ultrafast Phenomena XI: Proceedings of the 11th International Conference, Garmisch-Partenkirchen, Germany, July 12–17, 1998*, pages 57–59. Springer.

Ferraro, A., Aolita, L., Cavalcanti, D., Cucchietti, F. M., and Acín, A. (2010). Almost all quantum states have nonclassical correlations. *Physical Review A*, 81(5):052318.

Fogliano, F., Besga, B., Reigue, A., Heringlake, P., Mercier de Lépinay, L., Vaneph, C., Reichel, J., Pigeau, B., and Arcizet, O. (2021). Mapping the cavity optomechanical interaction with subwavelength-sized ultrasensitive nanomechanical force sensors. *Physical Review X*, 11(2):021009.

Frisch, R. (1933). Experimental demonstration of einstein's radiation recoil. *Zeitschrift für Phys*, 86:42–45.

Gardiner, C. and Zoller, P. (2004). *Quantum noise: a handbook of Markovian and non-Markovian quantum stochastic methods with applications to quantum optics*. Springer Science & Business Media.

Gebremariam, T., Mazaheri, M., Zeng, Y., and Li, C. (2019). Dynamical quantum steering in a pulsed hybrid opto-electro-mechanical system. *JOSA B*, 36(2):168–177.

Gebremariam, T., Zeng, Y.-X., Chen, X.-Y., and Li, C. (2017). Observation and measures of robust correlations for continuous variable system. *Communications in Theoretical Physics*, 68(5):661.

Gebremariam, T., Zeng, Y.-X., Mazaheri, M., and Li, C. (2020). Enhancing optomechanical force sensing via precooling and quantum noise cancellation. *Science China Physics, Mechanics & Astronomy*, 63:1–11.

Genes, C., Mari, A., Tombesi, P., and Vitali, D. (2008). Robust entanglement of a micromechanical resonator with output optical fields. *Physical Review A*, 78(3):032316.

Genes, C., Mari, A., Vitali, D., and Tombesi, P. (2009a). Quantum effects in optomechanical systems. *Advances in atomic, molecular, and optical physics*, 57:33–86.

Genes, C., Ritsch, H., and Vitali, D. (2009b). Micromechanical oscillator ground-state cooling via resonant intracavity optical gain or absorption. *Physical Review A*, 80(6):061803.

Gigan, S., Böhm, H., Paternostro, M., Blaser, F., Langer, G., Hertzberg, J., Schwab, K. C., Bäuerle, D., Aspelmeyer, M., and Zeilinger, A. (2006). Self-cooling of a micromirror by radiation pressure. *Nature*, 444(7115):67–70.

Giorda, P. and Paris, M. G. (2010). Gaussian quantum discord. *Physical review letters*, 105(2):020503.

Giovannetti, V. and Vitali, D. (2001). Phase-noise measurement in a cavity with a movable mirror undergoing quantum brownian motion. *Physical Review A*, 63(2):023812.

Gröblacher, S. (2012). *Quantum opto-mechanics with micromirrors: combining nano-mechanics with quantum optics*. Springer Science & Business Media.

Gröblacher, S., Hammerer, K., Vanner, M. R., and Aspelmeyer, M. (2009). Observation of strong coupling between a micromechanical resonator and an optical cavity field. *Nature*, 460(7256):724–727.

Gut, C., Winkler, K., Hoelscher-Obermaier, J., Hofer, S., Nia, R. M., Walk, N., Steffens, A., Eisert, J., Wieczorek, W., Slater, J., et al. (2020). Stationary optomechanical entanglement between a mechanical oscillator and its measurement apparatus. *Physical Review Research*, 2(3):033244.

Hammerer, K., Aspelmeyer, M., Polzik, E. S., and Zoller, P. (2009a). Establishing einstein-poldosky-rosen channels between nanomechanics and atomic ensembles. *Physical review letters*, 102(2):020501.

Hammerer, K., Wallquist, M., Genes, C., Ludwig, M., Marquardt, F., Treutlein, P., Zoller, P., Ye, J., and Kimble, H. J. (2009b). Strong coupling of a mechanical oscillator and a single atom. *Physical review letters*, 103(6):063005.

Hartmann, M. J. and Plenio, M. B. (2008). Steady state entanglement in the mechanical vibrations of two dielectric membranes. *Physical Review Letters*, 101(20):200503.

He, Q. and Ficek, Z. (2014). Einstein-podolsky-rosen paradox and quantum steering in a three-mode optomechanical system. *Physical Review A*, 89(2):022332.

Henderson, L. and Vedral, V. (2001). Classical, quantum and total correlations. *Journal of physics A: mathematical and general*, 34(35):6899.

Höhberger, C. and Karrai, K. (2004). Proceedings of the 4th ieee conference nanotechnology.

Holstein, T. and Primakoff, H. (1940). Field dependence of the intrinsic domain magnetization of a ferromagnet. *Physical Review*, 58(12):1098.

Horodecki, R., Horodecki, P., Horodecki, M., and Horodecki, K. (2009). Quantum entanglement. *Reviews of modern physics*, 81(2):865.

Huang, S. and Agarwal, G. (2009a). Enhancement of cavity cooling of a micromechanical mirror using parametric interactions. *Physical Review A*, 79(1):013821.

Huang, S. and Agarwal, G. (2009b). Entangling nanomechanical oscillators in a ring cavity by feeding squeezed light. *New Journal of Physics*, 11(10):103044.

Huang, S. and Agarwal, G. (2009c). Normal-mode splitting in a coupled system of a nanomechanical oscillator and a parametric amplifier cavity. *Physical Review A*, 80(3):033807.

Huang, S. and Agarwal, G. (2010). Normal-mode splitting and antibunching in stokes and anti-stokes processes in cavity optomechanics: radiation-pressure-induced four-wave-mixing cavity optomechanics. *Physical Review A*, 81(3):033830.

Huang, S. and Agarwal, G. (2011). Electromagnetically induced transparency with quantized fields in optocavity mechanics. *Physical Review A*, 83(4):043826.

Ian, H., Gong, Z., Liu, Y.-x., Sun, C., and Nori, F. (2008). Cavity optomechanical coupling assisted by an atomic gas. *Physical Review A*, 78(1):013824.

Kassahun, F. (2014). Refined quantum analysis of light. *Create Space Independent Publishing Platform*.

Kibret, A. A., Darge, T. Y., and Tesfahannes, T. G. (2024). Generation of stationary entanglement and quantum discord in an optomechanical system through three-level atoms. *JOSA B*, 41(8):C20–C28.

Kibret, A. A., Derge, T. Y., and Tesfahannes, T. G. (2023). Steady-state entanglement in a hybrid optomechanical system enhanced by optical parametric amplifiers. *Optics Continuum*, 2(10):2131–2143.

Kippenberg, T. J. and Vahala, K. J. (2007). Cavity opto-mechanics. *Optics express*, 15(25):17172–17205.

Kippenberg, T. J. and Vahala, K. J. (2008). Cavity optomechanics: back-action at the mesoscale. *science*, 321(5893):1172–1176.

Kleckner, D. and Bouwmeester, D. (2006). Sub-kelvin optical cooling of a micromechanical resonator. *Nature*, 444(7115):75–78.

Kogias, I., Lee, A. R., Ragy, S., and Adesso, G. (2015). Quantification of gaussian quantum steering. *Physical review letters*, 114(6):060403.

Kraus, B. and Cirac, J. I. (2004). Discrete entanglement distribution with squeezed light. *Physical review letters*, 92(1):013602.

Kuzyk, M. C., van Enk, S. J., and Wang, H. (2013). Generating robust optical entanglement in weak-coupling optomechanical systems. *Physical Review A*, 88(6):062341.

Lai, D.-G., Qin, W., Hou, B.-P., Miranowicz, A., and Nori, F. (2021). Significant enhancement in refrigeration and entanglement in auxiliary-cavity-assisted optomechanical systems. *Physical Review A*, 104(4):043521.

Lakhfif, A., Hidki, A., El Qars, J., and Nassik, M. (2022). Quantum versus classical correlations in a double cavity optomechanical system. *Journal of Physics B: Atomic, Molecular and Optical Physics*, 55(11):115501.

Lanyon, B. P., Barbieri, M., Almeida, M. P., and White, A. G. (2008). Experimental quantum computing without entanglement. *Physical review letters*, 101(20):200501.

Lebedev, P. (1901). The experimental study of the pressure of the light. *Ann. Phys*, 6:433.

Lee, Y. A. and Vidal, G. (2013). Entanglement negativity and topological order. *Physical Review A*, 88(4):042318.

Leng, H., Wang, J., Yu, Y., Yu, X., Xu, P., Xie, Z., Zhao, J., and Zhu, S. (2009). Scheme to generate continuous-variable quadripartite entanglement by intracavity down-conversion cascaded with double sum-frequency generations. *Physical Review A*, 79(3):032337.

Li, B.-B., Ou, L., Lei, Y., and Liu, Y.-C. (2021). Cavity optomechanical sensing. *Nanophotonics*, 10(11):2799–2832.

Li, G., Nie, W., Wu, Y., Liao, Q., Chen, A., and Lan, Y. (2020). Manipulating the steady-state entanglement via three-level atoms in a hybrid levitated optomechanical system. *Physical Review A*, 102(6):063501.

Li, J., Haghighi, I. M., Malossi, N., Zippilli, S., and Vitali, D. (2015a). Generation and detection of large and robust entanglement between two different mechanical resonators in cavity optomechanics. *New Journal of Physics*, 17(10):103037.

Li, J. and Paraoanu, G. (2009). Generation and propagation of entanglement in driven coupled-qubit systems. *New Journal of Physics*, 11(11):113020.

Li, W., Jiang, Y., Li, C., and Song, H. (2016). Parity-time-symmetry enhanced optomechanically-induced-transparency. *Scientific Reports*, 6(1):31095.

Li, W., Li, C., and Song, H. (2015b). Criterion of quantum synchronization and controllable quantum synchronization based on an optomechanical system. *Journal of Physics B: Atomic, Molecular and Optical Physics*, 48(3):035503.

Liao, C.-G., Xie, H., Chen, R.-X., Ye, M.-Y., and Lin, X.-M. (2020). Controlling one-way quantum steering in a modulated optomechanical system. *Physical Review A*, 101(3):032120.

Lin, Q., Rosenberg, J., Chang, D., Camacho, R., Eichenfield, M., Vahala, K. J., and Painter, O. (2010). Coherent mixing of mechanical excitations in nano-optomechanical structures. *Nature Photonics*, 4(4):236–242.

Lin, Y., Leibrandt, D. R., Leibfried, D., and Chou, C.-w. (2020). Quantum entanglement between an atom and a molecule. *Nature*, 581(7808):273–277.

Liu, S.-Y., Zhang, Y.-R., Yang, W.-L., and Fan, H. (2015). Global quantum discord and quantum phase transition in xy model. *Annals of Physics*, 362:805–813.

Liu, X., Hu, J., Li, Z.-F., Li, X., Li, P.-Y., Liang, P.-J., Zhou, Z.-Q., Li, C.-F., and Guo, G.-C. (2021). Heralded entanglement distribution between two absorptive quantum memories. *Nature*, 594(7861):41–45.

Liu, Y., Miao, H., Aksyuk, V., and Srinivasan, K. (2012). Wide cantilever stiffness range cavity optomechanical sensors for atomic force microscopy. *Optics express*, 20(16):18268–18280.

Liu, Y.-C., Hu, Y.-W., Wong, C. W., and Xiao, Y.-F. (2013). Review of cavity optomechanical cooling. *Chinese Physics B*, 22(11):114213.

Liu, Y.-l., Wang, C., Zhang, J., and Liu, Y.-x. (2018). Cavity optomechanics: Manipulating photons and phonons towards the single-photon strong coupling. *Chinese Physics B*, 27(2):024204.

Lü, X.-Y., Wu, Y., Johansson, J., Jing, H., Zhang, J., and Nori, F. (2015). Squeezed optomechanics with phase-matched amplification and dissipation. *Physical review letters*, 114(9):093602.

Ma, Y.-H. and Wu, E. (2015). Macroscopic entanglement of remote optomechanical systems assisted by parametric interactions. *International Journal of Theoretical Physics*, 54:1334–1341.

Ma, Y.-H. and Zhou, L. (2012). Enhanced entanglement between a movable mirror and a cavity field assisted by two-level atoms. *Journal of Applied Physics*, 111(10).

Mancini, S., Giovannetti, V., Vitali, D., and Tombesi, P. (2002). Entangling macroscopic oscillators exploiting radiation pressure. *Physical review letters*, 88(12):120401.

Maquedano, L. and Costa, A. C. (2024). Analysis of quantum steering measures. *Entropy*, 26(3):257.

Mari, A. (2012). *Signatures of non-classicality in optomechanical systems*. PhD thesis, Universität Potsdam.

Mari, A. and Eisert, J. (2009). Gently modulating optomechanical systems. *Physical Review Letters*, 103(21):213603.

Marquardt, F., Chen, J. P., Clerk, A. A., and Girvin, S. (2007). Quantum theory of cavity-assisted sideband cooling of mechanical motion. *Physical review letters*, 99(9):093902.

Marquardt, F., Clerk, A., and Girvin, S. (2008). Quantum theory of optomechanical cooling. *Journal of Modern Optics*, 55(19-20):3329–3338.

Mathieu, V., Kochelev, N., and Vento, V. (2009). The physics of glueballs. *International Journal of Modern Physics E*, 18(01):1–49.

McGee, S., Meiser, D., Regal, C., Lehnert, K., and Holland, M. (2013). Mechanical resonators for storage and transfer of electrical and optical quantum states. *Physical Review A*, 87(5):053818.

Mekonnen, H. D., Tesfahannes, T. G., Darge, T. Y., and Eshete, S. (2024). Boosting macroscopic entanglement in charged cavity optomechanical system through coherent feedback loop. *Journal of Optics*, pages 1–9.

Mekonnen, H. D., Tesfahannes, T. G., Darge, T. Y., and Kumela, A. G. (2023). Quantum correlation in a nano-electro-optomechanical system enhanced by an optical parametric amplifier and coulomb-type interaction. *Scientific Reports*, 13(1):13800.

Metcalfe, M. (2014). Applications of cavity optomechanics. *Applied Physics Reviews*, 1(3).

Metzger, C., Ludwig, M., Neuenhahn, C., Ortlieb, A., Favero, I., Karrai, . f. K., and Marquardt, F. (2008). Self-induced oscillations in an optomechanical system driven by bolometric backaction. *Physical review letters*, 101(13):133903.

Meystre, P. (2013). A short walk through quantum optomechanics. *Annalen der Physik*, 525(3):215–233.

Meystre, P., Wright, E. M., McCullen, J., and Vignes, E. (1985). Theory of radiation-pressure-driven interferometers. *JOSA B*, 2(11):1830–1840.

Mi, X., Bai, J., and Ke-hui, S. (2013). Robust entanglement between a movable mirror and a cavity field system with an optical parametric amplifier. *The European Physical Journal D*, 67:1–7.

Miao, H., Zhao, C., Ju, L., and Blair, D. G. (2009). Quantum ground-state cooling and tripartite entanglement with three-mode optoacoustic interactions. *Physical Review A*, 79(6):063801.

Modi, K., Paterek, T., Son, W., Vedral, V., and Williamson, M. (2010). Unified view of quantum and classical correlations. *Physical review letters*, 104(8):080501.

Navascués, M., Guryanova, Y., Hoban, M. J., and Acín, A. (2015). Almost quantum correlations. *Nature communications*, 6(1):6288.

Nichols, E. F. and Hull, G. F. (1901). A preliminary communication on the pressure of heat and light radiation. *Physical Review (Series I)*, 13(5):307.

Nielsen, M. A. and Chuang, I. L. (2010). *Quantum computation and quantum information*. Cambridge university press.

Ollivier, H. and Zurek, W. H. (2001). Quantum discord: a measure of the quantumness of correlations. *Physical review letters*, 88(1):017901.

Palomaki, T., Harlow, J., Teufel, J., Simmonds, R., and Lehnert, K. W. (2013). Coherent state transfer between itinerant microwave fields and a mechanical oscillator. *Nature*, 495(7440):210–214.

Pan, G., Xiao, R., and Zhai, C. (2023). Enhanced entanglement and output squeezing in electro-optomechanical system with an optical parametric amplifier. *The European Physical Journal D*, 77(2):25.

Paschotta, R. (2014). Optical parametric amplifiers. *Dostupné z: https://www. rpphotonics. com/optical_parametric_amplifiers. html (accessed March 9, 2022)*.

Pinard, M., Dantan, A., Vitali, D., Arcizet, O., Briant, T., and Heidmann, A. (2005). Entangling movable mirrors in a double-cavity system. *Europhysics Letters*, 72(5):747.

Regal, C., Teufel, J., and Lehnert, K. (2008). Measuring nanomechanical motion with a microwave cavity interferometer. *Nature Physics*, 4(7):555–560.

Reid, M. D., Drummond, P., Bowen, W., Cavalcanti, E. G., Lam, P. K., Bachor, H., Andersen, U. L., and Leuchs, G. (2009). Colloquium: the einstein-podolsky-rosen paradox: from concepts to applications. *Reviews of Modern Physics*, 81(4):1727.

Riedinger, R., Wallucks, A., Marinković, I., Löschnauer, C., Aspelmeyer, M., Hong, S., and Gröblacher, S. (2018). Remote quantum entanglement between two micromechanical oscillators. *Nature*, 556(7702):473–477.

Safavi-Naeini, A. H., Alegre, T. M., Chan, J., Eichenfield, M., Winger, M., Lin, Q., Hill, J. T., Chang, D. E., and Painter, O. (2011). Electromagnetically induced transparency and slow light with optomechanics. *Nature*, 472(7341):69–73.

Schliesser, A. and Kippenberg, T. (2014). Cavity optomechanics with whispering-gallery-mode microresonators. In *Cavity Optomechanics: Nano-and Micromechanical Resonators Interacting with Light*, pages 121–148. Springer.

Schmidt, M., Peano, V., and Marquardt, F. (2015). Optomechanical dirac physics. *New Journal of Physics*, 17(2):023025.

Scully, M. O. and Zubairy, M. (1988). Noise free amplification via the two-photon correlated spontaneous emission laser. *Optics communications*, 66(5-6):303–306.

Scully, M. O. and Zubairy, M. S. (1997). *Quantum optics*. Cambridge university press.

Sheard, B. S., Gray, M. B., Mow-Lowry, C. M., McClelland, D. E., and Whitcomb, S. E. (2004). Observation and characterization of an optical spring. *Physical Review A*, 69(5):051801.

Singh, S., Jing, H., Wright, E., and Meystre, P. (2012). Quantum-state transfer between a bose-einstein condensate and an optomechanical mirror. *Physical Review A*, 86(2):021801.

Tesfa, S. (2008). Two-mode squeezing in a coherently driven degenerate parametric down conversion. *The European Physical Journal D*, 46:351–358.

Tesfahannes, T. G. (2020). Generation of the bipartite entanglement and correlations in an optomechanical array. *JOSA B*, 37(11):A245–A252.

Tesfahannes, T. G. (2021). Enhanced optomechanically induced transparency via atomic ensemble in optomechanical system. *Quantum Information Processing*, 20(3):116.

Tesfahannes, T. G. and Getahune, M. D. (2020). Steady-state quantum correlation measurement in hybrid optomechanical systems. *International Journal of Quantum Information*, 18(07):2050046.

Teufel, J. D., Donner, T., Castellanos-Beltran, M., Harlow, J. W., and Lehnert, K. W. (2009). Nanomechanical motion measured with an imprecision below that at the standard quantum limit. *Nature nanotechnology*, 4(12):820–823.

Thompson, J., Zwickl, B., Jayich, A., Marquardt, F., Girvin, S., and Harris, J. (2008). Strong dispersive coupling of a high-finesse cavity to a micromechanical membrane. *Nature*, 452(7183):72–75.

Tian, L. (2012). Adiabatic state conversion and pulse transmission in optomechanical systems. *Physical review letters*, 108(15):153604.

Tian, L. and Wang, H. (2010). Optical wavelength conversion of quantum states with optomechanics. *Physical Review A*, 82(5):053806.

Vidal, G. and Werner, R. F. (2002). Computable measure of entanglement. *Physical Review A*, 65(3):032314.

Vitali, D., Gigan, S., Ferreira, A., Böhm, H., Tombesi, P., Guerreiro, A., Vedral, V., Zeilinger, A., and Aspelmeyer, M. (2007). Optomechanical entanglement between a movable mirror and a cavity field. *Physical review letters*, 98(3):030405.

Walls, D., Milburn, G., Walls, D., and Milburn, G. (1994). Atomic optics. *Quantum Optics*, pages 315–340.

Walls, D. and Milburn, G. J. (2008). Quantum information. In *Quantum Optics*, pages 307–346. Springer.

Wang, G., Huang, L., Lai, Y.-C., and Grebogi, C. (2014a). Nonlinear dynamics and quantum entanglement in optomechanical systems. *Physical review letters*, 112(11):110406.

Wang, H., Gu, X., Liu, Y.-x., Miranowicz, A., and Nori, F. (2014b). Optomechanical analog of two-color electromagnetically induced transparency: Photon transmission through an optomechanical device with a two-level system. *Physical Review A*, 90(2):023817.

Wang, Y.-D. and Clerk, A. A. (2012). Using interference for high fidelity quantum state transfer in optomechanics. *Physical review letters*, 108(15):153603.

Wang, Y.-D. and Clerk, A. A. (2013). Reservoir-engineered entanglement in optomechanical systems. *Physical review letters*, 110(25):253601.

Woolley, M. and Clerk, A. (2014). Two-mode squeezed states in cavity optomechanics via engineering of a single reservoir. *Physical Review A*, 89(6):063805.

Xiong, H., Si, L.-G., Lü, X.-Y., Yang, X., and Wu, Y. (2014). Nanosecond-pulse-controlled higher-order sideband comb in a gaas optomechanical disk resonator in the non-perturbative regime. *Annals of Physics*, 349:43–54.

Xu, J.-S., Xu, X.-Y., Li, C.-F., Zhang, C.-J., Zou, X.-B., and Guo, G.-C. (2010). Experimental investigation of classical and quantum correlations under decoherence. *Nature communications*, 1(1):7.

Yang, R.-G., Li, N., Zhang, J., Li, J., and Zhang, T.-C. (2017). Enhanced entanglement of two optical modes in optomechanical systems via an optical parametric amplifier. *Journal of Physics B: Atomic, Molecular and Optical Physics*, 50(8):085502.

Yang, X., Huang, G. H., and Fang, M. F. (2015). A study on quantum discord in gaussian states. *Optics Communications*, 341:91–96.

Yin, Z.-q., Li, T., Zhang, X., and Duan, L. (2013). Large quantum superpositions of a levitated nanodiamond through spin-optomechanical coupling. *Physical Review A*, 88(3):033614.

Zhang, C.-y., Li, H., Pan, G.-x., and Sheng, Z.-q. (2016a). Entanglement of movable mirror and cavity field enhanced by an optical parametric amplifier. *Chinese Physics B*, 25(7):074202.

Zhang, J., Peng, K., and Braunstein, S. L. (2003). Quantum-state transfer from light to macroscopic oscillators. *Physical Review A*, 68(1):013808.

Zhang, W.-Z., Cheng, J., Li, W.-D., and Zhou, L. (2016b). Optomechanical cooling in the non-markovian regime. *Physical Review A*, 93(6):063853.

Zhang, W.-Z., Cheng, J., Liu, J.-Y., and Zhou, L. (2015). Controlling photon transport in the single-photon weak-coupling regime of cavity optomechanics. *Physical Review A*, 91(6):063836.

Zhao, L.-C., Ling, L., Qi, J.-W., Yang, Z.-Y., and Yang, W.-L. (2017). Dynamics of rogue wave excitation pattern on stripe phase backgrounds in a two-component bose-einstein condensate. *Communications in Nonlinear Science and Numerical Simulation*, 49:39–47.

Zhou, L., Han, Y., Jing, J., and Zhang, W. (2011). Entanglement of nanomechanical oscillators and two-mode fields induced by atomic coherence. *Physical Review A*, 83(5):052117.

Zidan, M., Eleuch, H., and Abdel-Aty, M. (2021). Non-classical computing problems: Toward novel type of quantum computing problems. *Results in Physics*, 21:103536.

Zubair, A., Ahmad, Z., Mahmood, A., Cheong, W.-C., Ali, I., Khan, M. A., Chughtai, A. H., and Ashiq, M. N. (2017). Structural, morphological and magnetic properties of eu-doped cofe2o4 nano-ferrites. *Results in physics*, 7:3203–3208.